RECEIVED
LAWRENCE
RADIATION LABORATORY
FEB 11 1970
LIBRARY AND
DOCUMENTS SECTION

UCRL-19113

c.2

INTERSTITIAL ORDERING AND MECHANICAL PROPERTIES OF TANTALUM-CARBON ALLOYS

Prakash Rao
(Ph.D. Thesis)

December 1969

AEC Contract No. W-7405-eng-48

TWO-WEEK LOAN COPY

This is a Library Circulating Copy which may be borrowed for two weeks. For a personal retention copy, call Tech. Info. Division, Ext. 5545

LAWRENCE RADIATION LABORATORY
UNIVERSITY of CALIFORNIA BERKELEY

UCRL-19113 c.2

DISCLAIMER

This document was prepared as an account of work sponsored by the United States Government. While this document is believed to contain correct information, neither the United States Government nor any agency thereof, nor the Regents of the University of California, nor any of their employees, makes any warranty, express or implied, or assumes any legal responsibility for the accuracy, completeness, or usefulness of any information, apparatus, product, or process disclosed, or represents that its use would not infringe privately owned rights. Reference herein to any specific commercial product, process, or service by its trade name, trademark, manufacturer, or otherwise, does not necessarily constitute or imply its endorsement, recommendation, or favoring by the United States Government or any agency thereof, or the Regents of the University of California. The views and opinions of authors expressed herein do not necessarily state or reflect those of the United States Government or any agency thereof or the Regents of the University of California.

TABLES OF CONTENTS

ABSTRACT

I. INTRODUCTION---------- 1

A. Nature of Interstitial Sites in bcc Metals---------- 2

B. Evidence for Interstitial Ordering---------- 6

C. Mechanical Properties of Interstitial Alloys---------- 7

D. Field Ion Microscopy of Interstitial Alloys---------- 9

E. Computer Simulation of Field Ion Images from Interstitial Alloys---------- 10

F. Purpose of the Investigation---------- 12

II. EXPERIMENTAL PROCEDURE---------- 13

A. Specimen Preparation---------- 13

B. Analysis of Carbon Content---------- 14

C. Helium-3 Activation Analysis---------- 14

D. Determination of Tensile Properties---------- 15

E. Specimen Preparation for Electron Microscopy---------- 16

F. Preparation of Specimens for Field Ion Microscopy---------- 16

G. Method of Computation of Field Ion Images---------- 17

H. Computation of Images from Interstitial Alloys---------- 18

I. X-ray Analysis of Ta Containing 11.5 At.% C---------- 19

III. EXPERIMENTAL RESULTS AND INTERPRETATION---------- 20

A. Mechanical Properties of Tantalum-Carbon Alloys---------- 20

B. Electron Microscopy and Interpretation---------- 23

1. Stages of Transformation---------- 23

2. Initiation of Order---------- 25

3. Formation of Discrete Nuclei---------- 26

4. Impinging Domain Boundaries---------- 27

5. Large Non-Impinging Domains ---------- 28

6. Structure of the Ordered Phase ---------- 29

7. Development of Superlattice Diffraction Patterns --------- 31

8. Repeat Distances of Planes Containing Only Tantalum or Only Carbon Atoms in the Ordered Phase ---------- 32

C. Nature of Fractured Surfaces ---------- 34

D. Field Ion Microscopy of Tantalum-Carbon Alloys ---------- 36

E. Nature of Computed Images ---------- 39

F. X-ray Analysis ---------- 41

IV. DISCUSSION ---------- 43

A. Stages of the Ordering Transformation ---------- 43

B. Relation of Interstitial Interactions to Elastic Deformation of the bcc Lattice ---------- 45

C. Correlation of Mechanical Properties and Microstructure ---------- 48

D. Field Ion Microscopy of Tantalum-Carbon Alloys ---------- 54

E. The Superstructure ---------- 57

F. Correlation With Short Range Order ---------- 58

G. Nature of the Interstitial Ordering Transformation ---------- 59

V. SUMMARY AND CONCLUSIONS ---------- 62

ACKNOWLEDGEMENTS ---------- 66

APPENDIX I ---------- 67

APPENDIX II ---------- 71

REFERENCES ---------- 77

FIGURE CAPTIONS ---------- 81

FIGURES ---------- 86

INTERSTITIAL ORDERING AND MECHANICAL PROPERTIES OF TANTALUM-CARBON ALLOYS

Prakash Rao

Inorganic Materials Research Division, Lawrence Radiation Laboratory
Department of Materials Sciences and Engineering, College of Engineering
University of California, Berkeley, California

ABSTRACT

Small concentrations of interstitial solutes (carbon, oxygen, nitrogen, and hydrogen) in the Group VB body centered cubic metals (vanadium, niobium and tantalum) undergo interstitial ordering, whereby preferential occupation of one type of interstitial site leads to the formation of a regular periodic distribution of interstitial atoms forming superlattices.

Direct evidence for interstitial ordering in the tantalum-carbon system is obtained by transmission electron microscopy and field ion microscopy and is correlated with data on mechanical properties. Transmission electron microscopy indicates that the ordering transformation begins by fine scale fluctuations in carbon composition associated with the {110} planes. The fully ordered structure is realized locally when regions of ideal wavelength $\lambda = 4d_{110_{Ta}}$ are obtained. The alloy can be considered then to contain small "ordered particles". These small ordered regions align themselves along ⟨110⟩ and grow till impingement. The final stage of the ordering transformation occurs with the formation of long range highly ordered regions separated by coherent domain boundaries. At this stage the alloys become totally brittle.

Analyses of electron diffraction patterns of the ordered phase show that at the critical carbon composition (1.56 atomic percent), the structure of the ordered phase corresponds to body centered tetragonal $Ta_{64}C$.

Such a structure can be obtained by allowing carbon composition fluctuations to occur simultaneously along four sets of $\{110\}_{Ta}$ planes such that $d_{110_C} = 4d_{110_{Ta}}$.

At all other stages, only partial order exists. Confirmation of the ordering process is obtained from field ion microscopy whereby ordering can be detected even at 20°K by analysis of the imaging characteristics of atom rings around the $\langle 110 \rangle$ poles, with the aid of computer simulated field ion images expected from the ordered phase.

Investigation of the mechanical properties of tantalum containing varying amounts of carbon (determined by He^3 activation analysis) at 300°K, 196°K and 77°K shows that carbon causes a linear increase in yield strength and a decrease in ductility up to 1.56 atomic percent. At this point there is a sudden catastrophic loss in ductility. The linear dependence of yield stress on carbon composition reflects its dependence on the degree of order and on the volume fraction of the ordered phase. The onset of brittleness appears to be due to the development of large scale ordered domains of $Ta_{64}C$. Certain restrictions are placed on the relationships between elastic compliances to determine whether an alloy is ductile or brittle. When the carbon composition attains a critical value the strain energy is so large that the restrictions on the compliances are no longer satisfied. Then the crystal becomes energetically unstable and fails along a set of planes which release the maximum amount of strain energy. This maximum strain energy is reached on the $\{110\}$ planes, which are also the observed cleavage planes.

The fact that interstitial ordering occurs at such small solute concentrations, as compared to substitutional alloys, means that the driving force must be due to the larger strain energy term resulting from the

very large elastic deformations that occur. Since the $Ta_{64}C$ superlattice transformation is present in bulk material, a correction to the existing tantalum-carbon phase diagram is proposed.

I. INTRODUCTION

In recent years, evidence has been obtained by transmission electron microscopy which suggests that small concentrations of interstitials (carbon,[1] oxygen,[2,3] nitrogen,[4] and hydrogen[5]) in the Group V-B body centered cubic metals lead to (interstitial) ordering. Such ordered configurations are possible when the positions of the occupied interstices form a periodic lattice with periods exceeding the periods of the solvent lattice an integral number of times. Ordering in interstitial solutions means that process which leads to the formation of a regular periodic distribution from a random distribution of interstitial atoms among the interstices.

It has been shown experimentally[1-5] that ordering occurs for small concentrations of interstitials, of the order of one atomic percent, and that the period is two to four times the period of the solvent lattice. This is of particular interest since ordering has never been detected in substitutional solutions at concentrations on the order of one atomic percent. Ordering at room temperature of a substitutional solid solution containing 1 at.% of solute would require an ordering energy (displacement energy) of about 1 ev[6] though actually it may be two orders of magnitude higher.

As compared to a substitutional solid solution, one of the principal characteristics of an interstitial solid solution is the much larger magnitude of elastic deformation of the lattice. The concentration coefficient of variation of the lattice period for interstitial solutions in which ordering has been observed at low concentrations is an order of magnitude higher than the equivalent coefficients in substitutional solutions.[6]

This emphasizes the logic of relating the anomalously strong elastic interaction of impurity atoms in interstitial solutions in comparison with substitutional solutions, to elastic deformations of the lattice. Therefore, the hypothesis that elastic deformations have a dominant role in ordering in interstitial solutions explains the unusual character of the ordering in interstitial solutions explains the unusual character of the ordering at low concentrations, which is nonexistent in substitutional solutions. Khachaturyan's theory[6] relating interstitial interactions to elastic deformation of ordered lattice and its applicability to the tantalum-carbon system will be considered later.

A. Nature of Intersitial Sites in bcc Metals

Elements will small atomic radii such as H, O, N and C can be introduced into bcc metals on interstitial sites. Evidence for interstitial site occupation can be obtained from diffusion data.[7,8] The impurity interstitial always has vacant interstitial sites available and needs no lattice vacancy for a migration step. Therefore, diffusion is related to the migration of the impurity interstitial from one interstitial site to another. In the bcc lattice further evidence for interstitial site occupation can be obtained from electron diffraction[1-4] and anelastic studies.[9-10]

The bcc lattice has two kinds of interstitial sites, the octahedral site and the tetrahedral site, shown in Fig. 1. There are three octahedral and six tetrahedral interstices per lattice atom. In an octahedral site, the ⟨100⟩ axis is a four-fold rotation axis. However in the tetrahedral site the ⟨100⟩ axis is only a four fold inversion axis. The axis is a so-called $\bar{4}$ axis. Beshers[11] has investigated interstitial sites in the bcc lattice. Though the octahedral site accommodates a smaller sphere

in the undeformed lattice than does the tetrahedral site, atomic model calculations have shown that for carbon in α-iron and nitrogen in vanadium the octahedral site is preferred. This would depend on the "size" of the interstitial and the lattice. According to Pauling,[12] the atomic diameters in a co-valent configuration are H 0.60, O 1.32, N 1.40 and C 1.54 Å. The "size" of an atom or ion depends on its environment, bonding, etc., and it is an open question whether these values are applicable to a metallic interstice.

Beshers[11] has shown that diffusion appears to occur by octahedral-tetrahedral-octahedral jumps in all the systems except oxygen and nitrogen in niobium in which it appears that tetrahedral-tetrahedral jumps are preferred. The relative positioning of octahedral and tetrahedral sites in the bcc lattice is shown in Fig. 2. Beshers[11] discusses the distortions caused by impurity interstitials and the associated elastic strain energies. As a criterion, whether an octahedral or tetrahedral site should be preferred, he derived the expression

$$R = \frac{\Delta'}{QE_{100}}$$

where Δ' is the relaxation strength obtained from anelastic experiments referred to a common temperature, Q the activation energy for interstitial diffusion, and E_{100} Young's modulus. Large R values (2.5-3.2) should indicate preferred octahedral site occupation, low values (0.49-0.52) preferred tetrahedral site occupation. However, there is no critical value. According to this criterion, oxygen and nitrogen in tantalum and niobium as well as nitrogen and carbon in vanadium should prefer the tetrahedral site, whereas carbon and nitrogen in α-iron, carbon in tantalum and oxygen in vanadium should prefer octahedral sites (see Appendix I). In Appendix I, the applicability of Besher's calculations to the tantalum-carbon system

TABLE I. Known Interstitial Phases of Tantalum and Niobium Reported in Literature

Phase	Structure	Crystal Structure and Lattice Constants in Å	Reference
$Ta_{16}O$	$Ta_{16}O$		Usikov and Khachaturyan[13]
TaO_x	Ta_6O	Tetragonal; a = 13.5 $4a_{Ta}$; C = 13.1 $4a_{Ta}$	Steeb and Renner[14]
Ta_4O	Ta_4O		Usikov and Khachaturyan[13]
TaO_y	$Ta_{32}O_9$ $Ta_{3.56}O$	Cubic; a = 13.4 $4a_{Ta}$	Steeb and Renner[14] and Geiss and Lawless[15]
TaO_y		Orthorhombic; a = 3.271; c = 3.610	van Landuyt and Wayman[16]
TaO_2	Ta_2O	Cubic; a = 6.7 $2a_{Ta}$	Steeb and Renner[14]
$Ta_{27}N$	$Ta_{27}N$	Tetragonal; a $3a_{Ta}$	Seraphim et al.[4]
Ta_9N	Ta_9N		Usikov and Khachaturyan[13]
$Ta_{64}C$	$Ta_{64}C$	Tetragonal; a = 14.94; c = 13.22	Villagrana and Thomas[1]
Ta_2C	Ta_2C	C6 cadmium iodide antitype structure (hexagonal); a = 3.103; c = 4.9378	Bowman et al.[17]
TaC	TaC	Cubic; Nacl type; a = 4.45	

TABLE I cont.

Phase	Structure	Crystal Structure and Lattice Constant in Å	Reference
NbO_x	Nb_6O	Tetragonal; a = 13.5 $4a_{Nb}$; c = 13.1 $4a_{Nb}$	Steeb and Renner[14]
NbO_y	Nb_4O	Tetragonal; a = 6.65 $2a_{Nb}$; c = 3.32 a_{Nb}	" " "
NbO_z		Tetragonal; a = 26.75 $8a_{Nb}$; c = 19.25 $4\sqrt{2}a_{Nb}$	" " "
NbO	NbO	Cubic; a = 4.21	" " "
βNbN_x	$NbN_{0.39-0.45}$	Hexagonal (W_2C type) a = 3.05; c = 4.961	Guard et al.[18]
γNbN_x	$NbN_{0.75-0.80}$	Tetragonal; a = 4.386; c = 4.332	"
δNbN_x	$NbN_{0.88-0.91}$	Cubic (NaCl type); a = 4.3885	"
ϵNbN_x	$NbN_{0.92-1.00}$	Hexagonal; a = 2.958; c = 11.272	"

is outlined.

B. Evidence for Interstitial Ordering

In an investigation of the effect of interstitial nitrogen in tantalum, Seraphim, et al.[4] were the first to attempt to correlate transmission electron microscopy observations with interstitial ordering in the Group V-B body centered cubic metals. On the basis of X-ray Weissenberg camera investigations they proposed an ordered structure $Ta_{27}N$. Van Torne and Thomas[2] and van Landuyt, et al.[3] have made detailed electron microscopy s tudies on the phase transformation induced by interstitial oxygen in niobium and have observed that ordering followed by a definite phase transformation to fcc NbO occurred. Ordering of interstitial hydrogen in tantalum has also been suggested.[5]

Villagrana and Thomas[1] have shown that the introduction of up to 3 at. % carbon in tantalum leads to interstitial ordering. On the basis of electron diffraction data, the existence of a new ordered phase, $Ta_{64}C$ was predicted. Microscopic examination of bulk specimens showed many domain boundaries, separating regions in which the tetragonality associated with ordering was oriented in different directions. Direct observations of ordering in foils was also obtained.

In recent years, several other investigations have shown the existence of interstitial ordering accompanying the formation of ordered phases with different compositions. Table I summarizes all interstitial phases reported to date. It can be seen that there is an abundance of reported ordered phases.

It can be seen from Table I that all reported interstitial phases have empirical formulae corresponding to $M_{n2}I$ or $M_{n3}I$ where M = metal, I = interstitial and n = 1, 2, 3, 4. Therefore, the possibilities are:

n	$M_{n^2}I$	$M_{n^3}I$
1	MI	MI
2	M_4I	M_8I
3	M_9I	$M_{27}I$
4	$M_{16}I$	$M_{64}I$

The only unreported formula is M_8I.

Of particular interest is the structure reported by Steeb and Renner[14] and Geiss and Lawless[15] who assign a structure $Ta_{32}O_9$ to a diffraction pattern which corresponds exactly to that of the structure $Ta_{64}C$ obtained by Villagrana and Thomas.[1]

There have been reports[19,20] on anomalous behavior of the Snoek relaxation in the internal friction spectrum of Ta interstitial solid solutions in the range of one atomic percent interstitials. It was inferred from the internal friction data that the interstitials were interacting in pairs with neighboring interstitials to produce a second relaxation peak distinct from the Snoek effect. From the above observations it is certain that strong interactions are present in these solutions which tend to order the interstitials on specific sites.

C. Mechanical Properties of Interstitial Alloys

The effect of interstitials on the mechanical properties of the bcc metals have been investigated in recent years,[10,21-23] but the possible effect of some kind of interstitial ordering on the mechanical properties of these metals have not studied to any great extent. However, Van Torne and Thomas[22] have shown that the lower yield stress in niobium depends on the total impurity content, and that solute atom

clusters are the strongest barriers to dislocation motion, while Sherman et al.[23] have used some form of ordering to explain the tensile properties of vanadium containing hydrogen. The latter have observed an increase in ductility below 193°K of vanadium containing hydrogen.

Yielding and plastic deformation in bcc materials are usually investigated in terms on the empirical Petch relationship initially established for ferrous materials.[24] This relationship is

$$\tau_y = \tau_f + K^* d^{-1/2} \qquad (1)$$

where τ_y = yield stress

τ_f = friction stress

K^* = a parameter applying to the given metal (which is often taken as a measure of dislocation unlocking)

$2d$ = average grain diameter

The physical significance of the terms in the Petch relationship have been considered in detail by Van Torne and Thomas,[22] by a detailed comparison of substructure of niobium containing interstitials with mechanical properties.

Schoeck and Seeger[10] were the first to point out the significance of the dependence of the flow stress of iron on impurities. They showed that in the stress field of the dislocation, an ordering of solute interstitials takes place. By this Snoek effect dislocations are locked in times which are too short to allow the formation of Cottrell atmosphere.

The fundamental aspects of fracture of body centered cubic refractory metals have received a great deal of attention since brittle fracture during fabrication poses one of the most serious drawbacks to the development of these metals for use as structural materials. All of therefractory metals show a cleavage-shear transition at a temperature which

increases with increasing strain-rate and the presence of a notch.

Interstitial solutes such as hydrogen, carbon, nitrogen and oxygen are much more soluble in the Group V-B metals (V, Nb, Ta) than in the Group VI-B metals (Cr, Mo, W) and have a marked effect on the mechanical properties, causing embrittlement. Hydrogen is the most effective embrittling agent for V, Nb and Ta, while nitrogen oxygen and carbon are less effective in a decreasing order. The mechanism of interstitial embrittlement in the Group V-B metals is not well understood. It is known, however, that interstitial solutes raise the yield stress and hardness of the Group V-B metals.

D. Field Ion Microscopy of Interstitial Alloys

Very little work has been done to date on the field ion microscopy of interstitial solid solutions. Nakamura and Muller,[25] in a very interesting study of the Ta-O system, have shown that micrographs from that of a totally disordered structure (random distribution of spots) to that of a totally ordered structure (rings of bright spots) can be obtained by suitably varying the time and temperature of in situ annealing of Ta in the presence of oxygen. Smith et al.[26] have published a field ion micrograph of $TiC_{0.8}$ which shows a random image of extra bright spots. This kinds of an image is attributed to the bonding in titanium carbide which is complex, having ionic, covalent and metallic contributions.[26]

Field ion microscopy of interstitials has special interest in that the image contrast and imaging conditions from both species constituting the alloy is different from that obtained from substitutional solid solutions. The field ion images from substitutional alloys are easily distinguished from those of a pure metal from their gross irregularity. An exception is the case of the ordered alloy which, for all practical purposes, behaves like a pure metal and develops a regular image. The

irregularity of alloy micrographs can be attributed to the absence of a number of image spots. To explain this a visibility criterion is involved, whereby the characteristics of the solute can make the solute atoms totally invisible or either the solute and solvent atoms be partially visible. These effects have been considered in detail by Durai Raghavan, et al.[27] in a field ion study of the Ta-Mo system. Interstitials, on the other hand, by their very nature (particularly the sites they occupy) are unstable. There is usually no problem in their imaging. They appear as extra bright spots and are always unstable compared with the rest of the (matrix) atoms. Under the high hydrostatic stress field introduced by the large electric field in the process of field ionization, there is considerable stress relaxation at the tip. The interstitials, being devoid of constraints at the tip and in a layer below the tip, pop up to the surface and appear as large bright spots. Therefore, while the matrix atoms are stable, the interstitials keep popping to the surface and are field evaporated away. Photographic recording of such images is extremely difficult. It seems obvious from the image, that the evaporation field for the interstitials is much lower than the best imaging voltage for the Ta atoms. If the applied field is reduced to such an extent that the best imaging voltage (and therefore a stable image) for the interstitials is obtained, then the matrix Ta atoms are not imaged at all. This drawback, coupled with the low proportion of interstitials present makes the stable imaging of both species difficult. This can be overcome, as described later, by photographing the image when both species are field evaporating.

E. Computer Simulation of Field Ion Images From Interstitial Alloys

It is now well realized that the general features of the field ion image of a pure metal can be explained in terms of the geometry of an

approximately spherical surface which is obtained when a crystal lattice is cut by a sphere. Moore[28] was the first to point out that by assuming that only those atoms which lie within a shell of given thickness can give rise to spots, image patterns that strongly resemble the field ion image can be obtained with the help of a computer. Specifically, the computer obtains the coordinates of atoms which lie within the shell. Moore[29] later extended this work to solid solution alloys. To account for the different evaporative properties of the two species, different shell thicknesses were assigned. This work has been extended to ordered interstitial superlattices in the present investigation, and is described below.

Further detailed work on computer simulation of field ion images of metals, superlattices and interstitial solid solutions has been done by Perry and Brandon,[30] Ranganathan, et al.[31] and Perry.[32] Perry and Brandon[30] have extended Moore's model taking into account preferential field evaporation or retention of a second component in dilute solution, and also for condensation and adsorption on field-evaporation surfaces. Ranganathan et al.[31] have extended Moore's model to compute field ion images for the hexagonal lattice, the HCP structure and a few of the common superlattices. The results show that computations are in fact necessary for a detailed interpretation of the field-ion image. Perry[32] has determined the distribution of atomic bonding in simulated images of interstitial solid solutions, and has examined the consequences of relaxation of the surface interstitial atoms. In the calculations the interstitial thin shell image was assumed to lie between 0.16a and 0.577a based on the results obtained by Fortes and Ralph.[33] This gives rise to a high density of interstitials in the computed micrographs. It has been shown that any

possible relaxation effect will occur while the interstitial atom is passing through the 1.4 to 2.3 states (that is, immediately the coordination reduces from that of the bulk.)[32] However, it was assumed that interstitials in the bulk occupy the body centered and octahedral sites in fcc and bcc, respectively, in a purely random manner. No tendency to ordering or clustering was considered, nor was any definite composition assumed.

F. Purpose of the Investigation

The purpose of this investigation is to follow in detail the changes in microstructure accompanying the interstitial ordering transformation (particularly the intial stages)using the techniques of transmission electron microscopy and field ion microscopy. A modern sophisticated approach is required to try and solve the "classical" problem of the ductile-brittle transition in bcc metals. Microstructure is being correlated with the mechanical properties of tantalum-carbon alloys with respect to the variation of yield stress with carbon content and with temperature. Interstitial order is characterized and a structure is assigned to the ordered phase on the basis of electron diffraction data. The influence of the morphology of the ordered phase on the tensile properties of these alloys is examined.

The choice of the tantalum-carbon system for such an investigation rests on the fact that the existence of interstitial order in bulk had already been shown. Also, the ease of introducing carbon into tantalum (as compared to gaseous oxygen or nitrogen) made such an investigation worthwhile. The possibility of carbon occupying the octahedral sites in tantalum and thereby contributing to the tetragonality of the ordered regions must certainly affect the mechanical properties of these alloys. An attempt is made in this investigation to correlate all the above factors in an effort to characterize interstitial order.

II. EXPERIMENTAL PROCEDURES

A. Specimen Preparation

Pure tnatalum stock in the form of 1/4 in. diam rods were grown into high purity single crystals using the MRC electron beam zone refiner. The crystals were usually grown by three passes at a speed of 4.6 mm/min. The power input required to melt the 1/4 in. rods is about 1.1 kw. This can be achieved by various combinations of beam voltage and beam current. However, it was found that a beam voltage of 6kV and a beam current of 180 ma were the optimum setting from the standpoint of uniformity of diameter of the zone melted rod. Three passes on the zone refiner were sufficient to give a resistivity ratio of $\rho_{273}/\rho_{4.2}$ of 50,000 (according to Van Torne,[34] $\rho_{273}/\rho_{4.2}$ = 10,000 corresponds to 3 impurity atoms in 10^9 matrix atoms).

The single crystals were then rolled into strips 5/1000 in. thick using a precision rolling mill. The strips (3 in × 0.5 in × 0.005 in) were then washed with methyl alcohol, and annealed at 2000°C for 2 hours in a BREW furnace in a dynamic vacuum of 10^{-7} mm Hg. All the specimens were treated similarly and allowed to cool in the furnace under vacuum so as to minimize impurity pickup and to get uniform grain size. After annealing, the resistivity ratio did not change.

The tantalum strips were then cleaned by dipping in hydrofluoric acid and washing with methyl alcohol. The clean strips were weighed on a Mettler type BC 1000 substitution balance to an accuracy of ±0.0001 gm, and there transferred to a vacuum evaporator where a film of carbon was deposited on both surfaces of the strips. The specimens were then annealed at various temperatures for 24 hours under high vacuum. At the

end of the annealing period the specimens were allowed to cool in the furnace under vacuum. Finally all the specimens were annealed at 2000°C for 2 hours to obtain a uniform grain size (400μ) so that non-uniformity of grain size would not complicate the interpretation of tensile data.

B. Analysis of Carbon Content

One of the difficulties in the study of bcc metals containing interstitial impurities is that there is no easy and accurate method for obtaining the exact interstitial content. The usual methods of determining carbon, such as the LECO 70 second carbon analyser, are totally unsuitable for the determination of carbon in refractory metals probably because of the high melting points and high retentivity of carbon, as these techniques depend on the complete conversion of all interstitial carbon present to carbon dioxide. The use of difference in weight before and after carbon pick up as a measure of carbon content is rather inaccurate as it does not necessarily isolate carbon from other impurities that might have also been picked up.

C. Helium-3-Activation Analysis

A single, rapid and absolute method for detection of carbon and other elements over the concentration range of 1 ppb to 100% is the helium-3 activation analysis.[35] Only a few milligrams of the total sample material are required. The key feature of this method is the use of the He^3 ions accelerated to comparatively low kinetic energies to induce unclear reactions which give radioactive products. These products, which decay mainly by emission of positrons or negatrons, can be detected by conventional nuclear techniques. In the case of carbon, the C^{12} (He^3,α) C^{11} reaction is used. The analysis* was done by bombarding the specimens (placed after two 0.005 in. aluminum in foils and one 0.005 in gold foil

*Analysis done by the Nuclear Chemistry Division of Lawrence Radiation Laboratory, University of California, Berkeley.

to decrease the energy of the beam) with a 30 MeV He^3 beam from the Berkeley 88-inch cyclotron and measuring the α-decay rate as a function of time, according to the above nuclear reaction. The carbon contents obtained are given below:

Table II

Sample No.	Atomic Percent Carbon
1	0
2	0.76 ± 0.0076
3	1.27 ± 0.0127
4	1.53 ± 0.0153
5	2.05 ± 0.0205
Oxygen: 0.02 at % maximum.	

D. Determination of Tensile Properties

Tensile specimens from strip tantalum, treated as above, were tested at three temperatures 300°K, 196°K and 77°K using the Instron Universal testing machine at a strain rate of 3.33×10^{-4} sec^{-1}. The tensile specimens were 1/2 inch wide and had a one inch gage length.

The fractured surfaces were examined in the Cambridge Stereoscan Mark IIa Scanning Electron Microscope. Scanning electron fractography has several advantages over conventional electron fractography in the ease of specimen preparation. However, resolution seems to be a limiting factor, as also the difficulty in image interpretation as a result of the large depth of focus. Resolution of the Stereoscan is always better than that of a light optical microscope for a similar magnification by a factor of at least 300. Magnification can be varied from 20× to 50,000× with ease. Specimen mounting is extremely simple, being glued on with a con-

ductive cement. Specimens are directly observed, there being no need for replication.

E. Specimen Preparation for Electron Microscopy

Foils suitable for transmission electron microscopy were easily prepared by chemical polishing. The 5/1000 in. thick specimens of tantalum containing different amounts of carbon were chemically polished in a solution of 3:1 HNO_3:HF at or slightly below room temperature until the foils were too thin to handle. Then the edges and one side of the foil were masked with masking lacquer and chemical polishing was continued until thin enough for electron transmission.

Observations were made using the Siemens IA electron microscope equipped with a double-tilting stage. Great care was taken to see that the beam current never rose above 5μA since otherwise bcc metals do undergo interstitial ordering in the microscope as a result of beam heating and carbon pick up. Most of the foils obtained had either a [112] or[113] orientation. Since a [100] orientation is needed to uniquely characterize the morphology of the ordered phase, a 15° wedge had to be used in the double tilt holder to obtain the [100] orientation.

Dark field images taken using superlattice reflections from ordered regions prove very useful, since coherency strains tend to obscure the particle dimensions and shapes in bright-field micrographs or in dark field of fundamental reflections particularly when the particles are small.

F. Preparation of Specimens for Field Ion Microscopy

Tips for field ion microscopy were prepared by the precision shearing of foils used in tensile testing the electron microscopy. Strips of 0.005 in. width were cut from each of the 0.005 in. thick foils using a specially designed precision shearing device. This gives an approxi-

mately square cross section to the "wires." Three polishing techniques were tried. Two of these mentioned in the literature[25,36] involved electropolishing of the tips. However, the third method involving simple chemical polishing using a 50:50 mixture of HF and HNo_3 proved to be the fastest and best way. The only drawback is that the method does not give reproducible results. It may be noted that the specimen containing 0.76 at.% carbon was most difficult to polish. All the other specimens gave tips with relative ease. Possible reasons for this difficulty in polishing are discussed later.

Imaging was done at 15-20°K in a glass field ion microscope which uses cold Helium gas from liquid helium as the coolant. Helium at $1\text{-}3\times10^{-4}$ torr was used as the imaging gas. Images were easily obtained but the tips flashed very easily. This would be expected from bcc metals containing impurities, as the latter make such fine sections inherently brittle.

Images obtained at 77°K and at 20°K were recorded.

G. Method of Computation of Field Ion Images

Since the field ion images of Ta had either a (110) or (100) texture, it was decided to obtain computed images correspondingly to both orientations. For this purpose the program developed by Ranganathan et al.[31] was suitably modified and used. In this method, a given crystal structure is considered in terms of the Bravais lattice. If the latter has centering then the structure can be generated by repeated application of the method to the primitive lattice with different coordinates for the origin. To obtain a (100) orientation one chooses the coordinate axes [100], [010] and [001]. Two simple cubic lattices need to be considered with origins at 000 and $\frac{1}{2}\,\frac{1}{2}\,\frac{1}{2}$. The crystal is projected onto the [100]

planes and the radii R_A and R_B obtained by the intersection of the spherical shell with the [100] planes are determined (Fig. 3). The coordinates of an atom are recorded only if it falls within any set of these values. Since the stereographic projection is a closer approximation to the field ion image, the orthographic coordinates are first converted to stereographic ones and the Cal Comp Plotter Subroutine is used to plot the simulated image. The computations were programmed in FORTRAN for the Control Data 6600 computer. Similarly, to obtain a (110) orientation, coordinate axes [110] [1$\bar{1}$0] and [001] are chosen. With this set of axes, the bcc lattice becomes a face centered tetragonal lattice with a c/a ratio of 0.703 ($= 1/\sqrt{2}$). It is therefore necessary to consider four primitive tetragonal lattices with origins at 000; $\frac{1}{2}\ \frac{1}{2}\ 0$; $\frac{1}{2}\ 0\ \frac{1}{2}$; and $0\ \frac{1}{2}\ \frac{1}{2}$.

H. Computation of Images from Interstitial Alloys

The ideal ordered composition $Ta_{64}C$ predicted by Villagrana and Thomas[1] was assumed. Then the simulation of matrix atoms was produced for both the [100] and [110] orientations assuming a c/a ratio of 1.08 as predicted by a hard sphere model of $Ta_{64}C$. This involves changing the size of the primitive lattices to incorporate the c/a ratio. This leads to two primitive tetragonal lattices for the [100] orientation and four primitive tetragonal lattices for the [110] orientation. The atom coordinates of the carbon interstitials were then supplied, taking into account the fact that their primitive lattices were four times the size of the primitive Ta lattices. The $[\frac{1}{2}\ 0\ 0]$ octahedral site occupancy was assumed for the carbon interstitials and the tip radius was taken to be 100a where "a" is the lattice parameter. For this tip radius, Moore[29] has predicted a shell thickness P of 0.0736a. Since the shell thickness for the interstitial atoms is still unknown,

various shell thicknesses were tried, and are tabulated below.

Orientation	[100]	[110]
Shell thickness, P	0.0736a (same as that for the matrix atoms)	0.104a
	0.1104a[0.0736x1.5]	0.156a
	0.1472a[0.0736x2.0]	0.208a
	0.1840a[0.0736x2.5]	0.260a

I. X-ray Analysis of Ta Containing 11.5 At.% C

As it was required to determine what phases coexist in Ta containing much greater amounts of carbon, an alloy was prepared containing 11.5 at.% carbon. This sample was analyzed using the Picker x-ray diffractometer with Cu k_α radiation.

This alloy is extremely brittle. All attempts at spark cutting to prepare foils suitable for electron microscopy were completely unsuccessful. The result is just a powder.

III. EXPERIMENTAL RESULTS AND INTERPRETATION

A. Mechanical Properties of Tantalum Carbon Alloys

Upon deformation, tantalum exhibits a semidiscontinuous stress-strain tensile curve. Figures 4, 5 and 6 show a series of tensile stress-strain curves for specimens with varying carbon content, at three temperatures 300, 196 and 77°K. It is immediately evident that the level of interstitial content has a marked influence on the stress-strain curve. The effect of increasing the interstitial content is to shift the curve in the plastic strain range to higher stress levels. The effect of decreasing temperature is similar in that at any one carbon composition, the specimens yield at higher stress levels with decreasing temperature.

It is generally accepted that the plastic deformation of bcc metals is accompanied with the initiation of a Luders band at points of stress concentration within the specimens. The band front usually progresses from the tensile grips toward the center of the gage length. Luders bands have also been observed in the deformation of polycrystalline niobium.[22]

Upper yield points were observed for all the tantalum specimens. The lower yield stress is a more reproducible measure of the strength of the specimen since τ_{LY} is not sensitive to specimen alignment in the tensile machine as τ_{uy} (τ refers to shear stress, which is taken as one-half the measured tensile stress σ). From Figs. 4, 5 and 6 it can be seen that the plastic region of the stress-strain curve is nearly horizontal i.e., no appreciable increase in flow stress with strain to fracture. This is a common feature in bcc metals, particularly at room temperature.[21-23] It can be seen from Figs. 4, 5, and 6 that at any test temperature, the

TABLE III. Summary of Tensile Data

Atomic percent carbon in tantalum	Shear stress in kg/mm^2					Percent elongation		
	τ_{yp}	τ_{uy}	τ_{LY}	τ_{Fl}	τ_{FY}	Elastic	Plastic	Total
A. Test Temperature 300°K								
0	5.28	6.97	6.69	6.94	6.76	0.72	14.98	15.70
0.76	9.51	10.38	9.65	10.04	10.14	1.00	10.70	11.70
1.27	9.87	11.74	11.74	11.09	10.91	0.82	7.28	8.10
1.53	15.67	16.26	15.31	15.50	15.14	0.61	2.36	2.97
2.05	-	-	-	-	5.81	0.70	-	0.70
B. Test Temperature 196°K								
0	11.97	13.44	12.32	12.74	13.10	1.00	11.32	12.32
0.76	13.38	17.68	17.18	16.87	15.84	1.00	8.50	9.50
1.27	17.60	20.25	19.72	19.58	19.00	1.08	5.32	6.60
1.53	24.65	24.80	24.80	-	24.80	1.45	0.33	1.78
2.05	-	-	-	-	10.84	0.75	-	0.75
C. Test Temperature 77°K								
0	24.30	28.20	27.45	27.45	25.00	1.58	2.40	3.98
0.76	31.30	32.55	31.50	31.50	29.60	1.92	1.66	3.58
1.27	35.20	38.20	-	-	35.55	1.84	0.61	2.45
1.53	31.70	37.20	-	-	37.00	2.00	0.65	2.65
2.05	-	-	-	-	18.82	12.00	-	1.20

ductility (plastic region of stress-strain curve) decreases with increasing carbon content. The specimens containing 2.05 at.% carbon show total low of ductility and fail at elastic stresses far below the expected upper yield stress. Figure 7 summarizes the ductile-brittle behavior of tantalum-carbon alloys containing up to 2.05 at.% carbon in a plot of test temperature vs atomic percent carbon in tantalum. Specimens containing ~1.5 at.% carbon and above show total loss of ductility. It would seem from this plot that 1.5 at.% carbon is some critical composition responsible for the onset of brittleness in tantalum carbon alloys, over the temperature range investigated.

A summary of all the data obtained in Figs. 4, 5, and 6 is given in Table III. Figures 8 thru 11 are plots of this data with either varying atomic percent carbon in tantalum or varying test temperature, and the results obtained from these plots are discussed below.

When τ_{LY} is plotted vs. atomic percent carbon in tantalum, straight lines of positive slope result, as shown in Fig. 8. The range of τ_{LY} observed is shown together with the average points yields for the three temperatures:

$$\text{At } 300^\circ\text{K}, \quad \tau_{LY} \left(\frac{kg}{mm^2}\right) = 6.0 + \{5.3 \times (\text{atomic percent carbon})\}$$

$$\text{At } 196^\circ\text{K}, \quad \tau_{LY} \left(\frac{kg}{mm^2}\right) = 12.2 + \{7.0 \times (\text{atomic percent carbon})\}$$

$$\text{At } 77^\circ\text{K}, \quad \tau_{LY} \left(\frac{kg}{mm^2}\right) = 26.4 + \{8.0 \times (\text{atomic percent carbon})\}$$

It can be seen that there is a very slight change in slope of the lines with temperature. Points marked B on the plot show the fracture stresses of those alloys exhibiting brittle failure (i.e. tantalum containing 2.05 at.% carbon). The implications of this plot of τ_{LY} vs at.% carbon will be discussed later.

When stress at lower yield or fracture stress is plotted as a function of temperature, a series of curves are obtained one for each carbon composition as shown in Fig. 9. There is an obvious increase in yield stress with decreasing temperature, and the lines curve upward with decreasing temperature. However when specimens fracture before yielding (i.e. are brittle) there is a practically linear increase of fracture stress with decreasing temperature. It will be observed that tantalum containing 1.53 and 2.05 at.% carbon behave differently from those specimens containing lesser carbon. This fact is clearly displayed in plots of total percent elongation (Fig. 10,11) and percent plastic elongation vs. test temperature. While the plots for tantalum containing less than 1.5 at.% carbon behave similarly and curve downwards, those for 1.53 and 2.05 at.% curve upwards. This shows that the latter alloys behave totally differently, at least mechanically.

In summary, the fact that tantalum carbon alloys show decreasing ductility and increasing yield strength till the critical 1.5 at.% percent carbon composition is amply borne out by all the plots in Figs. 7-11. There is total loss of ductility above 1.5 at.% carbon. An examination of the electron micrographs of these alloys gives reasons why such mechanical behavior might be expected.

B. Electron Microscopy and Interpretation

1. Stages of Transformation

When carbon is introduced into pure tantalum (Fig. 12a) the transformation begins by fine fluctuations in carbon composition (Fig. 12b) along the {110} planes of bcc tantalum. These carbon composition fluctuations take place homogeneously until the diffusion process sets up regions of ideal

wavelength, resulting in the formation of "ordered particles" (Fig. 12c). These small ordered regions grow and align themselves along ⟨110⟩ directions (Fig. 12d). Further growth until impingement is followed by the final stage of the ordering transformation involving the formation of highly ordered regions separated by coherent antiphase domain boundaries (Fig. 12e). Figures 12a, b, c, d and e correspond to micrographs obtained from pure tantalum, Ta-0.76 at.% carbon, Ta-1.27C, Ta-1.53C and Ta-2.05C. The electron diffraction pattern obtained from the critical ordering composition is shown in Fig. 12f, and will be discussed later.

Electron diffraction patterns obtained from each one of the stages in this ordering transformation are shown in Fig. 13. Figure 13a corresponds to the diffraction pattern obtained from Fig. 12a and so on. These diffraction patterns are disccused later when the development of the superlattice diffraction pattern is correlated with carbon composition fluctuations. Figure 12 shows only the bright field micrographs. In the following interpretation bright-field and dark field electron microscopy is used to follow each of the above stages of the transformation.

Seraphim, et al.[4] have noted that the transformation proceeds similarly in the tantalum-nitrogen system. That is, the transformation proceeds first by the formation of a herringbone (maze) structure, which broadens in texture; and finally transforms catastrophically to an entirely new pattern consisting of highly ordered regions separated by coherent domain boundaries.

Van Torne and Thomas[2] have shown in a study of the Nb-O system that the general sequence of the transformation results in the formation of a cross hatched pattern of contrast. Then within the initially transformed area, prisms are nucleated, bounded by [110] Nb planes. These prisms

possess internal striations, until they grow to converge together with the elimination of the internal structure.

2. Initiation of Order

The earliest stages of the low temperature decomposition of supersaturated solid solutions proceeds through a series of intermediate stages prior to the formation of an equilibrium precipitate.[38] In the very early stages, there is a localized rearrangement of solute atoms to produce small regions of new composition, of < 100Å size, coherent with the matrix.

During the early stages, a uniform mottling is observed in all grains with excellent contrast at extinction and bend contours. Dislocations are in good contrast at this stage but not at all during later stages of the transformation. The striations have a rather diffuse basket weave of light and dark contrast, that is, they do not possess a distinct image. They are uniformly distributed and have a high density.

Examples of the bright and dark field images obtained from Ta-0.76 atomic percent carbon are shown in Figs. 14a and 14b. The dark field image of a matrix reflection (Fig. 14b) shows the uniform mottling . In fact, the dark field image resembles small particle formation.

The matrix spots in diffraction patterns are streaked in the ⟨110⟩ directions, normal to the {110} striations in contrast. This streaking is similar to that observed in Cu-2% Be.[39]

It must be noted that there is no development of a superlattice diffraction pattern at this stage. The only indication of a transformation in progress is the streaking of matrix spots in the ⟨110⟩ directions.

Elastic distortions due to tetragonal coherency produceds streaking at reciprocal lattice points. Tyapkin[40] has shown that coherency induces

pure shear on {110} planes in $\langle 1\bar{1}0 \rangle$ directions resulting in the extension of diffraction intensity along the normal to the shear planes. The magnitude of the shear strain depends on the value of the anisotropy factor, A, defined as

$$A = \frac{G_{\langle 100 \rangle}}{G_{\langle 110 \rangle}} = \left(\frac{2C_{44}}{C_{11} - C_{12}}\right)$$

When the cubic crystal $A_{Ta} = 1.58$ is isotropic A=1, while when A > 1, then $G_{\langle 110 \rangle}$ becomes a minimum. Therefore given the condition of tetragonality associated with ordering, there will be relatively low resistance to shear on {110} $(1\bar{1}0)$.

3. Formation of Discrete Nuclei

Tantalum containing 1.27 at.% carbon shows the formation of discrete nuclei which lie along $\langle 110 \rangle$. Figure 15 shows bright and dark field micrographs in the [001] orientation. Dark field micrographs of matrix (Figs. 15.1, 15.2 and 15.3) and superlattice (Figs. 15.1a, 15.2a and 15.3a) reflections show the formation of discrete nuclei along [110]. For g $\langle 110 \rangle$ type dark field images, only one set of nuclei (platelets) are visible (Figure 15.1a, 15.3a) However for g $\langle 200 \rangle$ type reflections both sets of (110) platelets are visible (see black arrows) (Fig. 15.2a) This shows that the nuclei do indeed lie along $\langle 110 \rangle$. Using the matrix reflection for dark field imaging only g.R contrast is visible, while using superlattice reflections the individual particles themselves are visible.

The strain contrast images show interstitial contrast (that is, the dark side of the black-white image in the direction of g). The volume fraction of the ordered regions is relatively high and the contrast gives the distinct impression that they are lined up in a regular array.

4. Impinging Domain Boundaries

Tantalum containing 1.53 at.% carbon corresponds to the fully ordered state consisting of impinging small to medium sized domains. Figure 16 shows bright and dark field micrographs from such an alloy. Figures 16.1 and 16.3 correspond to dark field micrographs from g ⟨110⟩ type matrix reflections while Figs. 16.1a and 16.3a are dark field micrographs from corresponding superlattice reflections. Figures 16.1a and 16.3a show the development of cuboids of ordered regions with internal striations along the ⟨100⟩ (see black arrows), lining up along the [110] directions. It seems from the micrographs that ordered regions cuboid in shape and bounded by {110} planes are stacked up along the ⟨110⟩ directions.

Ardell and Nicholson[41] have shown that spherical γ' particles exist when the lattice misfit with the matrix is less than 0.1%, a good example being the system Fe-15% Ni-15% Cr-3.5%Ti. It is also significant that alignment does not occur in this system. Only when the misfit is greater than 0.1%, as in the systems Ni-Al (misfit ~ 0.5%) does γ' appear as cubes and possibly as a consequence, does alignment occur.

An observation of Fig. 16 shows that there are many particles separated by distances that are very small compared to their linear dimensions. Similar observations have been made in several Ni base alloys.[41] There seems no simple explanation for this although a number of possible reasons can be advanced. Since the particles are not free to wander about in the matrix, certain particles must certainly coarsen selectively by virtue of their position. Therefore, two or more particles favorably located and aligned will grow at the expense of each other.

The strain contrast observed is the net strain from the individual particles themselves. This concept of net strain arises from the fact

that the high volume fraction of the ordered phase with overlapping individual strain fields produces a net strain.

The contrast observed is similar to that observed for order-induced strains in Cu-Be,[42] Cu-Au,[43] Fe-Al[58] and Ni-Mo.

The effect of ordering of interstitials between the [110] Ta habit planes is to produce localized ordering, partially or totally, depending on the interstitial concentration. Such changes distort the reciprocal lattice from the ideal point lattice for a perfect crystal.

5. Large Non-Impinging Domains

Tantalum containing 2.05 at.% carbon shows a complete change in microstructure in that large non-impinging domains are observed (Fig. 17).

A detailed dynamical theory explaining contrast from domain boundaries has been developed by Gevers, et al.[44] Its applicability to domain boundaries in the tantalum carbon system has been considered by Villagrana and Thomas.[1] Domains result from the preferential occupation of one set of interstices rather than another in a given domain.

In a single domain, the carbon fills partly and in an ordered way the octahedral sites of the same kind. There are three different kinds of octahedral interstices, of the ⟨1/2 00⟩ ⟨0 1/2 0⟩ or ⟨00 1/2⟩ variety. The preferential occupation of any one of these types of sites gives rise to an ordered domain.

The theory of domain boundary contrast[44] is based upon the fact that tetragonal regions with c-axes oriented normal to each other are separated by a domain boundary at 45° to each of the c-axes, that is the domain boundary divides the crystal into two wedged segments with the

crystal structure differing slightly in dimension in each segment. The contrast associated with a boundary arises from three sources. (1) differences in extinction distances in each segment for the same reflection; (2) a change in the phase angle at the boundary; (3) a difference in the deviation parameter's on either side of the domain boundary as a result of the different diffracting conditions in the two crystals on either side of the domain boundary. Gevers, et al.[44] have shown that the fringe patterns associated with domain boundaries are different from those of stacking faults or twin boundaries. In bright field the first and last fringes from domain boundaries are assymetrical, while in dark field they are symmetrical with respect to the fringe at the surface of the foil in bright field. Figure 17.3 shows a schematic representation of domain boundary contrast under different imaging conditions. From this schematic representation, the crystals I and II, and the top (T) and bottom (B) fringes are marked in Fig. 17.1b.

Distant spots of a diffraction pattern arising from an area covering two domains are split in two components. The vector joining the two components and which is the component of Δg parallel to the foil surface, is as should be, normal to the intersection of the surface and the domain wall. Diffraction patterns over a single domain never present split spots.

6. Structure of The Ordered Phase

Selected area diffraction patterns from Fig. 16 corresponding to a composition Ta-1.53 at.% carbon show that ordering has occurred, since besides the basic tantalum diffraction pattern there is a superposition of a second, smaller spaced, diffraction pattern corresponding to the ordered phase. This superlattice structure corresponds exactly to that obtained by Villagrana and Thomas,[1] who have empirically assigned the

composition $Ta_{64}C$ and have assigned a superlattice unit cell on the basis of electron diffraction data obtained.

A detailed examination of the selected area diffraction patterns obtained from Ta-1.53 at.% carbon will show how such a structure can be obtained. Figure 18a shows an [001] bcc tantalum diffraction pattern with a superlattice diffraction relpoints are spaced parallel to the $(\bar{1}\bar{1}0)_{bcc}$ and $(110)_{bcc}$ relpoints are a distance of $1/4(\bar{g}_{110})_{bcc}$. This means that in real space there are superlattice planes parallel to $[110]_{bcc}$ at a d-spacing four times that of $(110)_{bcc}$. Similarly, there are first order superlattice planes parallel to $[200]_{bcc}$ each at a d-spacing four times that of $(200)_{bcc}$. From this it can be said that the superlattice unit cell should be four a_o on edge, where a_o is the lattice parameter of bcc tantalum.

The position of the carbon atoms in relation to the superlattice unit cell, defined by tantalum atoms, can be decided upon keeping in mind that according to Beshers[11] calculations carbon should go into the $(\frac{1}{2}\,00)$ type octahedral interstitial sites in bcc tantalum.

On the basis of such a structure, Villagrana and Thomas[1] determined the structure factor equation. This is

$$F_{hkl} = f_{Ta}[T] + f_C[C]$$

where

$$T = \sum_{x=0}^{3}\sum_{y=0}^{3}\sum_{z=0}^{3} e^{2\pi i\left(\frac{hx}{4}+\frac{ky}{4}+\frac{\ell z}{4}\right)} + \sum_{x=1}^{7}\sum_{y=1}^{7}\sum_{z=1}^{7} e^{2\pi i\left(\frac{hx}{8}+\frac{ky}{8}+\frac{\ell z}{8}\right)}$$

and

$$C = e^{2\pi i\left(\frac{u}{8}\right)} + e^{2\pi i\left(\frac{h}{2}+\frac{5k}{8}+\frac{\ell}{2}\right)}$$

Here the f_C terms correspond to a body-centered arrangement of carbon atoms. The selection rules predicted by the above equation are the same as those for the body centered space lattice, that is reflections are present only when $(h + k + \ell)$ is even.

The superlattice unit cell is shown in Fig. 18c. The squares represent the bcc tantalum unit cells while the spheres represent carbon atoms in $0\ \frac{1}{2}\ 0$ octahedral positions. The superlattice unit cell is tetragonal since placing carbon atoms in $0\ \frac{1}{2}\ 0$ octahedral sites causes an expansion in the [010] direction accompanied by a slight contraction in the [100] and [001] directions. This tetragonality is confirmed by the observed slight contraction of one of the $(\bar{g}_{200})_{bcc}$ vectors and a corresponding change in the angle between $(\bar{g}_{110})_{bcc}$ vectors. The tetragonality, and therefore the existence of a $\frac{c}{a}$ ratio, is also obvious from the morphology of the ordered phase and the nature of the domain boundaries observed. Therefore, $Ta_{64}C$ is a body-centered tetragonal, and corresponds to a chemical composition of 1.56 at.% carbon.

Indexing of the superlattice is easy using a similarity matrix wherein $(hk\ell)_s$ corresponds to $4(hk\ell)_{Ta}$ (Fig. 18b). Indexing of superlattice relpoints has to be done carefully since a slight tilting off the reflecting sphere brings the second layer superlattice relpoints into the reflecting sphere thereby confusing the simple exact orientation diffraction pattern.

7. Development of Superlattice Diffraction Patterns

Figure 13 shows the development of the superlattice structure as the transformation proceeds to completion. The fully developed ordered structure is only observed in specimens with the critical 1.5 at.% carbon composition (for example, Fig. 13d). All lower carbon compositions show only a partial development of the superlattice. The first sign of change in the [001] Ta diffraction pattern (Fig. 13a) is the streaking of matrix spots in the ⟨110⟩ directions (Fig. 13b) and the appearance of superlattice spots streaked in the ⟨100⟩ directions (Fig. 13c). The

streaking of matrix spots can be attributed to the net elastic strain set up in the ⟨110⟩ directions. The introduction of interstitial carbon into the ⟨0 1/2 0⟩ octahedral sites would result in the variation of d spacing along the ⟨100⟩ directions. Such a Δd variation along ⟨100⟩ in the early stages of development of the superlattice can result in the streaking of superlattice along ⟨100⟩. The development of a periodic variation in carbon composition giving rise to the observed ordered structure is considered below.

8. Repeat Distances of Planes Containing Only Tantalum or Only Carbon Atoms in the Ordered Phase

In the ordered phase only four of the six possible {110} planes in bcc Ta can be occupied by carbon atoms alone. This arises from the nature of octahedral sites in the bcc lattice. For example, a 1/2 00 octahedral site lies on both the (001) and (010) planes passing through the origin, but not on the (100) plane. That is, only two of the three {100} planes passing through the origin contain the 1/2 00 octahedral site. Similarly, there can only be four of six possible {110} planes which possess only carbon atoms in the structure $Ta_{64}C$.

This can be shown by assuming that the carbon atoms in $Ta_{64}C$ occupy the 1/2 00 octahedral sites, (that is, the c-axis of the bct $Ta_{64}C$ unit cell is the [100] direction), then the planes containing only carbon atoms are the (110), $(1\bar{1}0)$ (both perpendicular to the (001) plane) and (101), $(10\bar{1})$ (both perpendicular to (010)) planes (see Fig. 19). These are the only planes containing carbon atoms along which C atom fluctuations are possible in the ordered structure. Of course, other combinations of the (110) planes will become possible, if the octahedral sites are other than 1/2 00 (that is 0 1/2 0 or 00 1/2). In any case, only four of the six possible {110} planes are occupied by only carbon atoms.

There is one carbon containing (110) plane after every four Ta containing (110) planes in the ordered structure. However, since we are dealing with an interstitial alloy, the spacing between a carbon containing (110) plane and a neighboring Ta containing (110) plane is not the same as between two neighboring Ta containing (110) planes. The spacing in the former case is less than (in fact, equal to 1/2) that in the latter case (see Fig. 19).

$$d_{110_C} = 4d_{110_{Ta}}$$

The spacing between neighboring planes of same or different species:

$$\{110\}_{Ta} \longleftrightarrow \{110\}_{Ta} = d_{110_{Ta}}$$

$$\{110\}_{Ta} \longleftrightarrow \{110\}_{C} = \frac{d_{110_{Ta}}}{2}$$

$$\{110\}_{C} \longleftrightarrow \{110\}_{C} = 4d_{110_{Ta}}$$

It will be observed that on the basis of a periodic fluctuation of carbon in tantalum, the $Ta_{64}C$ structure can only be obtained when there are simultaneous carbon fluctuations with frequency corresponding to $4d_{110_{Ta}}$ on four of the six possible {110} type planes in bcc tantalum. However, in the early stages of ordering, all four sets of fluctuation may not exist, and therefore, the diffraction pattern may not be fully developed. However, every fluctuation with $d_{110_C} = 4d_{110_{Ta}}$ will give rise to a superlattice spot at $1/4\ g_{110_{Ta}}$. This is exactly what is observed during the early stages of the transformation (for example, Fig. 13c). There is a superlattice spot at $1/4\ g_{110_{Ta}}$ around every matrix Ta spot, each set of spots in any one ⟨110⟩ direction being due to a set of fluctuations in that direction.

The intensities of the superlattice spots tend to increase with increasing carbon content. However, the superlattice is not present in

every specimen nor does it appear in every specimen with the appropriate carbon content.

It is observed that at times superlattice diffraction patterns are not obtained from apparently ordered areas. This can be explained if one considers the high degree of order necessary to produce a superlattice diffraction pattern. It is also possible that in certain regions the superlattice pattern is not reinforced due to the different diffracting conditions from domain to domain.

C. Nature of Fractured Surfaces

Figures 20 and 21 show scanning electron fractographs of the specimens. Magnifications were chosen so as to get first an overall picture of the fractured surface, and then a detailed picture of interesting features. Fractographs from specimens tested at two temperatures, 300°K and 77°K, are shown. Some general comments are first made below.

The pure tantalum fractured surface shown in Fig. 20a shows only slip bands, and a knife-like fracture edge.

Tantalum containing 0.76 at.% carbon presents a similar picture (Fig. 20b). There is a slight difference in slip band spacing from that in the pure metal. Ordered particles, if any, present at this stage should be small enough to be below the resolution limit.

Tantalum containing 1.27 at.% carbon presents fractographs that would be expected from the presence of "particles" of a second phase (Fig. 21b) shown circled. The fine "particle" dispersion is evident in Figs. 21b and 21c. The significance of these "particles" is discussed later, in correlation with electron microscopy data.

Tantalum containing 1.53 at.% carbon shows microvoid formation around large "particles" (Fig. 20c and 20d). The same slip bands are

also evident. There should be a 1:1 relationship between the number of particles and the number of microvoids.

Tantalum containing 2.05 at.% carbon shows the presence of fine dimples which is evidence of microvoid coalescence (Fig. 20e and 20f). An important observation is that there is no cleavage of "particles." Also, examination of the grain boundary interfaces of regions undergoing intergranular fracture showed no preferential precipitation of any form of carbide along the boundaries.

All fractures may be divided into two broad categories according to the fracture path: transgranular and intergranular.[37] Each fracture path may be further subdivided according to the mechanism by which the fracture propagated in order to provide a clearer, more detailed definition and illustration.

All fractures found in "engineering" metals fall into one or more of the following general classiciations.

1. <u>Transgranular Fracture Path</u>
   a. by microvoid coalescence
   b. by cleavage
   c. by fatigue
2. <u>Intergranular Fracture Path</u>
   a. by grain boundary separation with microvoid coalescence.
   b. by grain boundary separation without microvoid coalsecence.

A detailed description of each fracture mode is available.[37] Application of these fracture modes to the fractographs in Figs. 20-21 gives results summarized in Table IV.

Figure 21.h shows the nature of intergranular and transgranular fracture in a specimen that has undergone brittle failure. The fracture surfaces are sharp and clean.

Table IV Predominating Fracture Modes in Tantalum Containing 0-2.05 at.% carbon

Atomic Percent Carbon in Tantalum	Fracture Mode
0	Transgranular Fracture - By Cleavage
0.76	Transgranular Fracture - By Cleavage
1.37	Transgranular Fracture - By Microvoid Coalescence
1.53	Transgranular Fracture - By Microvoid Coalescence
2.05	Transgranular Fracture - By Microvoid Coalescence "Quasi-Cleavage"
	Intergranular Fracture - By Grain Boundary Separation Without Microvoid Coalescence

D. Field Ion Microscopy of Tantalum-Carbon Alloys

Since the field evaporation end form of Ta has been discussed by Nakamura and Muller[55] in detail, only the important observations, which will be useful in subsequent discussions, are being made here. Tantalum develops a large number of [200] planes with excellent resolution. These planes are poorly developed in W and Mo. The micrographs show a characteristic intensity distribution - the square [002] region bounded by {011} planes is bright, whereas the triangular [222] region also bounded by [011] planes is dim except for the [222] planes themselves. This intensity difference is found to be more marked with micrographs obtained at 77°K. Also characteristic for tantalum is the relatively low image intensity in the triangular region between the [011] planes. This presents certain difficulties discussed later.

Tantalum containing 0.76 at.% carbon proved to be the most difficult to polish to a tip and also the most difficult to image. The reasons are evident from the images shown in Fig. 22. Characteristic is the occurrence of large bright blobs throughout the bulk of the metal, which probably represents a homogeneous nucleation of ordered particles. This is not a surface phenomenon as these bright blobs were obtained even after field evaporating over a range of 15 kV. Figures 22a and 22b show these clusters imaged at 77°K. They are about the size of 3 Ta atoms, that is, about 10Å in diameter. Tips at 77°K showed the coexistence of clusters and a ring pattern of the matrix (Fig. 22a and 22b). In this case, the clusters tend to line up radially at the (011) poles. Figures 22c, d, e show the same alloy imaged at 20°K. Here the "particles" are more specific in dimensions rather than bright blobs, and are seen to be composed of up to three atoms (see arrow in Fig. 22e). Presence of ordered particles would be a good reason for the poor polishing and imaging characteristics of this alloy.

Tantalum containing 1.53% carbon yields interesting results. It is a critical composition, which has little or no ductility. As mentioned earlier, photographic recording of specimens containing interstitials, which give an unstable image, is enhanced by picturing them while they are field evaporating. When both species are field evaporating, though an overall fuzzy image is obtained, the interstitial atoms pop up and remain at the surface longer than do matrix atoms. This gives rise to a picture showing interstitials as bright spots relative to the fuzzy background of field evaporating matrix atoms. However, since as a result of field evaporation more interstitials are visible than at any one instant, development of ring patterns, if any, of interstitials

should give an indication of ordering. This is exactly what happens in Ta containing 1.53 atomic percent carbon as can be seen around the [011] planes in Fig. 23c. Two sets of rings can be seen around each 110 pole. Comparison of Figs. 23a and 23c shows the advantage of taking pictures during field evaporation. Though by this technique, an accurate count of the number of interstitials at any instant cannot be estimated, the general morphology of interstitial atoms appearing at the tip is obtained. This is more important in the present case for deciding between a random or an ordered distribution of interstitials. It is evident from the pseudo-ring patterns obtained that ordering of interstitials is occurring. Careful examination of the spacing of the rings shows, by measurements, that there is one ring of carbon atoms after every four Ta rings. (see plane markings in Figs. 23a). As discussed earlier, and as shown by the computer simulated patterns discussed later, ordering of carbon interstitials leading finally to the structure $Ta_{64}C$ should result in rings of C atoms at the [100], [110] and [111] poles such that there is one ring of carbon atoms after every four rings of Ta atoms. Figure 23a shows clearly that there are 2 carbon atoms in the fourth ring of atoms around the [111] pole and one carbon atom in the eighth ring. Figure 23c shows the same tip field evaporating continuously with rings of carbon interstitials around the [011] poles (marked by arrows).with the applied field lowered to give a stable image. Compared to Fig. 23c, the bright spots denoting interstitials in Fig. 23a and 23b are few and far between. There is a preferential appearance of bright spots on or close to every fourth ring of Ta atoms around the [110] and [111] poles. This fits in perfectly with the previous observation that the ordered structure $Ta_{64}C$ required the existence of such rings of interstitial atoms. Further proof is

obtained by computer simulation.

Tantalum containing 2.05 at.% carbon is very brittle and though comparatively easy to polish, is difficult to image. The tips flash very easily and stability of the image is rather poor. Tips give distorted images in most cases. Figure 24 is an image of the alloy at 20°K. As can be seen, there are a larger number of bright spots in this case, as would be expected from the high carbon content of this alloy. Close examination of the [110] pole in Fig. 24 shows bright spots preferentially along the lines joining the [110] to the adjoining [111] poles. Computed images of $Ta_{64}C$ (discussed later) show exactly the same result. According to computer simulation, there should be more carbon interstitials in the [110]-[111] region than in any other region. All these results add to the conviction that tantalum containing increasing amounts of carbon in the range 0-2 at.% undergoes an ordering process whereby interstitial carbon occupies octahedral sites preferentially to give an ordered structure.

E. Nature of Computer Simulated Images

The simulated images obtained for the [100] orientation are shown in Fig. 25 while those obtained for the [110] orientation are shown in Fig. 26.

The first striking observation from Fig. 25 is that there is one layer of carbon interstitials after every four layers (rings) of matrix atoms of the ordered structure at each one of the [100], [110] and [111] poles. This proves to be a very helpful guide for detecting the ordering of interstitials owing to the lack of a stable image. Increasing the shell thickness only results in an increased number of interstitials but does not change the nature of the picture. Another observation from images with lower shell thicknesses in Fig. 25 is that

TABLE V. d_{hkl}- spacing, 2θ values and relative intensities of Ta, $Ta_{64}C$ and Ta_2C using Cu k_α radiation.

hkl			d (Å)	2θ °	$I/I_{110_{Ta_6}}$	$I/I_{110_{Ta}}$
Ta	$Ta_{64}C$	Ta_2C				
	011 101		9.825	8.94	100	35.2
	110		9.35	9.46	50	17.6
	020 200		6.612	13.38	29.3	10.3
	112		5.83	15.18	25.1	8.83
	121 211		5.396	16.12	44	15.5
	013 103		4.654	19.06	20.8	7.35
		100		33.33	22	
		002		36.40	24	
		101		38.10	100	
110				38.50		100
		102		50.18	22	
200				55.59		21
		110		59.61	23	
		103		66.66	27	
211				69.58		38
		200		69.94	6	
		112		71.84	28	
		201		73.00	21	

there are large bands of interstitials around the central [100] pole, the spacing between these bands being nearly half the tip radius. This would again result from an ordered structure.

Examination of the field ion micrographs obtained shows that more information can be obtained from interstitials around the [110] and [111] poles than from around the [100] poles. There is a very good contrast from matrix atoms around the [100] poles with the result that interstitial atoms may not be readily detectable.

From an approximate count of the number of interstitials visible in practice, it seems more reasonable to assume a shell thickness equal to or 1.5 times that for matrix atoms, that is, $P = 0.0736a - 0.1104a$, rather than the very large P values used by Perry.[32]

It can be seen from the foregoing discussion that though an exact 1:1 correspondence may not be obtained between simulated and actual images, the former go a long way in helping the analysis of the latter. In fact, it seems essential to compute images to more fully understand experimental images.

F. X-Ray Analysis

The 2θ scan obtained from an area of a specimen containing 11.5 at.% carbon is shown in Fig. 27. The diffraction peaks expected from a two phase region consisting of $Ta_{64}C$ and Ta_2C are shown in Table V. It is observed from the traces that two distinct peaks corresponding to $(101)_{Ta_{64}C}$ and $(110)_{Ta_{64}C}$ are obtained at 2θ values of 8.94° and 9.46°. Most other $Ta_{64}C$ peaks have intensities which are not high enough to show up above the high background intensity in the low 2θ region. It is also observed that the only other diffraction peaks that show up are those due to Ta_2C. The Ta_2C 2θ values observed correspond exactly to those of

Bowman et al.[17] who has assinged a C6 cadmium iodide antitype structure to Ta_2C on the basis of neutron and x-ray diffraction. The relative intensities of $Ta_{64}C$ peaks were determined from a computer program set up using the structure factor equation mentioned earlier.[1]

The diffractometer traces show that 11.5 at.% carbon in tantalum corresponds to a two phase region consisting of $Ta_{64}C$ and Ta_2C only.

IV. DISCUSSION

A. Stages of the Ordering Transformation

Whenever the number of non-metal atoms in an interstitial alloy is less than the number of available interstitial sites there is the possibility of order or disorder. The tendency for interstitial atoms to avoid one another might be expected to increase with their increasing concentration and to be particularly marked at simple atom ratios when a definite fraction of the number of interstitial sites is filled. Since a non-metal atom always expands the interstice that it occupies, minimization of lattice strain is an important factor in promoting order, and so also is the difference in electronegativity between metal and non-metal atoms. The tendency for minimization of lattice strains can lead to fluctuations in carbon composition along those planes in the crystal which show least resistance to shear, that is, the {110} planes.

Electron microscopy data presented earlier indicate that the ordering transformation begins with a fine mottling of the structure where-in no second (ordered) phase is visible; only fine striations due to the strain fields involved in the introduction of a new tetragonal phase into the matrix. This is followed by the formation of discrete nuclei. The transformation takes place as a result of carbon composition fluctuations throughout the specimen. As a result, in the very early stages of ordering, there is a variation in both the wavelength, λ, and the amplitude, A, of these carbon composition fluctuations (Fig. 28b). The total amplitude of the fluctuations along the different {110} planes will be the Fourier summation of the individual (110) fluctuations. At this stage of imperfect order there is no particle formation as such but a tendency towards achieving a wavelength $\lambda_C = d_{110}/4$ (discussed earlier) and perfect order.

As the carbon concentration increases and the number of sets of {110} planes on which fluctuations can occur increase, perfect order is developed wherein ideal $\lambda = 4d_{110}$ and A= constant (Fig. 28c). Such a transformation does not require a nucleation stage. The diffusion process sets up regions of ideal λ. Once ideal λ is obtained, an "ordered particle" with coherent interfaces is formed. The size of the ordered regions depend on the number of wavelengths involved in that set of fluctuations (Fig. 28d). The alignment of the ordered regions along {110} can be due to the strain energy and/or the volume fraction leading to the fully ordered stage. The degree of order may also vary not only from particle to particle but also within each particle. Neither the volume fraction nor degree of order of the ordered phase can be determined to any accuracy except that the volume fraction is high and the degree of order is varying. Once the ordered regions are formed they align themselves along ⟨110⟩ Fig. 28e and grow into the disordered matrix till they impinge along common [100] directions (see Fig. 16). This stage corresponds to that in Fig. 28 f and g. It must be noted that although the domains impinge along [100] directions, they are probably bounded by (110) prism planes (as observed in the Nb-O system by Van Torne and Thomas).[2] The [100] impingement could be because four of the six possible (110) planes in a crystal cut any (001) surface along ⟨100⟩ directions. Further growth involves the formation of large cuboids bounded by {110} planes, aligning themselves along ⟨110⟩ (see Fig. 28g). The final stage involves the growth of crystals with one type of c-axis in preference to any other, to give rise to large non-impinging ordered domains (see Fig. 28h). This mode of formation is borne out by the electron microscopy data. To determine how the nucleation of an interstitially ordered phase would

proceed, interstitial interactions need to be related to the elastic deformation of the bcc lattice.

B. Relation of Interstitial Interactions to Elastic Deformation of the BCC Lattice

The hypothesis that elastic deformations play a dominant role in atomic interaction was first advanced by Zener[46] and was used by him to explain the tendency toward the predominant allocation of interstitial atoms in one of three equivalent sublattices of octahedral interstices. This redistribution is very similar to the process of ordering and results in tetragonality on the part of bcc interstitial solutions. This explains, for example, the tetragonality of iron-carbon martensite. The theory[46] describes the basic features of the phenomenon but does not account for the dependence of the interaction energy on the configurations formed by the impurity atoms, and on the possibility of the symmetry of the filled interstices being lower than the symmetry of the crystal class (for example, octahedral interstices in the bcc lattice having tetragonal symmetry.)

The intrusion of interstitials causes very considerable distortion of the bcc unit cell, due to the small volume of the octahedral vacancies. This suggests that interaction over the field of elastic displacements of solvent atoms makes a considerable contribution to the interaction energy of the interstitial atoms.

Assuming that interstitial atoms do not interact with one another the supersaturated solid solutions should have cubic symmetry. Indeed, since all octahedral sites should be physically equivalent, they should be filled by interstitial atoms to an equal extent. On average, the number of interstitial atoms on all three cubic axis will be the same, and for this reason there will be no tetragonality.

The situation is different where there is interaction between the interstitial atoms. The interaction is responsible for the tendency of the atoms to assume energetically more favorable configurations. Generally speaking, these depart from those configurations which correspond to uniform occupation of octahedral sites. At high temperatures where $kT \gg V$ (where k = Blotzmann constant, T = absolute temperature and V = effective interaction energy), interaction between atoms ceases to be important and there is equal probability of interstitial atoms occupying octahedral sites. This corresponds to the disordered state.

However, as temperature decreases and ordering occurs, the following important questions arise:

(1) What is the shape of the new-phase particles to ensure minimum free energy?

(2) What is the orientation of the new-phase particles relative to the crystallographic axis of the matrix?

(3) What is the orientation relationship between the lattices of the two phases?

(4) What should be the crystallographic structure of the tetragonally ordered solution?

Answers to questions (3) and (4) have already been obtained from electron diffraction data. Questions (1) and (2) are considered presently.

Nabarro[47] was the first to show that depending on the elastic energy of a particle of precipitate, its shape varied. With increasing elastic energy, its shape can vary from a disk (polar diameter < equational diameter) to a sphere (polar diameter = equatorial diameter) to a needle (polar diameter > equatorial diameter).

On the basis of these elastic energy considerations, Khachaturyan[6,48-50] has developed a highly mathematical model considering solid solutions in

which the interstitial atoms occupy octahedral sites in bcc and fcc lattices. The equilibrium distribution of interstitial atoms is described by a non-linear integral equation whose singular points correspond to singularities of the equilibrium characteristics and symmetries of whose solution correspond to the space groups of the phases. This model has been extended in an effort to answer the first two questions above. Calculations have been made[51] of the energy due to elastic deformation of a crystal by formation of a coherent inclusion of a new phase possessing some arbitrary shape. The condition of minimum elastic energy in the crystal allows the optimum shape and the orientation of the inclusion to be established and also allows the orientation relationship between the two phases lattices to be determined. Khachaturyan's calculations and its applicability to the tantalum-carbon system is considered in Appendix II. In general, the calculations show that depending on the elastic properties and transformation crystal geometry the planes for nucleation may be either of the {h00} or the {hh0} type.

It has been shown in Appendix II that the {110} plane in the preferred one in tantalum for the nucleation of a tetragonal phase.

From Appendices I and II it can be seen that in the tantalum-carbon system, the octahedral sites are preferred for carbon interstitial occupancy (Appendix I) and that the tetragonal ordered phase prefers the (110) plane for nucleation (Appendix II).

Interstitial ordering can also be considered in terms of the Cahn model[52] for spinodal decomposition which predicts the formation of modulated structures with periodic variations in composition, as a function of composition, temperature and time.

According to Cahn,[52] in an isotropic binary solid solution free from imperfections, the total Helmholtz free energy

$$F = \int_V \left[f^1(c) + \frac{\eta^2 E}{1-\nu} (c-c_o)^2 + \eta (\nabla c)^2 \right] dV$$

where $f^1(c)$ = Helmholtz free energy of a unit volume of homogeneous material of composition c. $2c(\nabla c)^2$ = first term of an expansion representing the increase in free energy due to introduction of a gradient of composition. η = linear expansion per unit composition change. E = Young's Modulus for the average composition.

This equation also takes into account the elastic energy of an arbitrary composition fluctuation. By Fourier analyzing the composition, finding the elastic energy of each Fourier component and noting that the components do not interact, one obtains the total elastic energy of an infinite isotropic solid with an arbitrary composition fluctuation. In this equation, η, the linear expansion per unit composition change term, is the main controlling factor determining the elastic energy, as large lattice strains are involved in interstitial ordering. Khachaturyan's theory[51] considers this term in detail, and its effect on the total elastic energy of a system.

It must be remembered that the procedure described above can only give accurate results when the carbon atoms are in thermodynamic equilibrium. Thus, if there are elastic distortions of the lattice when carbon atoms are aided to it, this leads to the interaction energy. In principle, the magnitude of this energy may be sufficient for the ordered state to be achieved. But it is not impossible that another kind of interaction also plays an important part in the process of ordering the interstitial atoms.

C. Correlation of Mechanical Properties and Microstructure

It has been recognized for a long time that the yield phenomenon in bcc metals is closely connected with the presence of impurity atoms in interstitial positions. Cottrell and his co-workers were the first to

point out that the existence of a yield point might be related to the locking of dislocations by solute atoms. The yield phenomenon was attributed to the tearing of dislocations from impurity atmospheres by the applied stress. This locking should be especially pronounced if the solute atoms causes large lattice distortions which is the case for interstitial atoms. Although the locking of dislocations by an impurity atmosphere certainly plays an important role in yield phenomenon the total process of yielding is much more complex. Nabarro,[53] and later Schoeck and Seeger,[10] have shown that in the stress field of a dislocation an ordering of interstitials takes place. Nabarro has pointed out that due to the tetragonal distortion around an interstitial carbon (or nitrogen) atom in bcc metals there will be an interaction with the shear stresses around a screw dislocations. Schoeck and Seeger[10] have shown how such an ordering occurs, and have related this yielding to the Snoek effect which predicts the well established internal friction peak.

Investigations of the effect grain size on the lower yield stress of niobium[54] has shown that there is practically no dependence whatsoever of the yield stress on the grain size. However, in the present this investigation all the specimens were of one grain size to eliminate any possible variation in the yield stress. From Eq. (1) (that is $\tau_y = \tau_f + k^* d^{-1/2}$) it can be seen that since τ_y is nearly independent of $d^{-1/2}$, $K^* \approx 0$ or is very small and therefore $\tau_f \approx \tau_y$. Therefore, from Eq. (1) it follows that in tantalum containing interstitials (whose stress strain diagrams are very similar to those of Nb) the atmosphere locking of dislocations in rather slight. This result may seem suprising since the stress-strain curves show well-marked upper and lower yield points. It must be remembered, however, that the size of the yield drop is an unreli-

able quantitative measure of the amount of dislocation locking because the experimental value of the upper yield stress depends sensitively on specimen preparation and on tensile machine characteristics. One way in which the form of the tantalum tensile curves do indicate a small K^* value is from the amount of the lower yield elongation. If for the tests at 300°K and 196°K the portion of the curve (in Figs. 4 and 5) immediately following the yield elongation is extrapolated to zero strain, the stress value obtained is a rough measure of σ_f. Then from Eq. (1) the difference in stress $\Delta\sigma$ between the lower yield stress and the extrapolated value is equal to $K^* d^{-1/2}$. With smaller yield elongations and low rates of work hardening immediately afterwards, as observed in the present tests, the values of $\Delta\sigma$ and consequently of K^* are very small.

The yield strength of tantalum can be attributed chiefly to the friction stress σ_f resisting the movement of dislocation, and the dependence of yield strength on temperature primarily from variations of σ_f. Frictional resistance to dislocation movement could be caused by (a) randomly distributed impurity atoms (b) ordered distribution of interstitial atoms (c) other dislocations in the lattice (d) the Peierls-Nabarro force. It is proposed that in the case of tantalum containing carbon in interstital sites, the ordered distribution of these interstitials probably makes the most significant contribution.

The linear dependence of the shear stress at lower yield on the atomic percent carbon present (Fig. 8), can be interpreted in terms of composition fluctuations. Since according to the fluctuation concept the exact degree of order is not known, it is reasonable to assume that it increases carbon composition, as the tendency towards occupation of the "right" site would increase with increasing carbon. The ordering process can be interpreted in terms of "particles" (that is, size, volume fraction and

degree of order) or statistically. The linear increase in yield stress with carbon content can be interpreted in terms of increasing degree of order, that is, higher the degree of order higher the yield stress. The degree of order varies from 0 to 1 as the carbon composition varies from 0 to 1.5 at.% carbon.

Since the yield strength varies linearly with increasing carbon concentration from 0-1.5 at.% carbon, it is reasonable to assume that the yield strength is also volume fraction dependent. The sizes of individual ordered regions can only be measured from electron micrographs of the 1.27 and 1.53 at.% carbon alloys and the values are shown plotted in Fig. 29. Since only two points are available it is possible to draw either a curve (B) or a straight line (A) through the points. A gradual decrease in ordered region size (A) is more reasonable since there is no abrupt change in yield strength with composition. The appearance of ordered regions at about 0.75 at.% carbon would require an abrupt change in the slope of the yield stress vs. composition (Fig. 8) curve. Since no such change in observed, a gradual increase in "particle" size with composition is a valid assumption. The upper curve is obtained by measurements off scanning electron fractographs.

It has been suggested that in the vanadium-hydrogen system the ductile-to-brittle transition temperature could be coincident with the temperature for the formation of hydride from solid solution.[23] This is not the case in the tantalum carbon system. The appearance of the ordered phase is in itself not the cause of brittleness nor is the impingement. The real reason for brittleness is the formation of non-impinging {110} domains boundaries.

The minimum cleavage shear stress will occur when the elastic shear strain energy is at the maximum in some region and direction in the crystal. One would expect the maximum shear strain energy to be attained in regions and directions which possess the largest internal strain energy. The maximum shear strain energy will be attained in regions which lie parallel to the cleavage plane. In tantalum, the cleavage plane is {110} as opposed to {100} in tungsten. Therefore the maximum shear strain energy, on introduction of a critical concentration of interstitial should be attained on {110} planes.

When the alloys are brittle and cleave, the values of the elastic compliances are such that the restriction imposed on the compliances by the positive strain energy of a crystal are only marginally fulfilled. These restrictions are:

(a) $S_{44} > 0$

(b) $S_{11} > |S_{12}|$

(c) $S_{11} + 2S_{12} > 0$

Substitution of the values of pure tantalum, $S_{11} = 6.78 \times 10^{-13}$ cm^2/dyne, $S_{12} = -2.47 \times 10^{-13}$ cm^2/dyne and $S_{44} = 11.98 \times 10^{-13}$ cm^2/dyne, shows that an increase in $|S_{12}|$ of 0.92 is sufficient to violate the restriction $S_{11} + 2S_{12} > 0$. Therefore, it is probable that under the influence of interstitial introduction, a point is reached in carbon composition where the restrictions on the compliances, which are the same as on the stiffnesses, are not satisfied. The crystal then becomes energetically unstable and it fails along a crystallographic set of planes which releases a maximum amount of strain energy. Due to the lack of detailed knowledge of elastic coefficients of these alloy crystals, the propose mechanism cannot be tested in a quantatitive manner.

It may be noted that brittle behavior is expected in alloys formed between elements (in this case Ta and C) whose elastic compliances are very different.

The brittle nature of interstitial solid solutions containing about 1.5 at.% carbon is not due to atmospheres of interstitials around dislocations. Instead, the ordered structure presents a large barrier to dislocation motion. It seems impossible even to visualize a dislocation with a Burgers vector suitable for simple slip through a structure with such a large unit cell. Thus, to drive a dislocation through the ordered region, the ordering energy must be supplied for each carbon atom dislocated from the superlattice relation. Catastrophic failure can be expected before appropriate stress elvels are exceeded.

The typical features of the temperature dependence of the yield stress τ_{LY} are shown in Fig. 9. The yield stress below 300°K is strongly temperature dependent. The lower yield stress of Ta-20.5 at.% C was impossible to obtain because fracture always occurred at or before the upper yield stress was reached. The plot therefore shows fracture stress variation with temperature rather than lower yield stress for this alloy. It can be observed from this plot that though the rate of increase of lower yield stress increases very rapidly with decreasing temperature, the rate of increase of fracture stress with decreasing temperature is nearly constant. This shows the increasing temperature dependence of lower yield stress with decreasing temperature for the ductile alloys as compared to the constant temperature dependence for the brittle alloys.

Temperature dependence can be interpreted in terms of slower diffusion of carbon atoms required to form the ordered phase. However at the critical ordering composition, that is, at the correct C:Ta atom ratio

the wavelength of the carbon composition fluctuations is ideal (that is, $\lambda = 4d_{110_{Ta}}$) and ordering occurs at all temperatures in the range of the present investigation.

It has been shown that in vanadium containing 10-800 ppm hydrogen, there is a total loss in ductility between 233°K and 173°K followed by a recovery of half the original ductility (that it has at 300°K) at 77°K.[21] Therefore this ductile-to-brittle transition is not maintained with decreasing temperature. In the region where ductility is totally absent fracture occurred exclusively by cleavage.

Sherman et al[23] have used the concept of stress-induced ordering in the vanadium-hydrogen system to explain the sudden loss in ductility at around 230°K. An examination of Fig. 10 shows that a similar situation arises in the tantalum-carbon system also. Tantalum containing up to 1.27 at.% carbon shows decreasing elongation with decreasing temperature. However, tantalum containing 1.53 and 2.05 at.% carbon shows an unexpected increase in elongation below 200°K. This phenomenon could very well be due to stress induced ordering.

That is, the lattice extension associated with applied stress would effectively reduce the lattice distortion caused by the ordered carbon atoms, thus making the ordered state a lower energy state with respect to that in the unstressed condition. The apparent return to ductility as temperature is decreased below the brittle range would be explained by the slower diffusion of carbon atoms to form the stress induced ordered phase.

D. Field Ion Microscopy of Tantalum-Carbon Alloys

Field ion microscopy of tantalum specimens containing controlled amounts of carbon yield intersting results. Tantalum specimens containing

0.76 at.% carbon tend to show a kind of "particle" formation involving up to three atoms. The underlying matrix crystal structure is nearly absent. A very similar picture was obtained by Nakamura and Muller[25] on the introduction of 2×10^{-3} torr O_2 to the tip and annealing for 5 min at 900°K. Contamination by oxygen resulting in a similar picture in the present case can be ruled out because none of the other alloys showed such an effect even though polished and observed under similar conditions. The exact nature of these bright "particles" is not known, but they are believed to be nuclei of the ordered phase. These particles are relatively stable. There is a strong tendency for these particles to field evaporate as a group, sometimes leaving behind large dark holes. These clusters have to have a certain minimum size. The unit cell of the superlattice structure $Ta_{64}C$ is a = 13.21Å; c= 14.26Å (from a hard sphere model which yields a c/a ratio of 1.08). The three closest carbon atoms in such a structure would be 12.35Å - 13.21Å. Therefore the minimum three interstitial group size is ~12.5Å. It is therefore not surprising that dark field images of weak intensity maxima in the (110) directions around matrix spots in the electron diffraction patterns fail to resolve such particles in the 0.76 at.% carbon alloy.

The most significant result from tantalum containing 1.53 at.% carbon is the observance of rings of carbon atoms on field evaporation. The spacing of the carbon rings, one after every four tantalum rings is of special significance since this is exactly what would be expected from an ordered structure of carbon interstitials wherein the interstitials segregate preferentially along (110) planes. There is one plane of carbon atoms after every four (110) tantalum planes. Computer simulation shows that such a structure would give rise to similar rings with similar spacings

around the [100] and [111] poles, as observed in the micrographs.

It is unfortunate, however, that an accurate count cannot be obtained because of the low concentration of interstitials, and the instability of the interstitial image. There remains considerable ambiguity as to which spot is to be considered as a pair or cluster, and even whether some of the medium or small size bright spots might not be tantalum atoms on exposed, low coordination sites.[25]

As in the present case, Nakamura and Muller[25] found that direct observation of the crystal structure of tantalum oxide was impossible. Only a general morphological picture can be obtained. It is therefore not possible to get a 1:1 correspondence between the computer simulated and experimentally observed micrographs. The former, however, is necessary to get an idea of what to expect in the latter.

A wide variety of associated interstitial configurations have been observed but the exact geometry of the occupied sites is not obtainable at present. There are still several ambiguities that remain unexplained. For example, it is difficult enough to explain why single interstitial dots are so clearly seen in the (011)-(121)-(111) triangle, while almost none are visible in the (011)-(031) region.[25]

Again, the size of the interstitial spot may give an indication of whether the interstitial lies just below or at the surface. Interstitials lying just below the surface would raise matrix atoms lying in the layer above them, and this raised group (bump) of atoms would give a large, possible slightly elongated spot. However, an interstitial lying at the surface would give a sharp bright spot.

The outcome of the field ion investigation has been that the possibility of detecting interstitial order at ~20°K has been shown. The ordering of carbon in tantalum giving rise to rings around the [110] poles is

definite proof of the existence of order. The fact that a ring of carbon atoms appears after every four rings of tantalum atoms around the [110] poles is further proof for the existence of carbon composition fluctuations such that $\lambda_{ideal} = 4d_{110_{Ta}}$.

E. The Superstructure

Because the $Ta_{64}C$ superlattice transformation is present in bulk material, the tantalum carbon phase diagram should be corrected to include this phase. In all the specimens examined, the $Ta_{64}C$ structure was the only second phase material detected.

Though Villagrana and Thomas[1] suggested the $Ta_{64}C$ superstructure as a trial structure, it is now evident that this does actually exist. Beshers'[11] and Khachaturyans[51] calculations, when applied to the tantalum-carbon system. (Appendice I and II) show that carbon should go into octahedral sites causing a tetragonal deformation. If the carbon atoms did go into tetrahedral sites instead, then the superlattice would most probably have been orthorhombic (as in the case of TaO_y), and there would be no tetragonality.

Steeb and Renner,[14] and recently Geiss and Lawless,[15] have attributed a diffraction pattern in the Ta-O system similar to that obtained for $Ta_{64}C$, to a structure $Ta_{32}O_9$ with $a_0 = 4a_{Ta} = 13.4$Å. In the patterns shown in both cases, no comment has been made on several extra spots which cannot be identified with the $Ta_{32}O_9$ structure. A detailed chemical analysis would no doubt show that the structures obtained would correspond to $Ta_{64}O$ (or $Ta_{64}C$) rather than $Ta_{32}O_9$ since the former structure explains the existence of every spot in the diffraction pattern.

Tantalum containing oxygen has been shown to form orthorhombic oxide plates from the bcc parent phase.[16] The lattice parameters of the orthochombic TaO_y phase are a = 3.271Å, b = 3.201Å and d = 3.610Å, while a_{Ta} =

3.306Å. This orthorhombic structure can only be described in terms of tetrahedral site occupation by the oxygen atoms rather than octahedral site occupation in the case of carbon atoms. Besher's[11] calculations have shown that oxygen in tantalum should indeed go into terahedral sites. The important consequence in the present investigation is that all possibility of any oxygen contamination giving rise to the observed diffraction patterns and microstructures can be ruled out since no orthorhombic phase, as expected from oxygen in tantalum, has ever been observed.

From electron microscopic observations it is concluded that in the alloys ranging from 0-1.5 at.% carbon, two phases, one disordered (α-Ta) and one ordered ($Ta_{64}C$) are present. However, the exact $Ta_{64}C$ composition, electron diffraction pattern (1.56 at.% carbon) is observed only in the 1.53 at.% carbon specimen. There seems to be a variation in the degree of order below 1.5% though fluctuations of carbon atoms giving rise to a frequency of $4d_{110_{Ta}}$ seem to exist from the start of superlattice development (that is, as soon as the second phase becomes visible). On the basis, it is proposed that the tantalum-carbon phase diagram be altered as shown in Fig. 30. The existing diagram[62] is shown in heavy lines while proposed changes are shown as dotted lines.

F. Correlation with Short Range Order

Finely dispersed contrast effects, interpreted in terms of a profusion of weakly localized strain fields, have been observed in Cu-Al,[56] Cu-Zn,[57] Fe-Al[58] and Ni_4Mo.[59] The contrast effects, in general, cannot be resolved individually. However, in Fe-Al alloys, the strain centers were observed to be aligned in rows predominantly in ⟨110⟩ but also in ⟨100⟩ direction depending on the foil normal and the operating reflection. The average distance between these rows was found to be 100-200Å. Electron

diffraction patterns of these alloys show intense directional streaking of all fundamental reflections. In addition, the diffraction patterns contain extra reflections whose intensity increases with increasing solute content and degree of local order (for example, in Fe-Al[58] and Cu-Al[56] alloys).

These results are very similar to those in tantalum-carbon in that the streaking of all fundamental reflections in the latter case shows the existence of anisotropic lattice strains. These are accompanied by the increasing intensity of superlattice spots with increasing carbon content.

It has been observed in short range ordering systems that although the crystal structures of the ordered regions are identical or closely related to the stable superlattice structures occurring at higher solute contents or lower temperatures, the essential difference between the structural features of the small ordered regions in the states of short range order and the neighboring superlattice phases is given by a difference in lattice periodicity in the Cu-Al and Ni-Mo systems. In the tantalum carbon system there does not seem to be any change in lattice periodicity with onset of long range order. However, the number of carbon atoms contributing to each lattice period may vary depending on composition. That is, the structure may not correspond exactly to the stoichiometric composition $Ta_{64}C$ except at the ordering composition. It would be reasonable to assume in this case that the high degree of elastic interaction would set the lattice period ($d_{110_c} = 4d_{110_{Ta}}$) very early in the transformation.

G. Nature of the Interstitial Ordering Transformation

It appears, from the experimental data presented, that the ordering transformation in tantalum carbon is one of small localized composition fluctuations. The presence of such fluctuations is amply borne out by

the experimental data presented. The possibility of predicting the observed ordered structure on the basis of simultaneous carbon composition fluctuations on four sets of {110} planes and the observance of rings of carbon atoms after every four rings of carbon atoms around the ⟨110⟩ poles in field ion micrographs support such an explanation.

The free energy change of a system accompanying the formation of a second phase may be expressed by the following equation:

$$\Delta F = -\Delta F_v + \Delta F_s + \Delta F_m$$

where ΔF_v = free energy associated with the formation of the volume of the second phase, ΔF_s = energy of the surface created between the two phases and ΔF_m = strain energy arising from the formation of the particle.

It has been mentioned earlier that the high degree of elastic deformation of the lattice of interstitial solid solutions is a reason for the ordering of interstitials at relatively low concentrations of the latter. This elastic energy contributes mainly to the determination of which the fluctuations in carbon composition occur on the sets of planes during the early stages of transformation. That is, the contribution is to the ΔF_v term, which is large during the early stages of the ordering transformation. However, the degree of order is low during the early stages of the transformation (as shown by the absence of all superlattice reflections). The contribution of the ΔF_s term will therefore be small at this stage. When the degree of order reaches unity during the later stages then ΔF_s, which depends on the degree of order, becomes an important term contributing to ΔF.

Therefore, during the early stages of the transformation, ΔF is small since the ΔF_v term makes the greater contribution. This means that there is a small barrier, if any, to the start of the transformation,

as compared to no barrier whatsoever for spinodal decomposition. The low degree of order during the earlier stages and a gradual increase to perfect order later would also explain the linear increase in the yield strength with composition. Such a homogeneous process would result from fine fluctuations in carbon over the entire matrix. Large localized strain energy contributions come from the very introduction of carbon atoms into interstices.

V. SUMMARY AND CONCLUSIONS

1. Carbon in tantalum undergoes interstitial ordering as a result of preferential occupation of one type of interstitial site by the solute atoms. Octahedral occupancy predicted by Beshers[11] for carbon in tantalum is found to be true on the basis of the tetragonality of the ordered phase and from electron diffraction data.

2. Investigation of the mechanical properties of tantalum containing varying amounts of carbon (whose accurate analysis has been done using He^3 activation analysis) shows that carbon causes a linear increase in yield strength and a decrease in ductility till the critical 1.5 at.% carbon composition. At this carbon content, there is a sudden catastrophic loss in ductility. The yield strength increases with carbon content and with decreasing temperature, and the stress-strain curves exhibit upper and lower yield points.

3. Scanning electron fractography shows more transgranular than intergranular fracture by cleavage and by microvoid coalescence. Tantalum containing 1.27 at.% carbon and above shows the presence of a second phase in the fracture surface. Failures by intergranular separation show no preferential carbide formation along grain boundaries.

4. Electron microscopy shows that the ordering transformation begins by fine fluctuations in carbon composition along the {110} planes of bcc tantalum. These carbon composition fluctuations take place homogeneously until the diffusion process sets up regions of ideal wavelength, $\lambda = 4d_{110_{Ta}}$, resulting in the formation of "ordering particles."

These small domains grow until they impinge. The final stage of the ordering transformation, corresponding to total loss of ductility, occurs

with the formation of highly ordered regions eparated by coherent domain boundaries. Using dark field techniques, it has been shown that the ordered phase formed initially from a disordered matrix aligns itself and grows along {110} until impingement. The fully developed ordered electron diffraction pattern is obtained only at this stage. Large non-impinging domains observed at the final stage of the transformation show contrast expected from domain boundaries.

Analysis of electron diffraction patterns of the ordered phase show that at the critical composition of 1.56 at.% carbon, the structure of the ordered phase corresponds to body centered tetragonal $Ta_{64}C$, Such a structure can be obtained by allowing carbon composition fluctuations along $\{110\}_{Ta}$ planes such that $d_{(110)_c} = 4d_{\{110\}_{Ta}}$. The $Ta_{64}C$ structure is obtained only when such fluctuations occur simultaneously on four sets of {110} planes. At all other stages, only partial order exists, with respect to the ideal composition $Ta_{64}C$.

5. Field ion microscopy shows that the transformation starts with the formation of "particles" in the lowest carbon specimens to a fully ordered end form wherein ordering can be detected even at 20°K by the formation of rings of carbon atoms around the ⟨110⟩ poles. The spacing between these rings is four times the spacing between tantalum atom rings and carbon atoms preferentially appear after every four tantalum layers.

Computer simulation of field ion images expected shows that the above observations are consistent with those expected from an alloy undergoing interstitial ordering.

6. X-ray analysis of a specimen containing 11.5 at.% carbon shows diffraction peaks in diffractometer traces which correspond to those obtainable from a two-phase region consisting of $Ta_{64}C$ and Ta_2C.

7. On the basis of electron microscopic data the mode of formation of large domains starting with carbon composition fluctuations along the {110} planes in bcc tantalum is discussed. When the fluctuations reach an ideal wavelength $\lambda = 4d_{110}$, an "ordered" particle is obtained. These ordered regions line up along ⟨110⟩ as a result of the strain energy contribution and grow to impinge along common ⟨100⟩ directions to finally give large ⟨110⟩ domains.

8. On the basis of elasticity theory, it has been shown that in the initial stages of the ordering transformation, {110} nuclei are indeed possible.

9. The nature of the stress-strain curves show that solute atom locking of dislocations is slight. Therefore, yield strength can be attributed mainly to the friction stress, σ_f. The linear dependence of yield stress on carbon composition is an indication that yield stress is dependent on the degree of order and the volume fraction. This is consistent with the observation that there is a gradual increase in the size of the ordered regions. The appearance of the ordered phase is, in itself, not the cause of brittleness, but its morphology (large parallel domains) at a certain critical composition. In tantalum, the observed cleavage plane is {110}. Now the minimum cleavage stress will occur when the elastic shear strain energy is at a maximum in some region and direction in the crystal. This maximum shear strain energy will be attained on those planes which possess the largest internal energy and these planes will be parallel to the cleavage plane. The maximum shear strain energy should be attained on the {110} planes on the introduction of a critical concentration of carbon interstitials leading to {110} failure.

In brittle alloys, there are certain restrictions placed on the relationships between the elastic compliances. It is probable that under the influence of interstitial introduction, a point is reached in carbon composition where the restrictions on the compliances are no longer satisfied. Then the crystal becomes energetically unstable and fails along a crystallographic sets of planes (in this case {110}) which release a maximum amount of strain energy.

The slight recovery of ductility below 200°K in the higher carbon alloys may be due to some form of stress induced ordering, whereby untransformed regions order completely under the influence of stress at around 200°K whereas show diffusion at lower temperatures prevents complete ordering and therefore enhances ductility.

10. The different stages of interstitial ordering, as obtained from field ion microscopy is very similar to earlier observations on the Ta-O system which involved in situ introduction of oxygen and annealing.

11. Since the $Ta_{64}C$ superlattice transformation is present in bulk material, a correction to the existing tantalum-carbon phase diagram is proposed.

12. A fluctuation model is used to explain the observed microstructure and mechanical properties during interstitial ordering in tantalum-carbon alloys.

ACKNOWLEDGEMENTS

The author is deeply grateful to Professor Gareth Thomas for his guidance, encouragement, unfailing patience and support during this research. He is indebted to his collegue P. R. Okamoto for the many stimulating and helpful discussions. Thanks are also due to the Nuclear Chemistry Division for the help in activation analysis, and to the IMRD Technical Photography staff for their excellent support.

This research was carried out under the auspices of the United States Atomic Energy Commission through the Inorganic Materials Research Division of Lawrence Radiation Laboratory, University of California, Berkeley, California.

APPENDIX I

Besher's[11] findings from a geometrical description of interstitial sites in the bcc lattice are summarized below.

(1) Octahedral Site Size:

The radius of the largest sphere which will fit into the octahedral site without distortion,

$$r_0 = \left(\frac{a}{2}\right) \left(1 - \frac{\sqrt{3}}{2}\right) = 0.067a$$

Since $a_{Ta} = 3.3058\text{Å}$, $0.067 \times 3.3058 = 0.2215\text{Å}$

(2) Tetrahedral Site Size:

The tetrahedral site will accommodate, without distortion, a sphere of radius $r_T = 0.126a$.

Since $a_{Ta} = 3.3058\text{Å}$, $r_T = 0.126 \times 3.3058 = 0.4170\text{Å}$ which is nearly twice the size which will go into the octahedral sites.

In comparison, $r_{carbon} = 0.77\text{Å}$.

It should be remembered that though the tetrahedral site is nearly twice as large as the octahedral site, the introduction of an interstitial into the octahedral site involves the outward displacement of only two first lattice neighbors along ⟨100⟩ directions, while the introduction of an interstitial into the tetrahderal site involves the equal displacement of four first lattice neighbors in ⟨210⟩ directions.

(3) Strain Energies of Interstitial Sites:

Beshers supposes that when a lattice atom moves outward the contribution which it makes to the strain energy is proportional to the square of the displacement and to Young's modulus in the direction of motion. The expressions derived using the above rule are shown in Table I reproduced from Beshers.[11] The results of numerical evaluation of these

expressions for Ta are given in Table II. In Table II, each column contains the values of the several energies for a selected hypothetical system. (Solvent plus solute of specific radius), these values being referred to the strain energy about an octahedral site in that system. By comparing the site energies and activation energies for a given system (in one column) one decides upon the preferred site and the diffusion path with the lowest controlling barrier. Between systems (column) one compares only these preferences.

Certain conclusions may be drawn from Table II concerning both occupation and diffusion. For smaller radii (0.7Å) the tetrahedral sites are more stable, while for C (radius 0.77Å) in Ta, the octahedral sites are equally stable, as can be seen by comparing W_T/W_o values.

Comparing the values of activation energies in Table II, an octahedral - tetrahedral jump or a tetrahedral - octahedral jump is equally possible for larger interstitial diameters, while for smaller diameters of octahedral - tetrahedral - octahedral path is preferred. Similarly it can be seen that tetrahedral - tetrahedral jumps seem unlikely because of the high Q_{TT}/W_o value, while the direct octahedral - octahedral jump never occurs.

TABLE I. Expressions Used for Calculating Interstitial Site and Activation Energies

Site Energies:

Octahedral	$W_o = 2(r - r_o)^2 E_{100}$
Tetrahedral	$W_T = 4(r - r_T)^2 E_{210}$

Activation Energies:

O - O	$Q_{oo} = 2(r - r_o)^2 E_{100} = W_o$
O - T	$Q_{oT} = 2(r - r_T)^2 E_{210} = 1/2\ W_T$
T - O	$Q_{To} = 2(r - r_o)^2 E_{100} - 2(r - r_T)^2 E_{210}$
	$= W_o - 1/2\ W_T$
T - T	$Q_{TT} = 3\ E_{210} \left\{ \left[(r - r_T) + (r - r_{Sp}) \right]^2 - (r - r_T)^2 \right\} + (r - r_T)^2 E_{210}$
	$= 3\ E_{210} \left[(r - r_T) + (r - r_{Sp}) \right]^2 - 1/2\ W_T$

TABLE II. Interstitial site and activation energies relative to the octahedral site energy in Tantalum for selected values of the radius of the interstitial atom.

Radius (Å)	Interstial in Tantalum 0.70	0.80
W_T/W_o	0.78	0.96
Q_{oo}/W_o	1.00	1.00
Q_{ot}/W_o	0.39	0.48
Q_{To}/W_o	0.61	0.52
Q_{TT}/W_o	0.75	0.72

$E_{100Ta} = 1.46 \times 10^{12}$ dynes/cm^2

$E_{210}/E_{100Ta} = 1.09$

$r_H = 0.3$Å

$r_o = 0.66$Å

$r_N = 0.70$Å

$r_c = 0.77$Å

APPENDIX II

According to Khachaturyan,[51] the elastic energy of unit columns of the new phase particle-matrix system has the form

$$f(r) = \sigma_{ij}(r)\ \epsilon_{ij} + 1/2\ \lambda_{ijlm}\ \epsilon_{ij}\ \epsilon_{lm} \qquad (1)$$

where λ_{ijlm} = elasticity modulus tensor

ϵ_{ij} = deformation tensor

$\theta(r)$ = form function.

Inside the inclusion, $\theta(r) = 1$

Outside the inclusion, $\theta(r) = 0$

σ_{ij} = tensor characterising the crystal geometry of the transformation.

From this is obtained an expression for the elastic energy of the system in the unstressed state,

$$E_1 - E(\sigma_{ij} \equiv 0) = 1/2\ \lambda_{ijlm}\ \epsilon^{o}_{ij}\ \epsilon^{o}_{lm}\ V - \int \frac{d^3k}{(2\pi)^3}\ A\ (\frac{\bar{k}}{k})\ |\ \theta\ (k)|^2 \qquad (2)$$

where the state $\epsilon_{ij} \equiv 0$ is stressed, and its energy is not at a minimum. The minimum elastic energy is possessed by the state with $\sigma_{ij} \equiv 0$ when both phases are in the free state. When $\sigma_{ij} \equiv 0$, $\epsilon_{ij} = \epsilon_{ij}$ inside the inclusion and $\epsilon_{ij} = 0$ outside it. Using this property and the condition that when $\sigma_{ij} = 0$, Eq. (1) becomes

$$\frac{\partial f}{\partial \epsilon_{ij}} = \sigma_{ij} = 0 = \sigma_{ij} + \lambda_{ijlm}\ \epsilon^{o}_{lm} \qquad (3)$$

we obtain

$$E(\sigma_{ij} \equiv 0) = -1/2\ \sigma^{o}_{ij}\ \epsilon^{o}_{ij}\ V = -1/2\ \lambda_{ijlm}\ \epsilon^{o}_{ij}\ \epsilon^{o}_{lm}\ V \qquad (4)$$

where V = volume of the new phase.

Several further simplification steps lead to expressions for minimum elastic energy (detailed mathematics are given in Khachaturyan's article[51]):

$$E_1 = -1/2\ A\ (\frac{\bar{k}_o}{k_o})\ V \tag{5}$$

$$E = 1/2\ V \left\{ \lambda_{ijlm}\ \epsilon^o_{ij}\ \epsilon^o_{lm} - A\ (\frac{\bar{k}_o}{k_o}) \right\} \tag{5a}$$

where $A\ (\bar{k}_o/k_o)$ is a complex scalar product.

E_1 denotes the minimum elastic energy of the system and is negative with respect to E, the elastic energy of the system in the stressed state.

Khachaturyan[51] has also obtained an expression for the vector of rotation of the crystallographic axes of the new phase (in the shape of a plate) relative to the matrix:

$$\langle\phi\rangle = 1/2\ [\bar{k}_o,\ G^{-1}\ (\bar{k}_o)\ \hat{\sigma}\ \bar{k}_o] \tag{6}$$

where again the terms on the right hand side represent a complex scalar product.

On the basis of the above equations, Khachaturyan[51] predicts that the optimum shape of a new phase particle to ensure minimum elastic energy is that of a thin plate, with length and width much greater than its thickness.

The results obtained can best be illustrated by applying them to the tantalum-carbon system. Consider the case where the crystal geometry of the transformation is described by the tensor ϵ^o_{ji}, which has a tetragonal character, while the matrix is cubic[57] (Fig. 31). Here the tetragonal deformation transforms a cube into a rectangular parallelepiped with a square base. The deformation involves a lengthening Δc along the c axis and a shortening Δa along the a_1 and a_2 axes. In the cubic axes

$$\epsilon^o_{11} = \epsilon^o_{22} = -\frac{\Delta a}{a},\ \epsilon^o_{33} = \frac{\Delta c}{c},\ \epsilon^o_{ij} = 0 \text{ when } i \neq j$$

From Eq. (3), we have

$$\sigma^o_{ij} = \sigma_o \begin{pmatrix} 1 & 0 & 0 \\ 0 & 1 & 0 \\ 0 & 0 & 1 \end{pmatrix} + k_o \begin{pmatrix} -1/2 & 0 & 0 \\ 0 & -1/2 & 0 \\ 0 & 0 & 1 \end{pmatrix} \tag{7}$$

where

$$\sigma_o = \frac{c_{11} + 2c_{12}}{3} \left(-2\frac{\Delta a}{a} + \frac{c}{c}\right)$$

$$k_o = \frac{2(c_{11} - c_{12})}{3} \left(\frac{\Delta c}{c} + \frac{a}{a}\right)$$

using the usual notation for independent components of the tensor λ_{ijlm}:

$$\lambda_{1111} = c_{11}, \ \lambda_{1122} = c_{12}, \ \lambda_{1212} = c_{44}$$

For the case of a cubic lattice the matrix $(\hat{G}^{-1})^{ij}$ has the following form[18]

$$(\hat{G}^{-1}(\bar{k}))^{11} = \frac{1}{k^2} \frac{c_{11} - (c_{11} - c_{44})\, n_1^2 + \Delta\,(c_{11} + c_{12})\, n_3^2\, n_3^2}{c_{44}\, D(n)}$$

$$(\hat{G}_1^{-1}(\bar{k}))^{12} = -\frac{1}{k^2} \frac{(c_{12} + c_{44})\,(1 + \Delta n_3^2)\, n_1 n_2}{c_{44}\, D(n)} \tag{8}$$

where

$$D(n) = c_{11} + \Delta(c_{11} + c_{12})\,(n_1^2\, n_2^2 + n_1^2\, n_3^2 + n_2^2\, n_3^2) + \Delta^2(c_{11} + 2c_{12} + c_{44})\, n_1^2\, n_2^2\, n_3^2$$

$$\Delta = \frac{c_{11} - c_{12} - 2c_{44}}{c_{44}}$$

Making the appropriate substitutions in Eq. (5a), the minimum elastic energy of the system,

$$E_1 = -\frac{(\sigma_o + k_o)^2}{2D(n)} \left[r^2 + n_1^2 A - n_1^4 B + \Delta c\, n_1^2\, n_2^2\, n_3^2 + 2\Delta r^2 n_2^2\, n_3^2\right] \tag{9}$$

where

$$r = \frac{\sigma_o - k_o/2}{\sigma_o + k_o}$$

$$A = \left[\frac{c_{11}}{c_{44}}\right] + \left[\frac{c_{11}}{c_{44}}^{-2}\right] \left[\frac{c_{12}}{c_{44}} + 1\right]$$

$$B = \frac{c_{11}}{c_{44}} - 1 + r^2 \left[\frac{c_{11}}{c_{44}} - 1\right]^{-2} \left[\frac{c_{12}}{c_{44}} + 1\right]$$

$$C = \frac{c_{11}}{c_{44}} + \frac{c_{12}}{c_{44}} + 2r^2 \left[\frac{c_{12}}{c_{44}}^{-1}\right].$$

From Eq. (9) it follows that the elastic energy of the crystal takes on its least value when the normal to the new-phase plate, n, is oriented in such a way that the right hand side of (9) is at a minimum. The components of the vector n are related to the Miller indices of a plane of type (hkl) by very simple expressions.

$$n_1 = \frac{h}{\sqrt{h^2 + k^2 + l^2}} \; ; \; n_2 = \frac{k}{\sqrt{h^2 + k^2 + l^2}} ; \; n_3 = \frac{l}{\sqrt{h^2 + k^2 + l^2}}$$

The direction of the vector n depends on the value of γ, which varies from 1, when the phase change is accompanied by pure expansion (nucleation along ⟨100⟩), to -1/2 when the transformation results in pure displacement (nucleation along ⟨110⟩), If the geometry of the emerging phase changes during the transformation, then the direction of the vector n will also change. In corresponding fashion, the orientation of the new phase (its crystal habit) will also change. On analyzing Eq. (9), it is easy to establish that, depending on the relationship between the elastic constants c_{ij} and the value of the numerical factor γ, the energy E_1 is at a minimum when the vector n lies either in plane (100) or in (110). This means that the Miller indices of the plane of the crystal form may either have the forms (hh0) or (h00).

Consider the tantalum-carbon system and let the c/a ratio of the new ordered phase vary from 1.00 to 1.20. The values of E_1 for nucleation in the (100) or (110) planes can be calculated using the above equations. Whichever values of E_1 are lower, give that set of invariant planes on which nucleation of the new phase occurs. It must be remembered that the deformation accompanying the phase change has a tetragonal nature and the main contribution to the energy of interaction between the new phase particle and the matrix is made by elastic stresses.

Elastic constants of tantalum in units of 10^{12} dynes/cm^2 [19]

T°K	c_{11}	c_{12}	c_{44}
300	2.6091	1.5743	0.8182

These values have been used to calculate the minimum elastic energies in the ⟨100⟩ and ⟨110⟩ directions, and the various values obtained for varying c/a ratio of the new phase, are tabulated in Tables I and II.

A plot of the minimum elastic energy E_1 vs c/a ratio in tantalum is shown in Fig. 42. It can be seen very clearly that the plane for nucleation of the new phase is predicted to be (110) as these represent planes of minimum elastic energy as compared to the (100) planes.

TABLE I

For the (010) invariant plane:

$\Delta c/c$	$\Delta a/a$	r	D(n)	n_1	E_1
0.025	0.013	-0.399	2.6091	1	-0.000154
0.050	0.024	-0.395	2.6091	1	-0.000578
0.075	0.039	-0.617	2.6091	1	-0.001022
0.100	0.053	-0.683	2.6091	1	-0.001694
0.125	0.068	-0.783	2.6091	1	-0.002415
0.150	0.082	-0.804	2.6091	1	-0.003390
0.175	0.100	-1.008	2.6091	1	-0.003865
0.200	0.116	-1.088	2.6091	1	-0.004700

TABLE II

For the (110) invariant plane:

$\Delta c/c$	$\Delta a/a$	r	D(n)	n_1, n_2	E_1
0.025	0.013	-0.399	1.8391	0.708	-0.00390
0.050	0.024	-0.395	1.8391	0.708	-0.001510
0.075	0.039	-0.617	1.8391	0.708	-0.003500
0.100	0.053	-0.683	1.8391	0.708	-0.006085
0.125	0.068	-0.783	1.8391	0.708	0.009720
0.150	0.082	-0.804	1.8391	0.708	-0.013400
0.175	0.100	-1.008	1.8391	0.708	-0.020450
0.200	0.116	-1.088	1.8391	0.708	-0.023950

REFERENCES

1. R. E. Villagrana and G. Thomas, Phys. Stat. Sol. 9, 499 (1965) see also Acta Met. 14, 1633 (1966).

2. L. I. Van Torne and G. Thomas, Acta Met. 14, 621 (1966).

3. J. Van Landuyt, R. Gevers and S. Amelinckx, Phys. Stat. Sol. 13 467 (1966).

4. D. P. Seraphim, N. R. Stemple and D. T. Novick, J. Appl. Phys. 33, 136 (1962).

5. D. Hull and D. C. Wynne, Proceedings of the Third European Regional Conference on Electron Microscopy, Prague, 1964, Czech. Acad. Sci. Prague 1964 (p. 239).

6. A G. Khachaturyan, Fizika Tverdogo Tela, 9, 2861 (1967).

7. A. Ferro, J. Appl. Phys. 28, 895 (1957).

8. R. W. Powers and M. V. Doyle, J. Appl. Phys. 30, 514 (1959).

9. J. Snoek, Physica 8, 711 (1941)

10. G. Schoeck and A. Seeger, Acta Met. 7, 469 (1959).

11. D. N. Beshers, J. Appl. Phys. 36, 290 (1965).

12. L. Pauling, The Nature of the Chemical Bond and the Structure of Molecules and Crystals, Cornell University Press, New York, 1960.

13. Usikov and Khachaturyan, Krystallographia, 13, 1045 (1968).

14. S. Steeb and J. Renner, Metall.

15. R. H. Geiss and K. R. Lawless, Proceedings of the Twenty Sixth Annual EMSA Meeting, New Orleans (1968).

16. J. Van Landuyt and C. M. Wayman, Acta. Met. 16, 8 (1968).

17. A. L. Bowman, T. C. Wallace, J. L. Yarnell, R. G. Wenzel and E. K. Storms, Acta, Cryst. 19, 6 (1965).

18. R. W. Guard, J. W. Savage and D. G. Swarthout, Trans. AIME, 239, 643 (1967).

19. R. W. Powers and M. V. Doyle, Acta Met. 4, 233 (1956).

20. R. W. Powers and M. V. Doyle, Trans. AIME, 215, 655 (1959).

21. A. L. Eustice and O. N. Carlson, Trans. AIME, 221, 238 (1961).

22. L. I. Van Torne and G. Thomas, Acta Met, 11, 881 (1963).

23. D. H. Sherman, C. V. Owen and T. E. Scott, Trans. AIME, 242, 1775 (1968).

24. N. J. Petch, J. Iron St. Inst. 174, 25 (1953).

25. S. Nakamura and E. W. Muller, J. Appl. Phys. 36, 3634 (1965).

26. D. A. Smith, B. Ralph and W. S. Williams, Phil Mag 16, 415 (1967).

27. N. V. Durai Raghavan, S. Ranganathan and G. Thomas, J. Less Common Metals, 18, 79 (1969).

28. A. J. W. Moore, J. Phys. Chem. Solids, 23, 907 (1962).

29. A. J. W. Moore, Phil Mag., 16, 793 (1967).

30. A. J. Perry and D. G. Brandon, Phil Mag. 16, 119 (1967).

31. S. Ranganathan, H. B. Lyon and G. Thomas, J. Appl. Phys. 38, 4957 (1967).

32. A. J. Perry, J. Appl. Phys. 39, 1462 (1968).

33. M. A. Fortes and B. Ralph, Acta Met. 15, 707 (1967).

34. L. I. Van Torne, Ph.D. Thesis, University of California, Berkeley UCRL-11752 (1965).

35. S. S. Markowitz and J. D. Mahony, Anal. Chem. 34, 329 (1962).

36. J. J. Hren and S. Ranganathan, Field Ion Microscopy, Plenium Press, New York (1968).

37. A. Phillips, V. Kerlins and B. V. Whiteson, Electron Fractography Handbook, Tech. Report, ML-TDR-64-416, Air Force Materials Laboratory (1965).

38. J. W. Christian, The Theory of Transformations in Metals and Alloys, Pergamon Press, Oxford (1965) p. 117, 606.

39. L. E. Tanner, Phil. Mag. 14, 111 (1966).

40. Yu. D. Tyapkin, Soviet Physics, Doklady 9, 1, 95 (1964).

41. A. J. Ardell and R. B. Nicholson, Acta Met. 14, 1295 (1966).

42. W. K. Armitage, P. M. Kelly and J. Nutting, Fifth Int. Congr. for Electron Microscopy, Philadelphia (1962) p. K4, Interscience, N.Y.

43. M. Hirayabashi and S. Weissmann, Acta Met. 10, 25 (1962).

44. R. Gevers, P. Delavignette, H. Blank, J. Van Landuyt, and S. Amelinckx Phys. Stat. Sol. 5, 595 (1964).

45. P. R. Okamoto (private communication).

46. C. Zener, Phys. Rev. 74, 639 (1948).

47. F. R. N. Nabarro, Proc. Phys. Soc., Lond., 52, 90 (1940).

48. A. G. Khachaturyan, Fizika Tverdogo Tela, 5, 15 (1963).

49. A. G. Khachaturyan, Fizika Tverdogo Tela, 5, 750 (1963).

50. A. G. Khachaturyan, Fiz. Metal. Metalloved, 19, 343 (1965).

51. A. G. Khachaturyan, Fizika Tverdogo Tela, 8, 2709 (1966).

52. J. W. Cahn, Acta Met. 9, 795 (1961).

53. F. R. N. Nabarro, Report of a Conference on the Strength of Solids, p. 38, The Physical Society, London (1948).

54. M. A. Adams, A. C. Roberts and R. E. Smallman, Acta Met., 8, 382 (1960).

55. S. Nakamura and E. W. Muller, J. Appl. Phys. 36, 2535 (1965).

56. S. Matsuo and L. M. Clarebrough, Acta Met. 11, 1195 (1963).

57. A. Kussmann and H. Wollenberger, Z.f. Metallkunde 50, 94 (1959).

58. H. Warlimont and G. Thomas, J. Materials Sci. (in press).

59. W. Geudig, P. Okamoto, G. Shanz, H. Warlimont and G. Thomas, Submitted to Trans. AIME.

60. L. D. Laudan and E. M. Lifshits, Theory of Elasticity, Addison-Wesley (1959).

61. F. H. Featherston and J. R. Neighbours, Phys. Rev., 130, 1324 (1963).

62. E. K. Storms, The Refractory Carbides, Academic Press, N.Y. (1967).

FIGURE CAPTIONS

Fig. 1. Nature of interstitial sites in bcc metals

(a) Tetrahedral interstitial site

(b) Octahedral interstitial site

Fig. 2. Relative positioning of octahedral (O) and tetrahedral (T) sites in the bcc lattice.

Fig. 3. Computer simulation of field ion images involving the imaging of those atoms which lie within a spherical shell of thickness R_A-R_B. Stereographic projection of these atom positions onto the x-y plane gives a computer simulated image.

Fig. 4. Stress-strain curves of tantalum containing upto 2.05 at.% carbon tested at 300°K.

Fig. 5. Stress-strain curves of tantalum containing upto 2.05 at.% carbon tested at 196°K.

Fig. 6. Stress-strain curves of tantalum containing upto 2.05 at.% carbon tested at 77°K.

Fig. 7. Summary of ductile-brittle behavior of tantalum-carbon alloys containing upto 2.05 at.% carbon in a plot of test temperature (°K) vs. atomic percent carbon in tantalum.

Fig. 8. Plot of shear stress at lower yield, τ_{LY}, vs. atomic percent carbon in tantalum.

Fig. 9. Plot of stress (kg/mm^2) at lower yield or fracture vs test temperature (°K).

Fig.10. Plot of total elongation (%) vs. test temperature (°K).

Fig.11. Plot of plastic elongation (%) vs. test temperature (°K).

Fig.12. Bright field electron micrographs of various stages of the interstitial ordering transformation:

Fig.12. (a) Pure tantalum

(b) Ta-0.76 at.% C showing contrast due to fine fluctuations in carbon composition.

(c) Ta - 1.27 at.% C showing the formation of "ordered particles" which align themselves along the ⟨110⟩ directions.

(d) Ta-1.53 at.% C showing growth along ⟨110⟩ till impingement.

(e) Ta-2.05 at.% C showing the formation of highly ordered regions separated by coherent antiphase domain boundaries.

(f) Electron diffraction pattern obtained from Ta-1.53 at.%C.

Fig.13. Electron diffraction patterns obtained from each of the above stages of the ordering transformation. Figure 13a corresponds to the diffraction pattern obtained from Fig. 12a and so on.

Fig.14. Bright field (a) and dark field (b) images obtained from Ta-0.76 at.% carbon showing a rather diffuse basket weave of light and dark contrast. Matrix spots in diffraction patterns are streaked in ⟨110⟩ normal to the {110} striations in contrast.

Fig.15. Bright field (A) and dark field (1,2,3,1a,2a,3a) images from Ta-1.27 at.% carbon showing the formation of discrete "particles" which align themselves along ⟨110⟩ (black arrows). Figures 15.1, 15.2 and 15.3 are obtained using matrix reflections while Figs. 15.1a, 15.2a and 15.3a are obtained using superlattice reflections.

Fig.16. Bright field (A) and dark field (1,2,3,1a,3a) images from Ta-1.53 at.% carbon showing the formation of impinging small to medium sized domains. Figures 16.1, 16.2 and 16.3 are obtained using matrix reflections while Figs. 16.1a and 16.3a are obtained using superlattice reflections.

Fig.17. Bright field (1,2) and dark field (1a,1b,2a) images from Ta-2.05 at.% carbon showing the development of highly ordered regions separated by coherent antiphase domain boundaries. Bright and dark field micrographs show domain boundary contrast expected from boundaries separating tetragonal regions with c-axes normal to each other. Figure 17.3 is a schematic representation of such domain boundary contrast under different imaging conditions. The top (T) and bottom (B) of the foil as obtained from the imaging conditions in Fig. 17.3 are marked in Fig. 17.1b.

Fig.18. Structure of the ordered phase

(a) [001] diffraction pattern showing the presence of a superlattice.

(b) Indexed superlattice relpoints

(c) Superlattice unit cell

Fig.19. Superlattice unit cell (outlined by heavy black lines) drawn to show that simultaneous carbon composition fluctuations along four of the six possible {110} planes, such that $\lambda = d_{110_C} = 4d_{110_{Ta}}$, can produce the superlattice. The four sets of {110} planes are marked. The small unit cell at the origin is a bcc Ta unit cell.

Fig.20. Scanning electron fractographs from tensile tests at 300°K

(a) Pure Ta, (b) Ta-0.76 at.% carbon, (c) and (d) Ta-1.53 at.% carbon, (e) and (f) Ta-2.05 at.% carbon (transgranular), (g) Ta-2.05 at.% carbon (intergranular).

Fig.21. Scanning electron fractographs from tensile tests at 77°K

(a) Pure Ta,(b) and (c) Ta-1.27 at.% carbon, (d) and (e) Ta-1.53 at.% carbon, (f) Ta-2.05 at.% carbon (transgranular) (g) Ta-2.05 at.% carbon (intergranular).

Fig. 21(h) shows the nature of intergranular and transgranular fracture in a specimen that has undergone brittle fracture.

Fig.22. Field ion micrographs of Ta-0.76 at.% carbon, (a) and (b) at 77°K (c), (d) and (e) at 20°K. Micrographs show particle formation with alignment (marked by arrows in (b)) at ⟨110⟩ poles. The bright spots are composed of upto three atoms (see arrow in (e)).

Fig.23. Field ion micrographs of Ta-1.53 at.% carbon at 20°K. (a) and (b) are part of a field evaporation sequence showing the presence of carbon atoms (extra bright spots) after every four planes (rings) of tantalum atoms at a [111] pole. (c) Picture taken during field evaporation shows rings of carbon atoms (marked by arrows) around ⟨110⟩ poles with a spacing four times that between adjacent tantalum planes.

Fig.24. Field ion micrograph of Ta-2.05 at.% carbon at 20°K, taken during the field evaporation process. Note the bright spots preferentially along lines joining, the [110] and adjoining [111] poles, a result predicted by computer simulation of images expected from the ordered structure.

Fig.25. Computer simulated field ion images of the ordered structure. Orientation [100]

(a) Pure Ta. Shell thickness, P = 0.0736a.

(b) P = 0.0736a

(c) P = 0.1104a

(d) P = 0.1472a

(e) P = 0.1840a

where a = lattice parameter.

Radius of tip = 100a.

Fig.26. Computer simulated field ion images of the ordered structure. Orientation [110]

(a) Pure Ta. P = 0.104a (b) P = 0.104a (c) P = 0.156a

(d) P = 0.208a (e) P = 0.260a.

Fig.27. 2θ x-ray scan of a specimen containing 11.5 at.% carbon.

Fig.28. Schematic representation of the different stages of the ordering transformation resulting in the formation of discrete nuclei which align themselves along ⟨110⟩ and grow till impingement.

(a) Starting average carbon composition;

(b) Small localized composition fluctuations with varying wavelength, λ, and amplitude.

(c) Composition fluctuations develop a fixed wavelength, λ, and finally,

(d) $\lambda_{ideal} = 4d_{110_{Ta}}$

(e) Regions of λ_{ideal} can be regarded as "ordered particles" which align themsleves along ⟨110⟩ and grown (f) till they impinge (g) and form large non-impinging domains (h).

(h) Only those areas visible when imaged with a ⟨110⟩ type reflection are shown bounded by heavy lines.

Fig.29. Plots of mean particle or microvoid size (Å) vs. atomic percent carbon in tantalum.

Fig.30. Tantalum-carbon phase diagram showning proposed changes (dotted lines) in the existing diagram (heavy lines).

Fig.31. Tetragonal deformation of a cube into a rectangular parallelepiped with a square base involving a lengthening Δc along the c-axis and a shortening Δa along the a_1 and a_2 axis.

Fig.32. Plot of minimum elastic energy, E_1, vs. c/a ratio in tantalum.

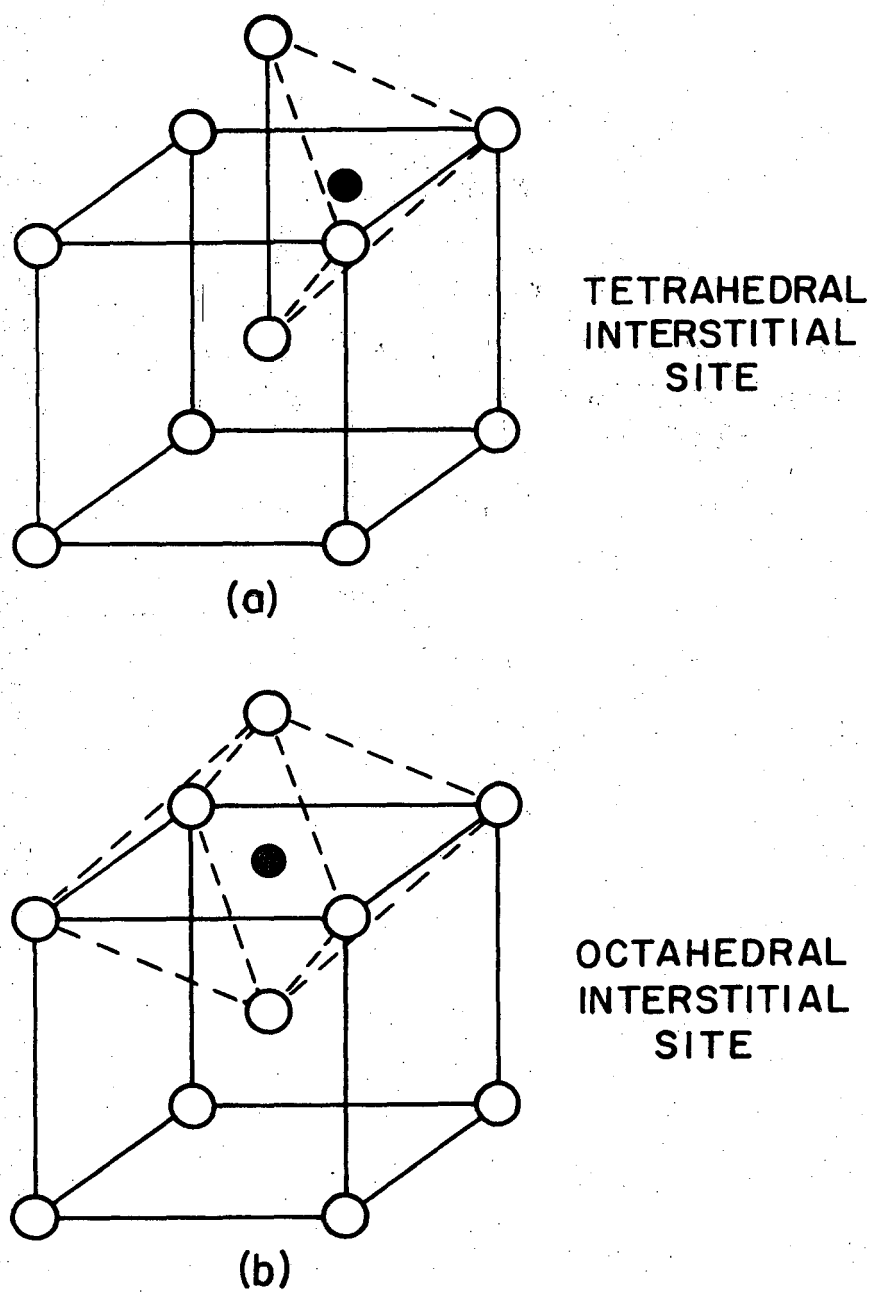

XBL 6910-5966

Figure 1

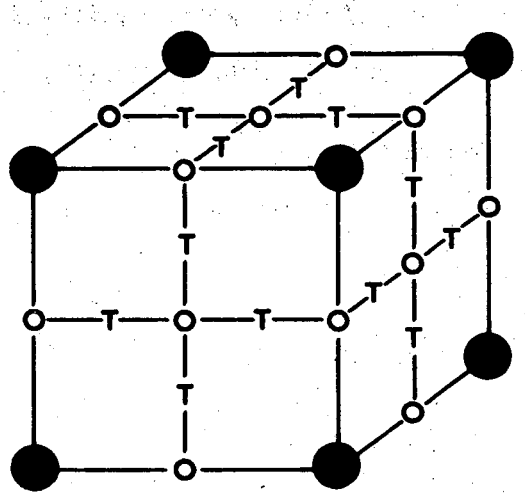

XBL 6910-5958

Figure 2

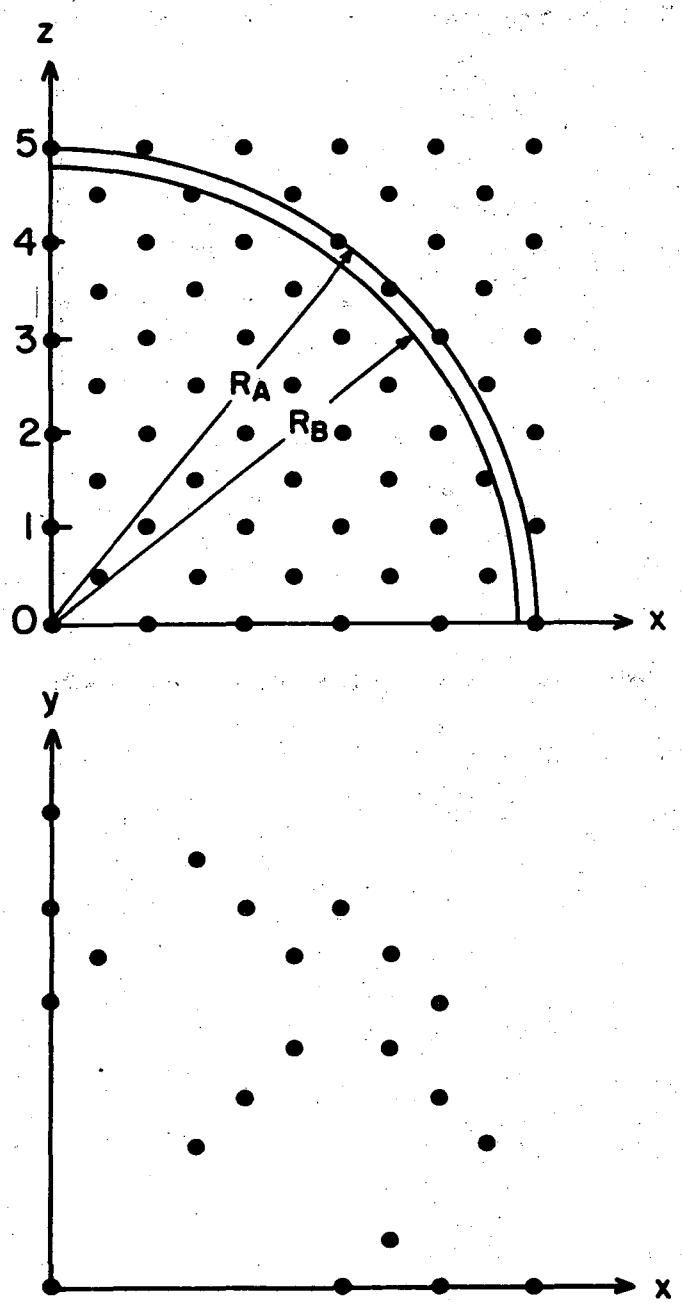

XBL 6910-5964

Figure 3

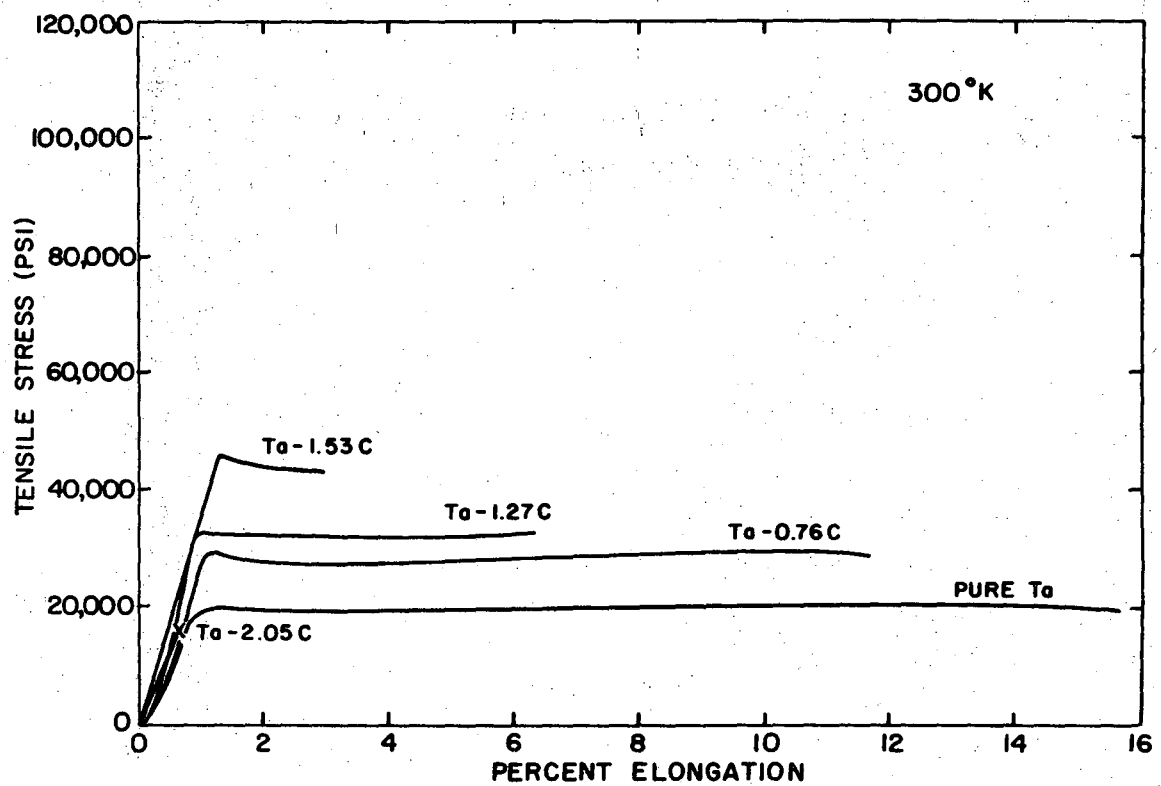

XBL 6910-5970

Figure 4

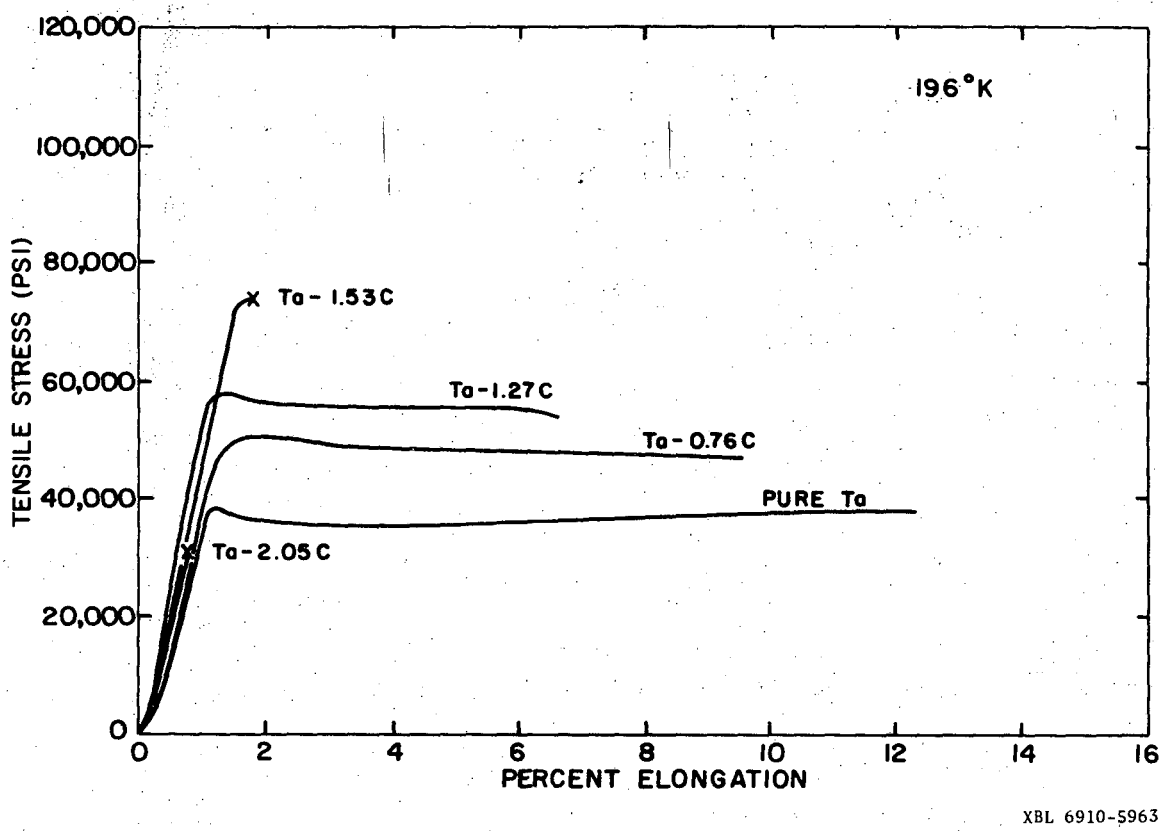
120,000
100,000
80,000
60,000
40,000
20,000
0
TENSILE STRESS (PSI)
196°K
Ta - 1.53C
Ta-1.27C
Ta-0.76C
PURE Ta
Ta-2.05C
0
2
4
6
8
10
12
14
16
PERCENT ELONGATION
XBL 6910-5963

Figure 5

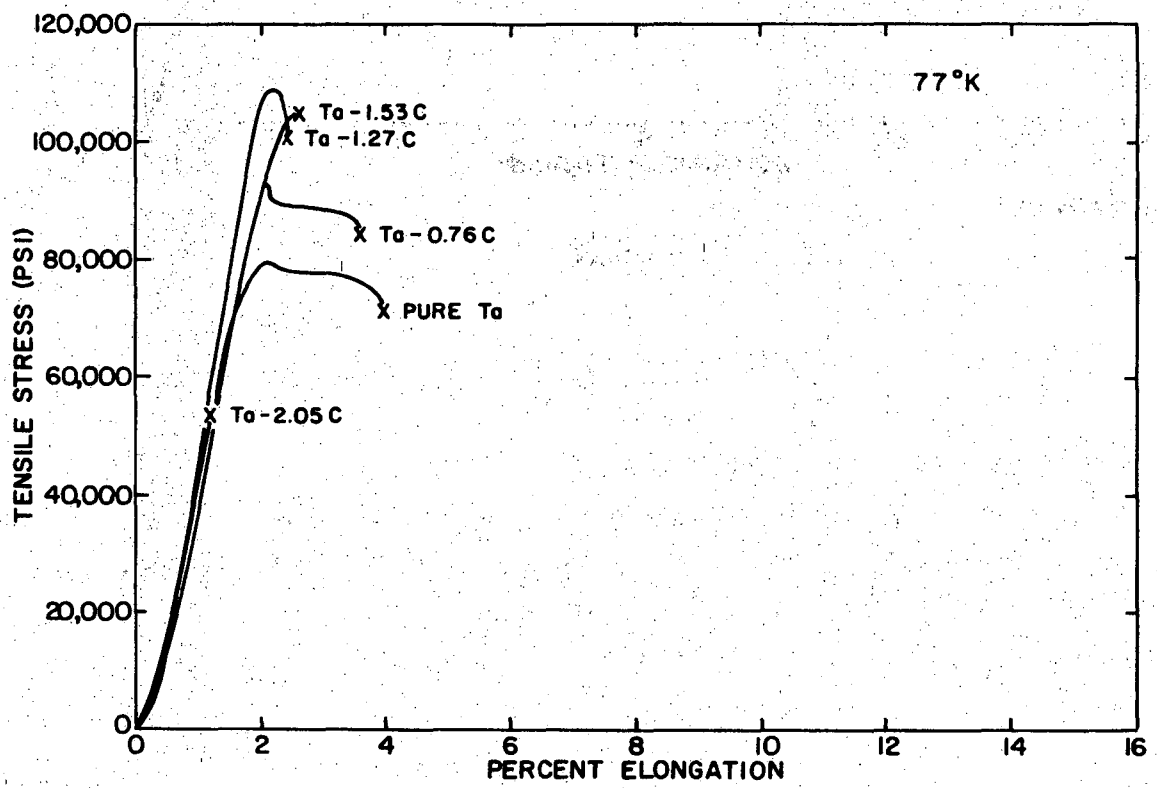

XBL 6910-5967

Figure 6

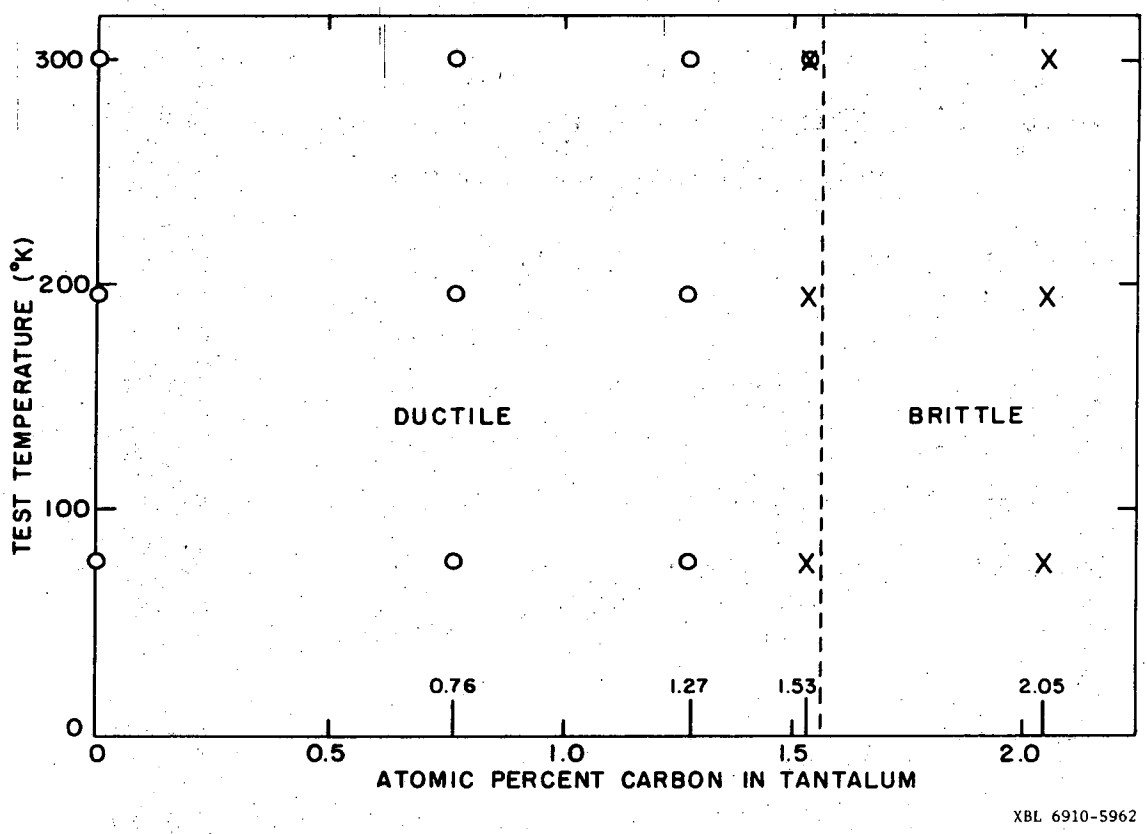
300
200
100
0
TEST TEMPERATURE (°K)
DUCTILE
BRITTLE
0.76
1.27
1.53
2.05
0
0.5
1.0
1.5
2.0
ATOMIC PERCENT CARBON IN TANTALUM
XBL 6910-5962

Figure 7

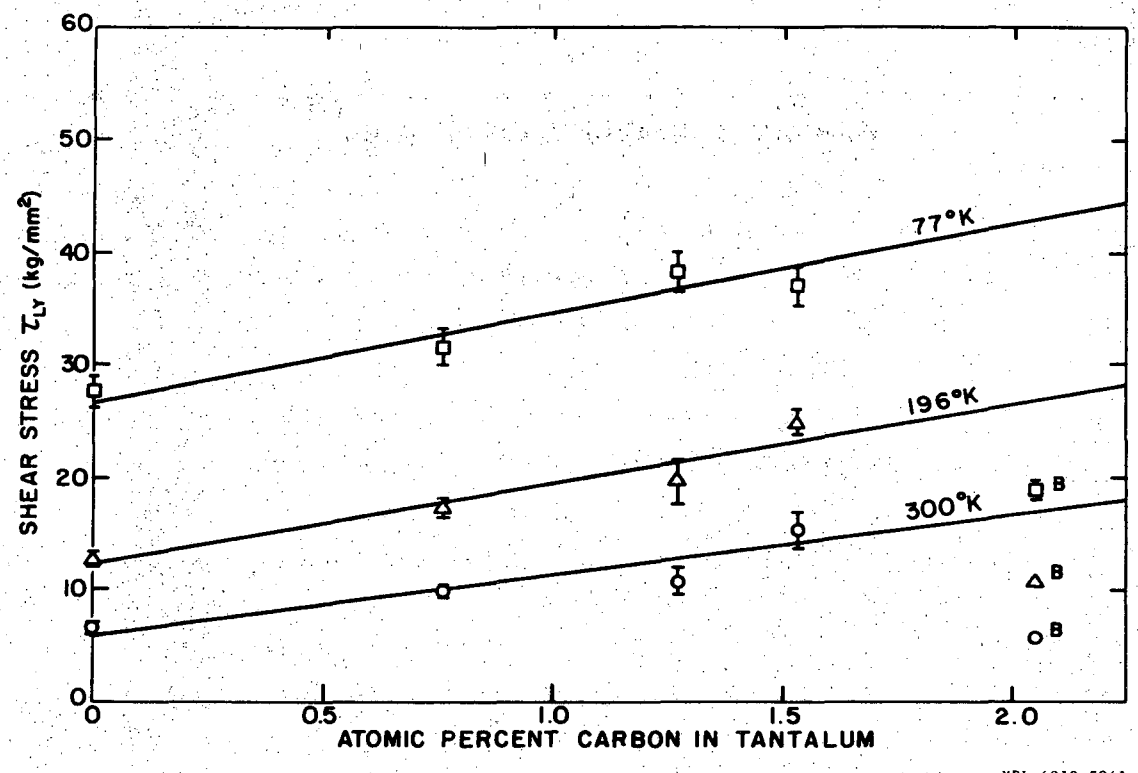

XBL 6910-5961

Figure 8

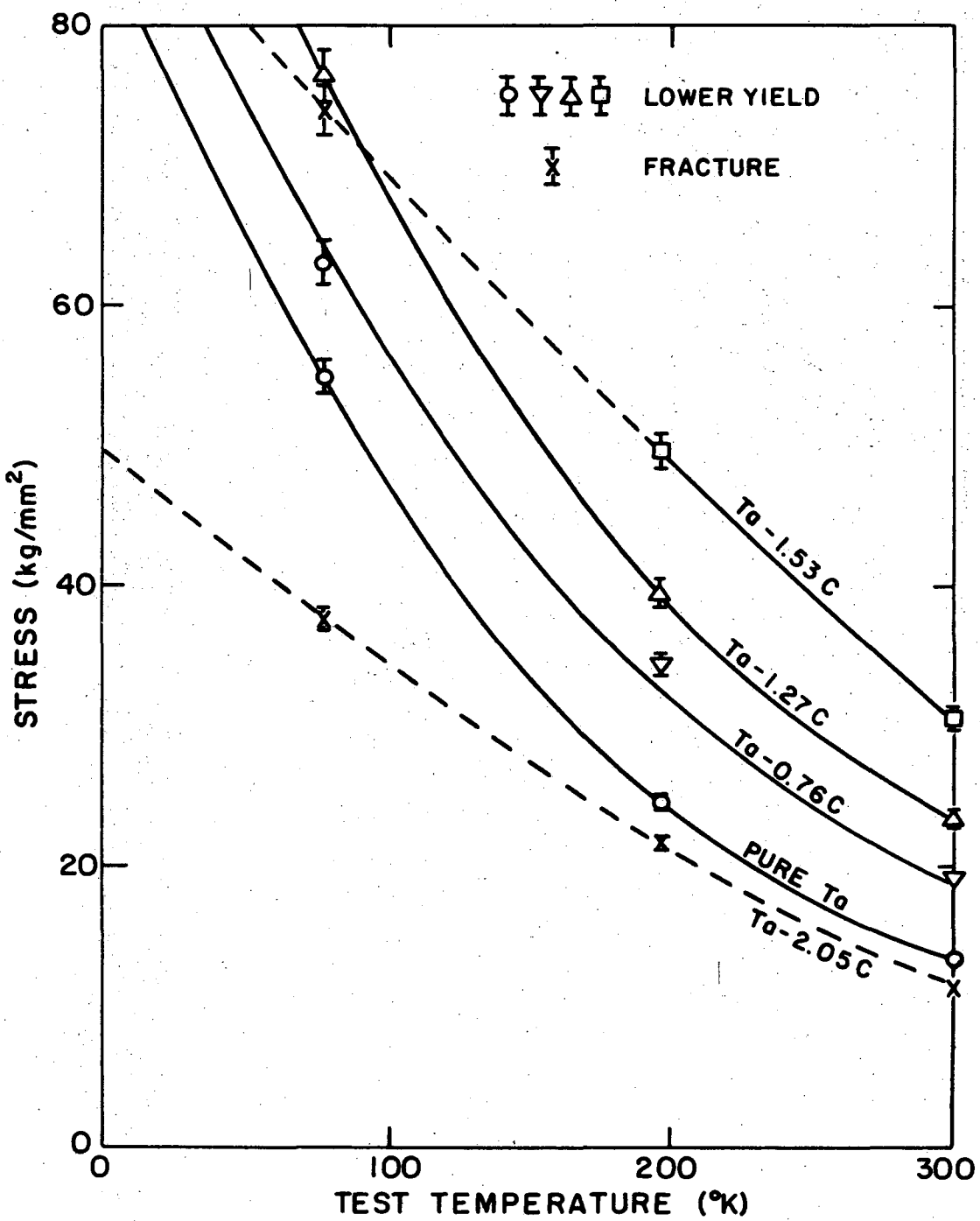

XBL 6910-5959

Figure 9

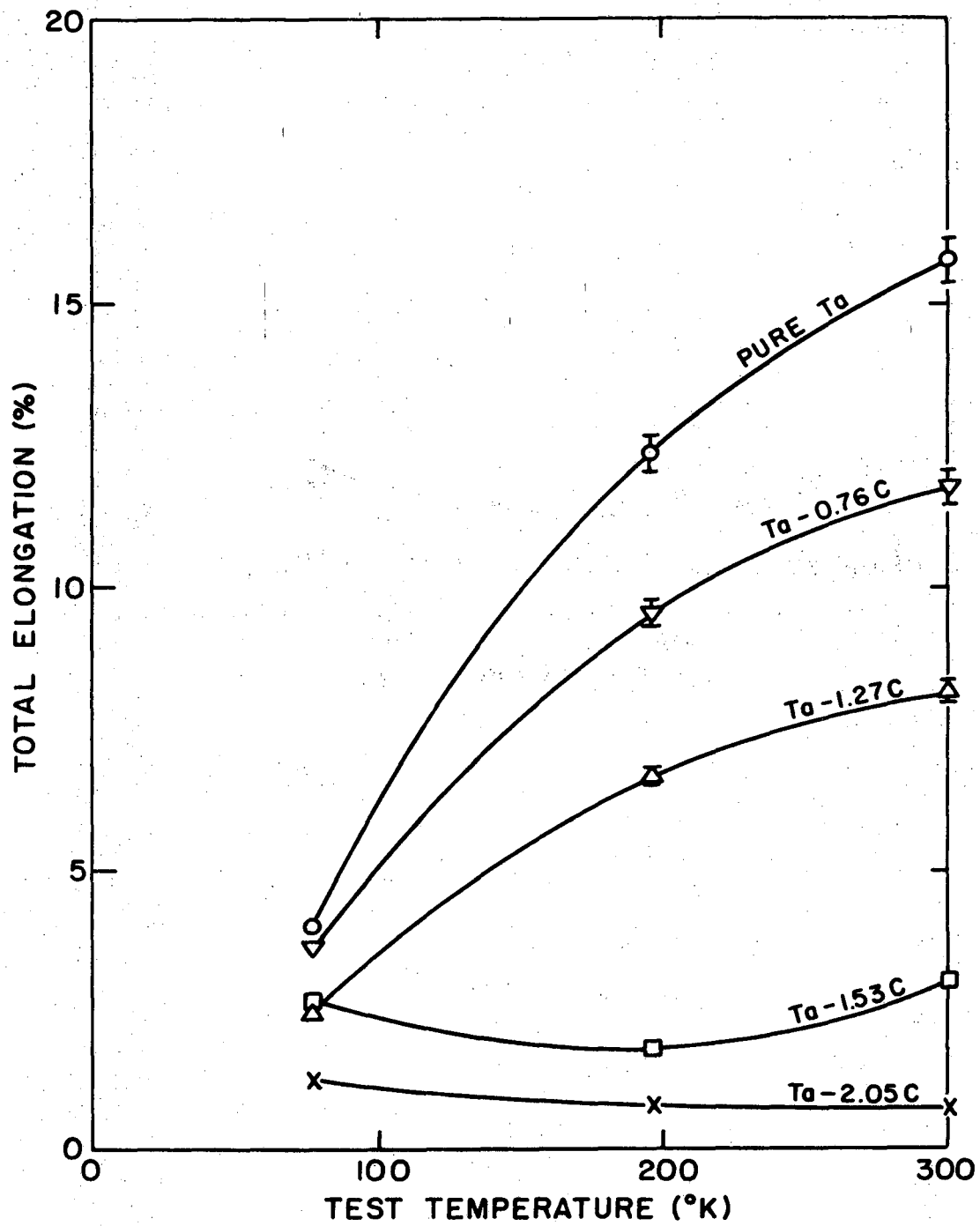

XBL 6910-5957

Figure 10

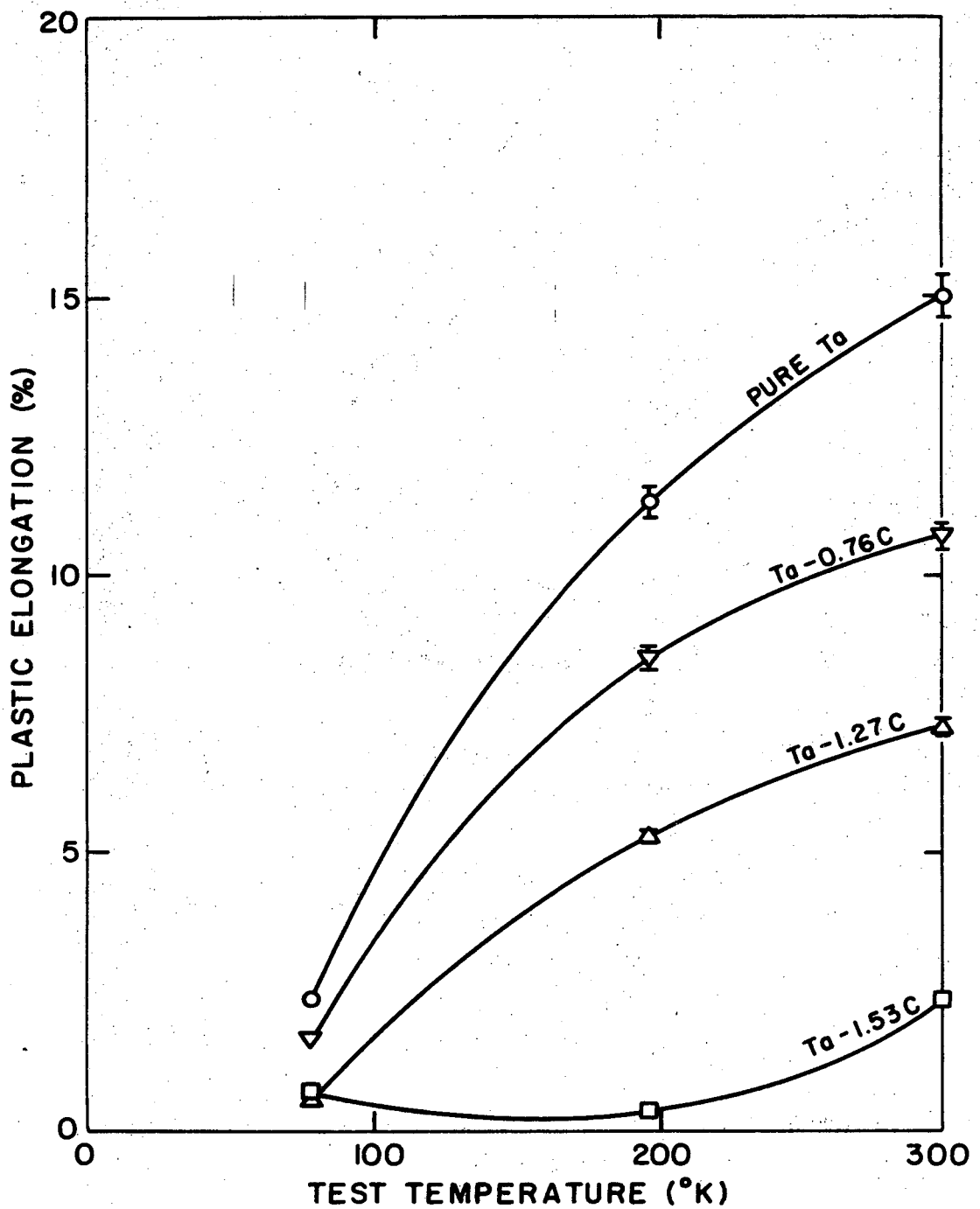

XBL 6910-5969

Figure 11

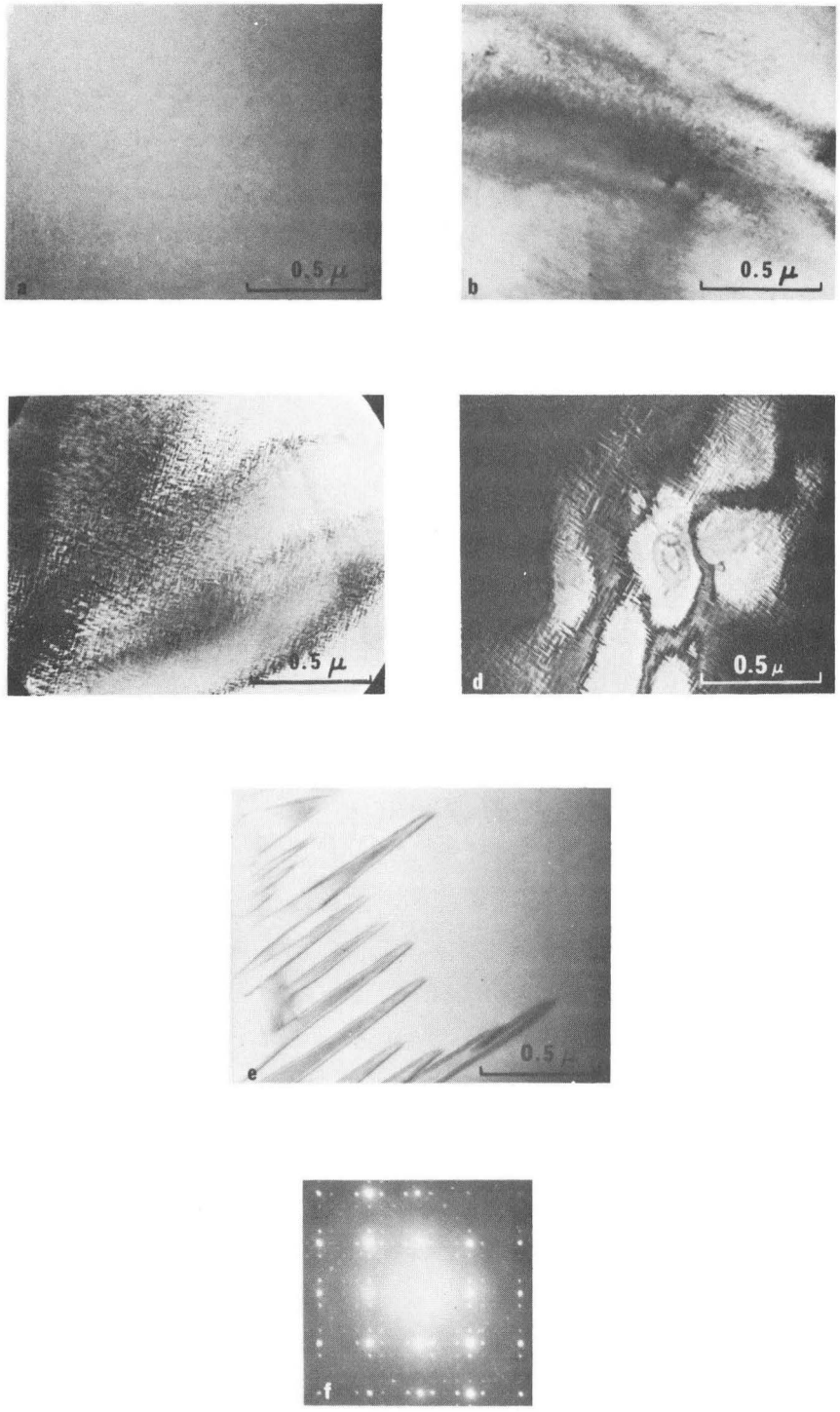

XBB 6911-7115

Figure 12

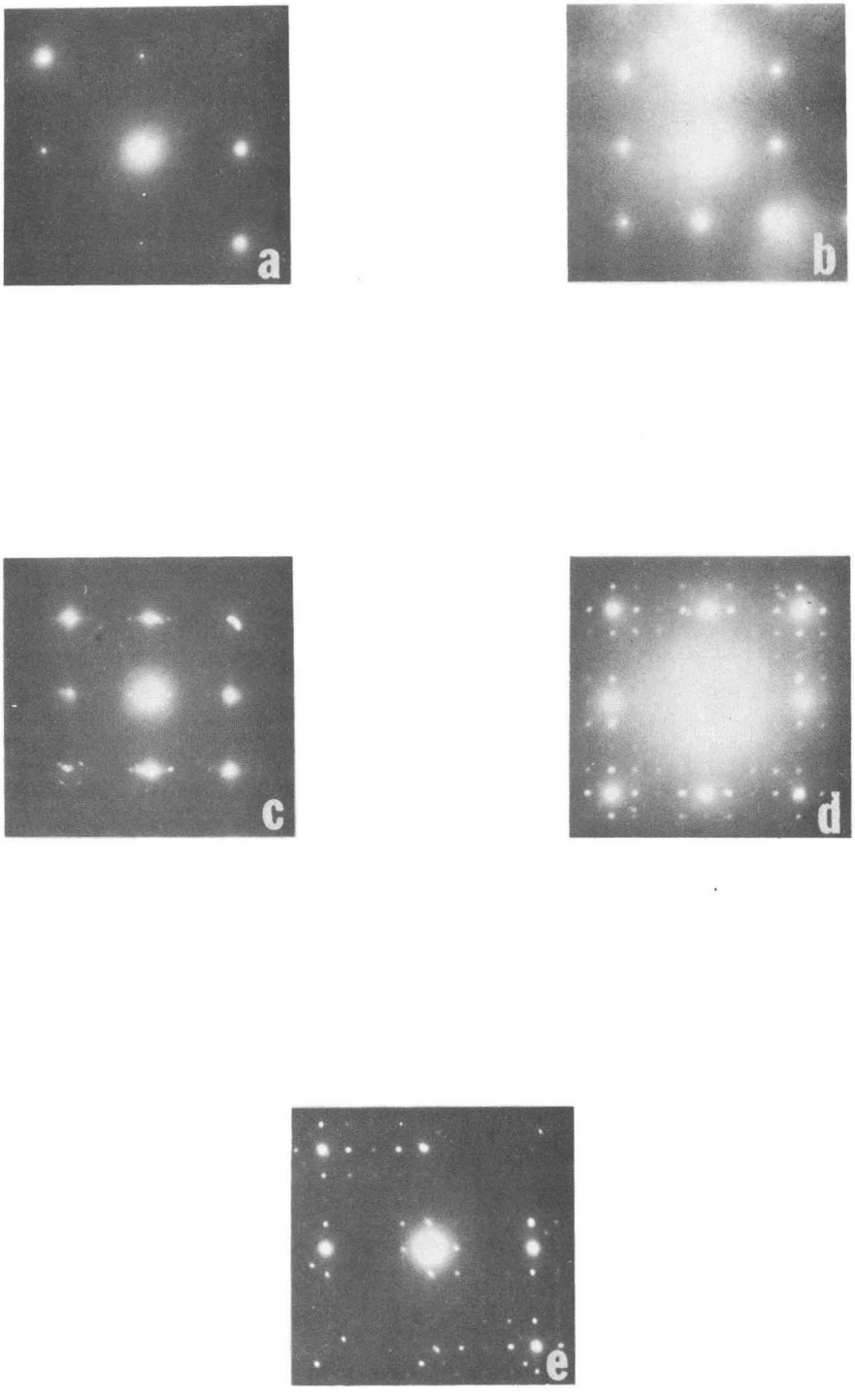

XBB 6911-7114

Figure 13

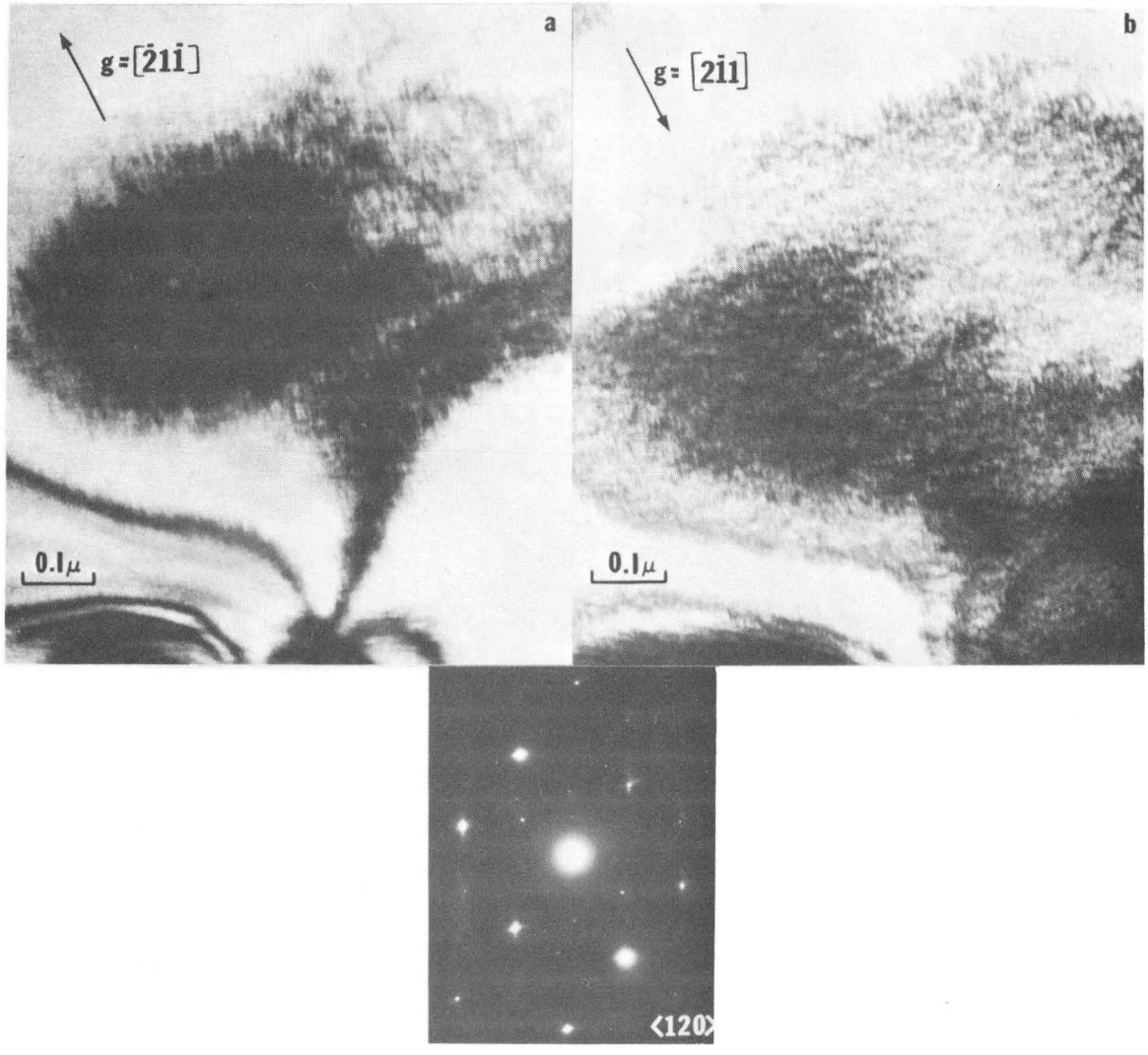

XBB 6911-7117

Figure 14

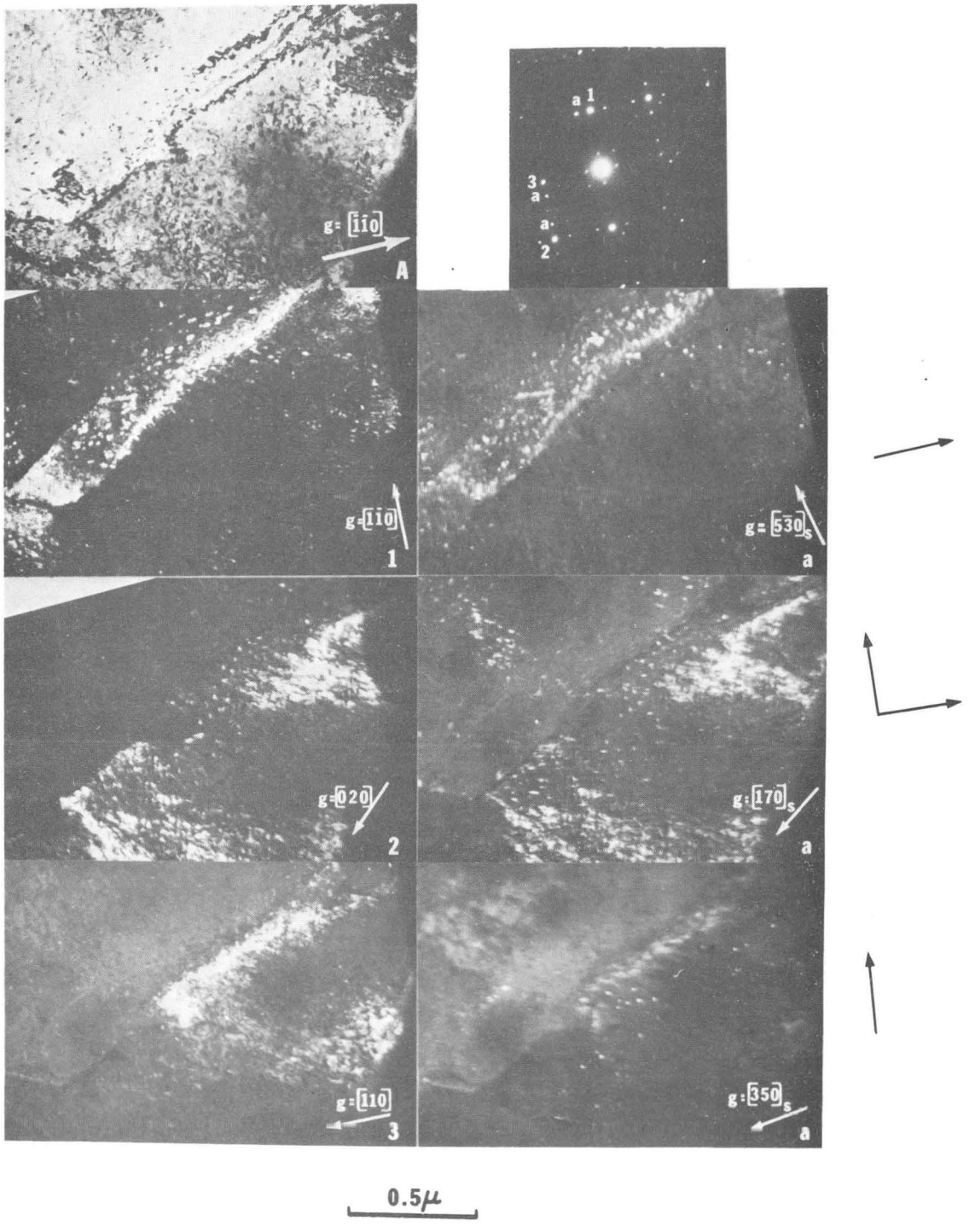

XBB 6911-7118

Figure 15

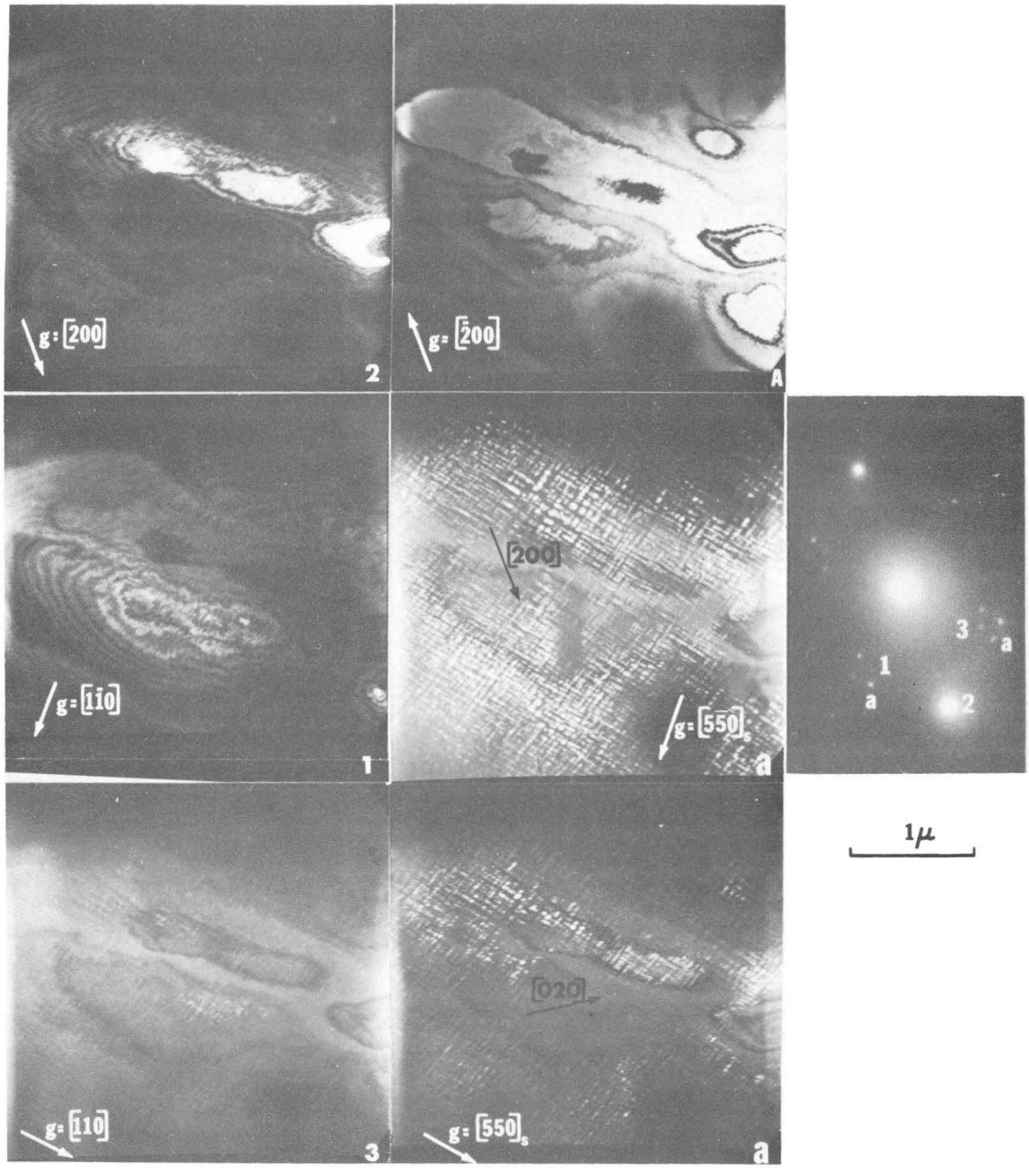

XBB 6911-7121

Figure 16

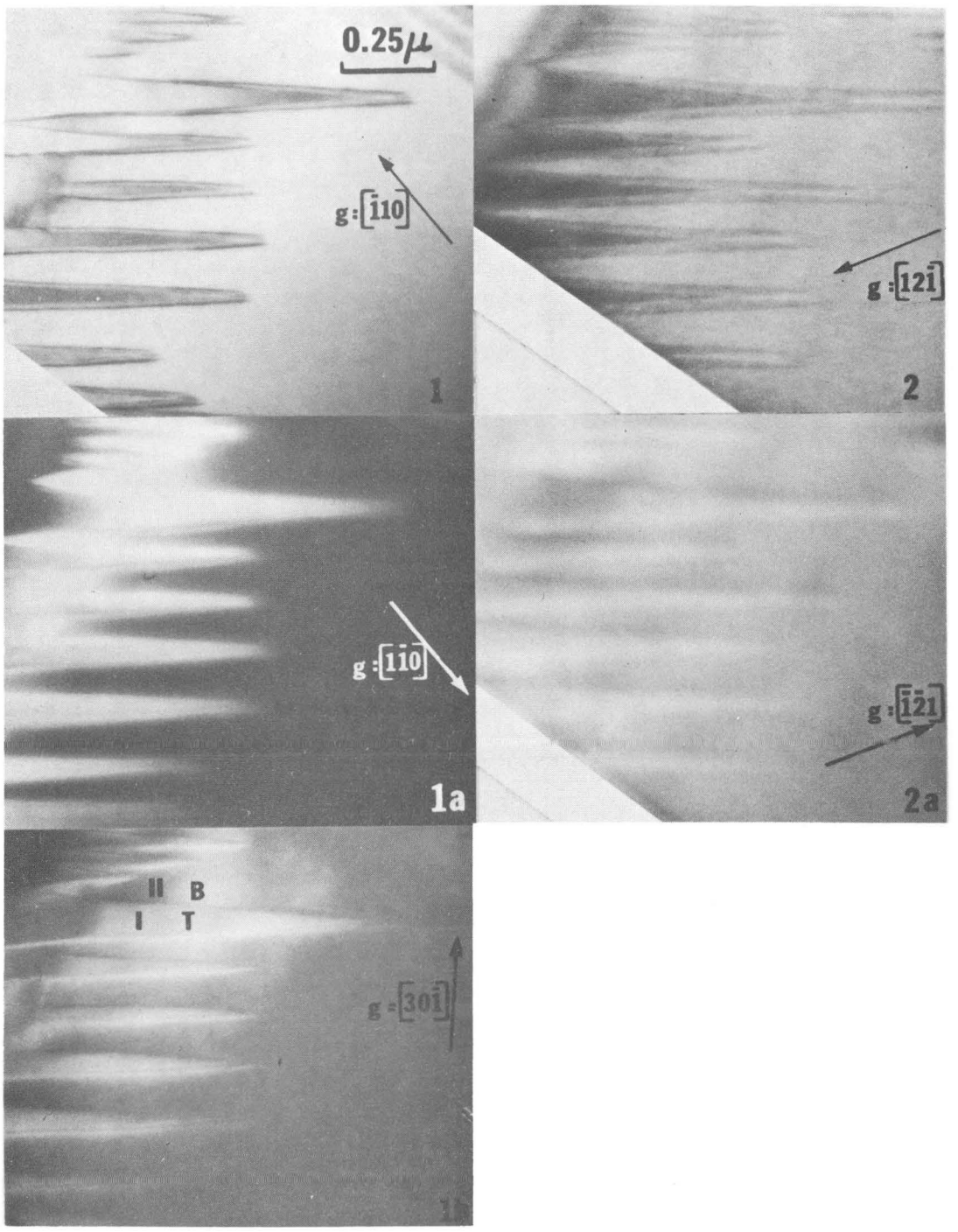

XBB 6911-7123

Figure 17

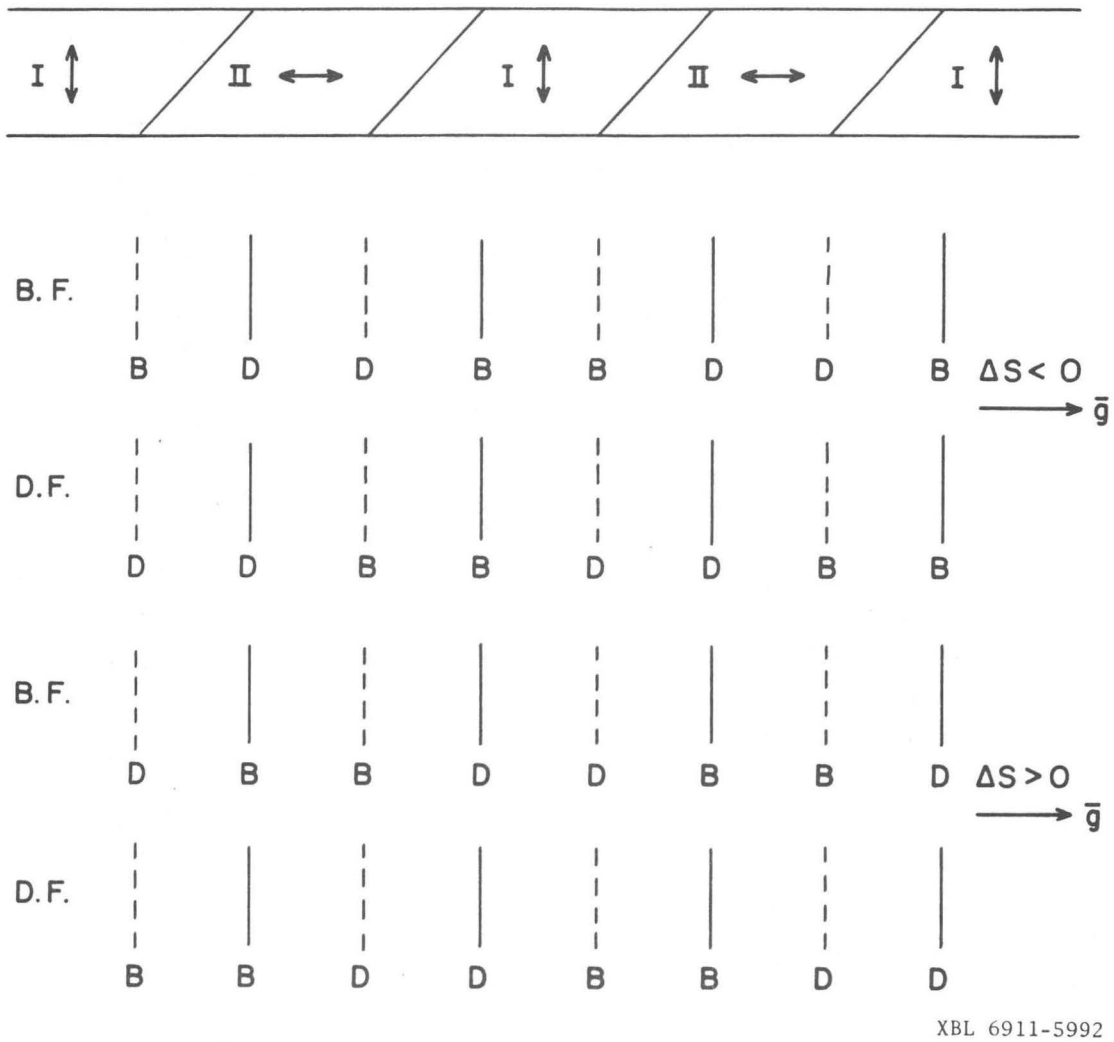
I
II
I
II
I
B. F.
B D D B B D D B
ΔS < O
g
D.F.
D D B B D D B B
B. F.
D B B D D B B D
ΔS > O
g
D.F.
B B D D B B D D
XBL 6911-5992

Figure 17.3

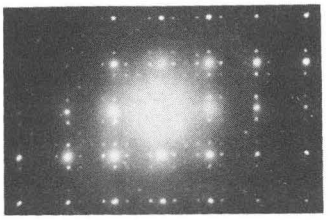

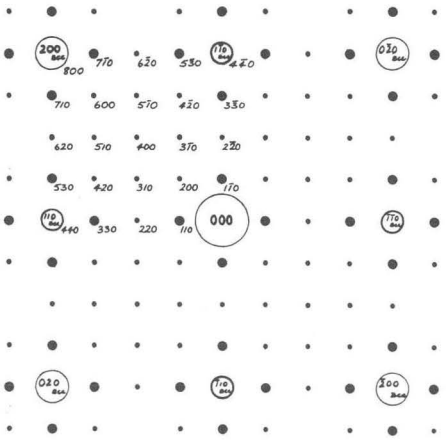

b

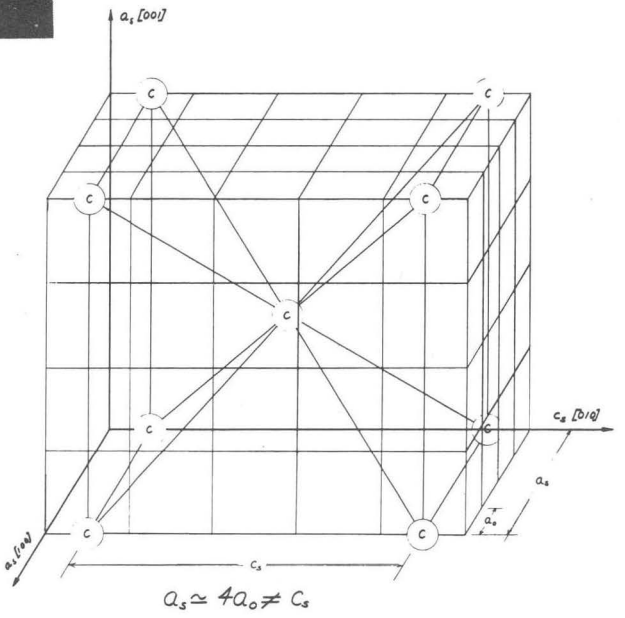

c

XBB 6911-7122

Figure 18

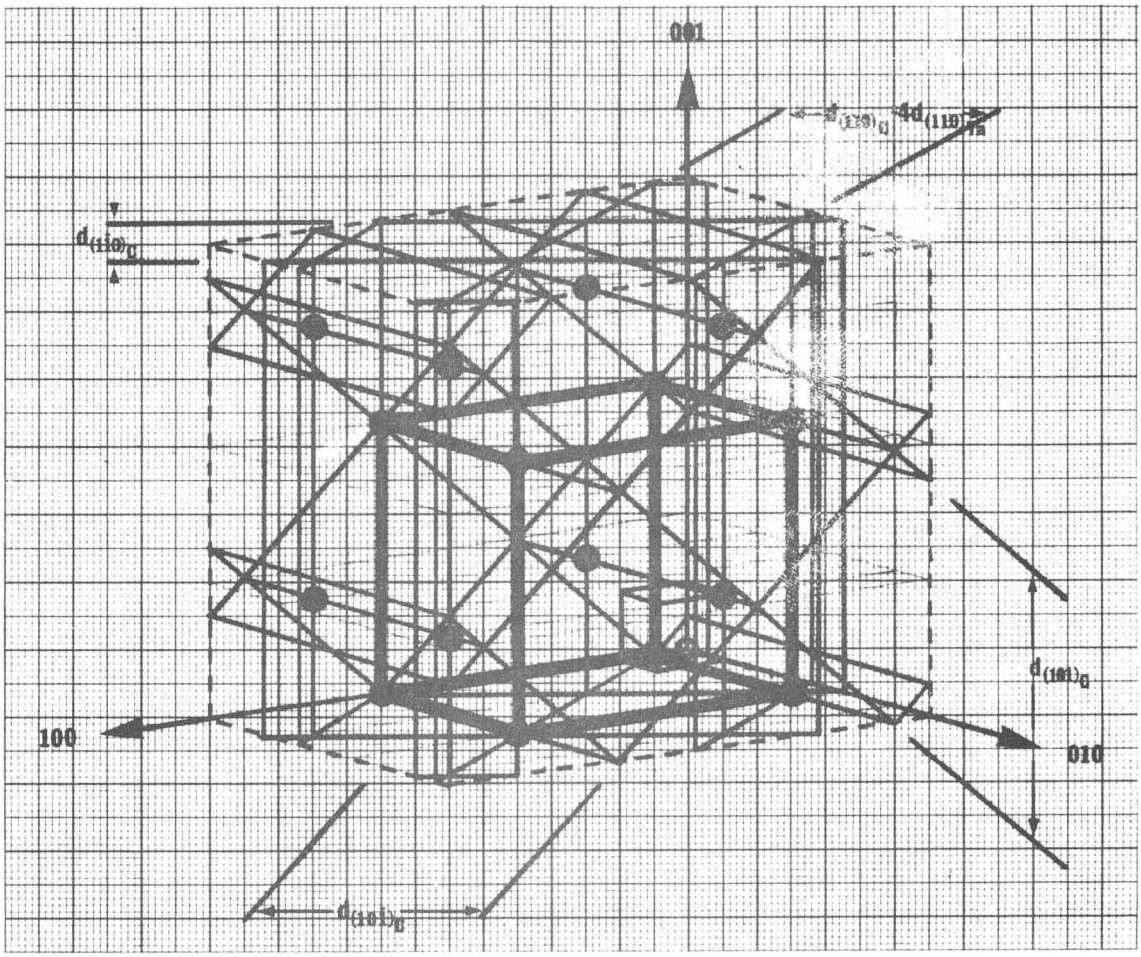

XBL 6910-5965

Figure 19

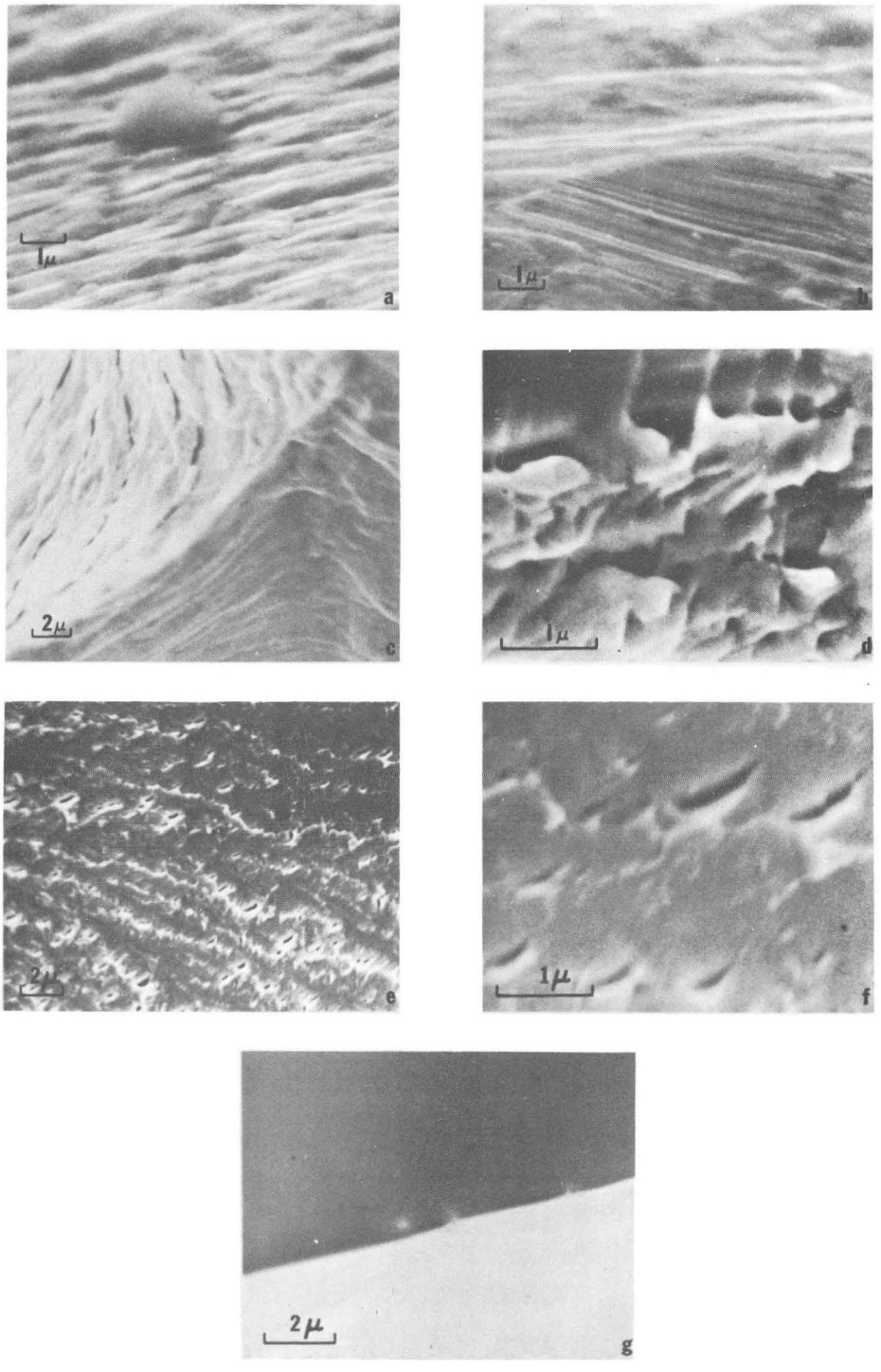

XBB 6911-7119

Figure 20

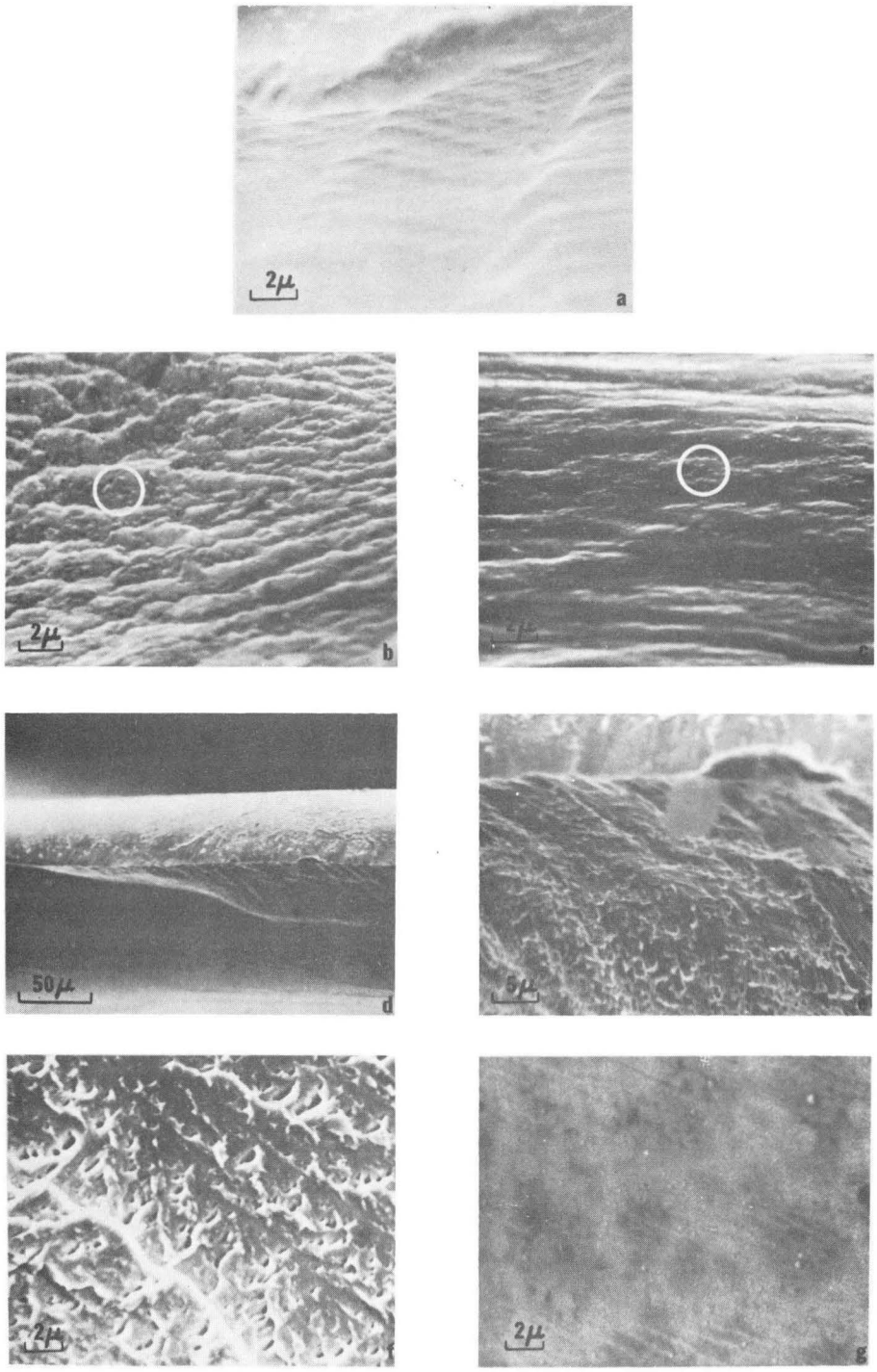

XBB 6911-7125

Figure 21

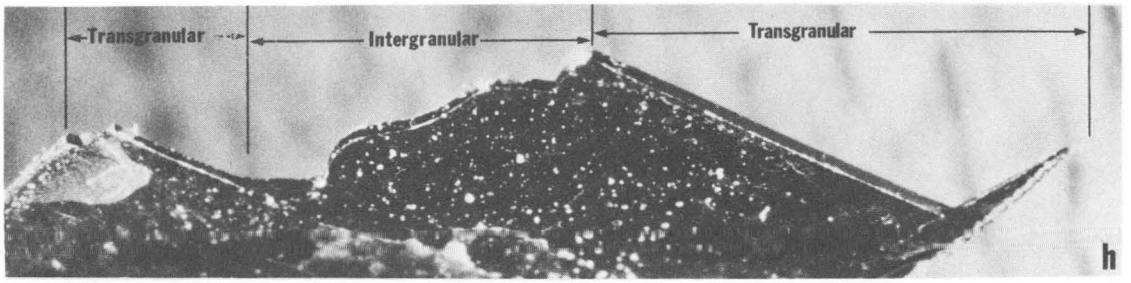

XBB 6911-7124

Figure 21h

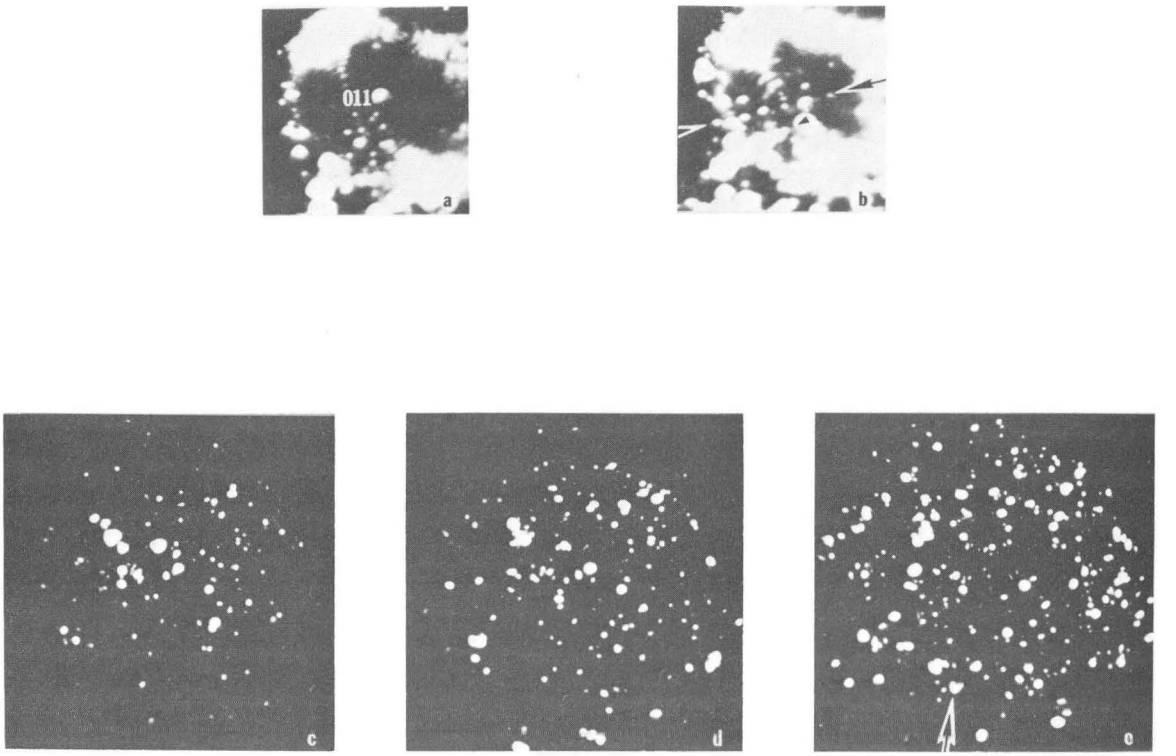

XBB 6911-7126

Figure 22

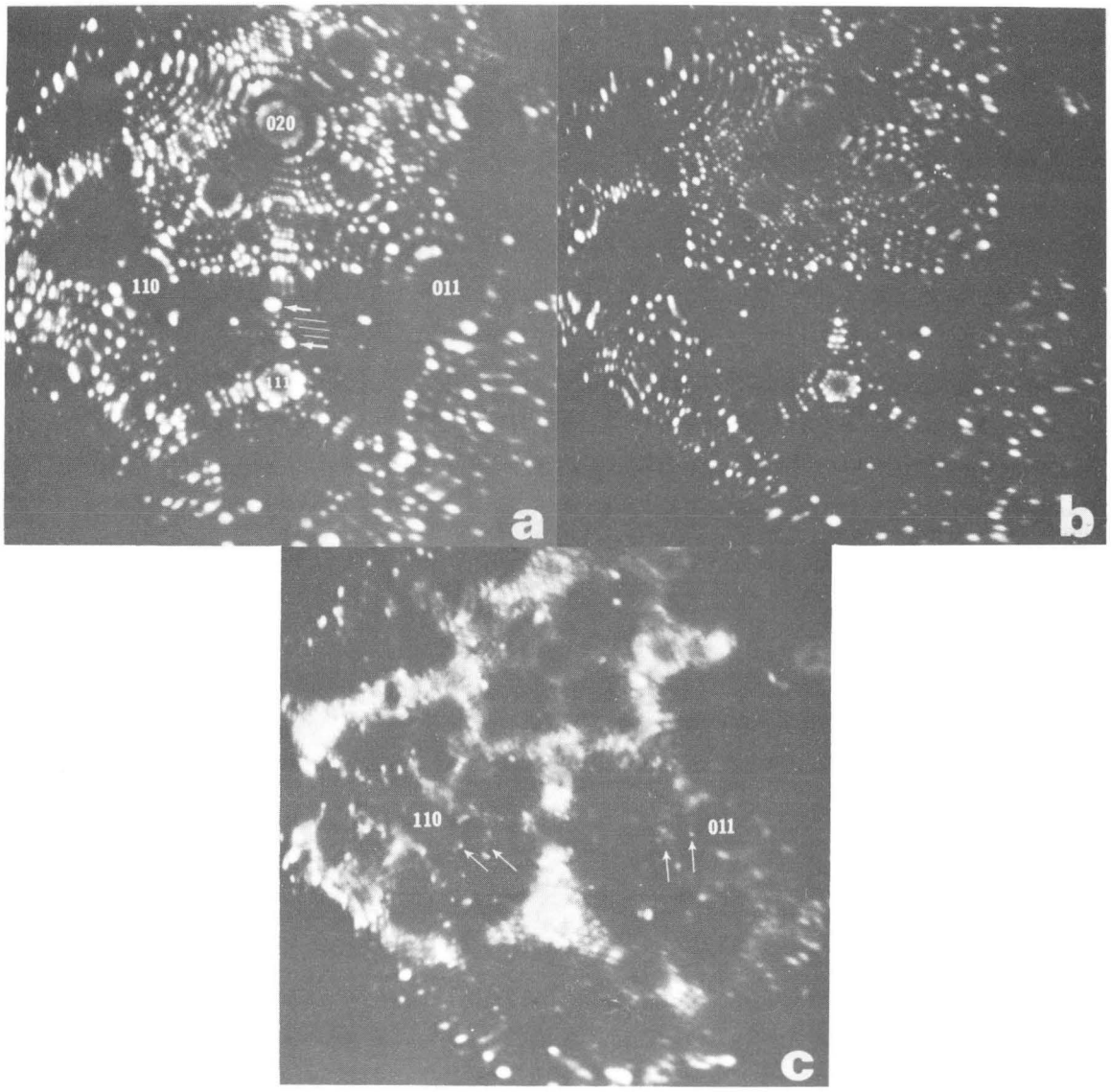

XBB 6911-7128

Figure 23

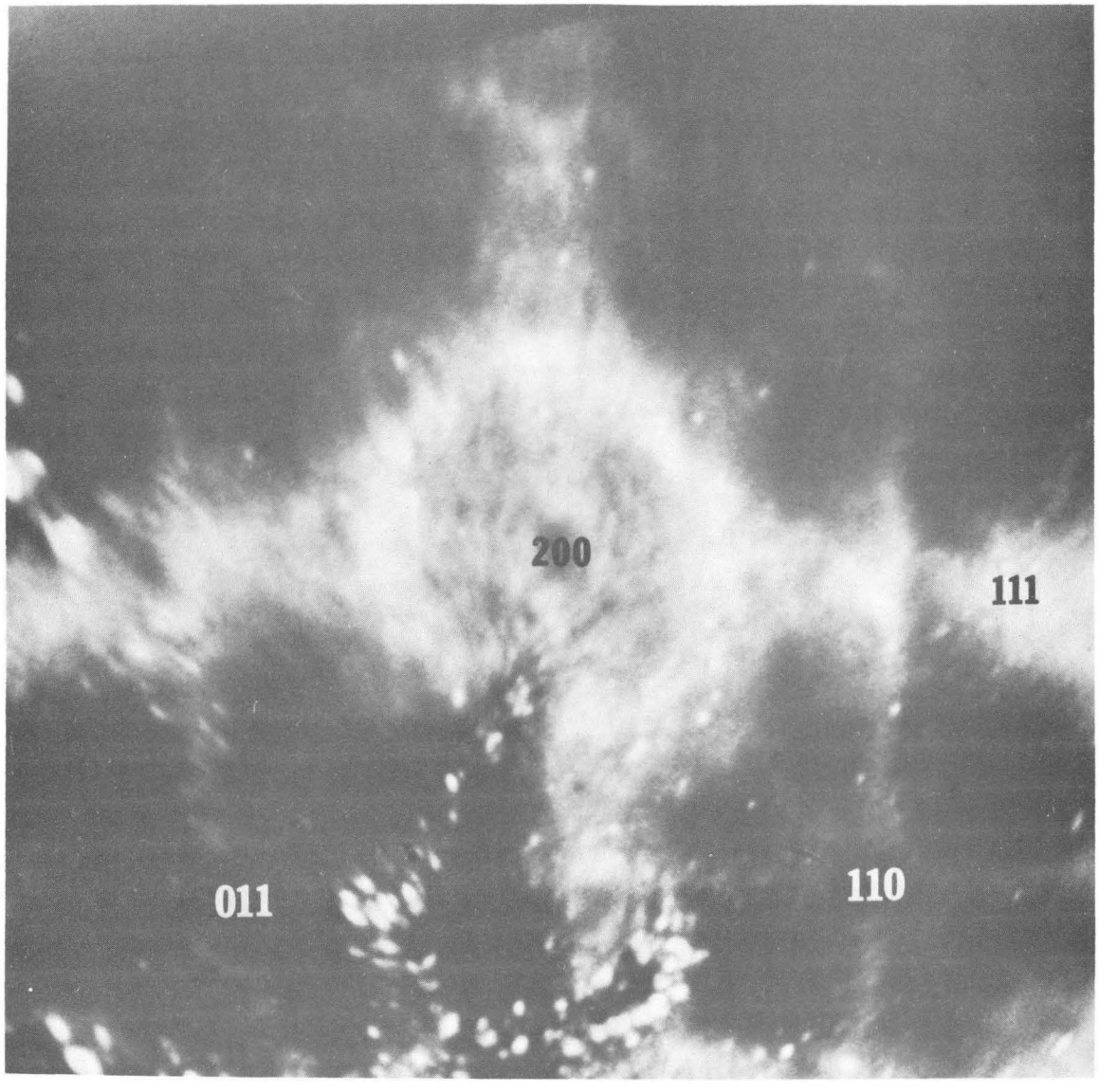

XBB 6911-7127

Figure 24

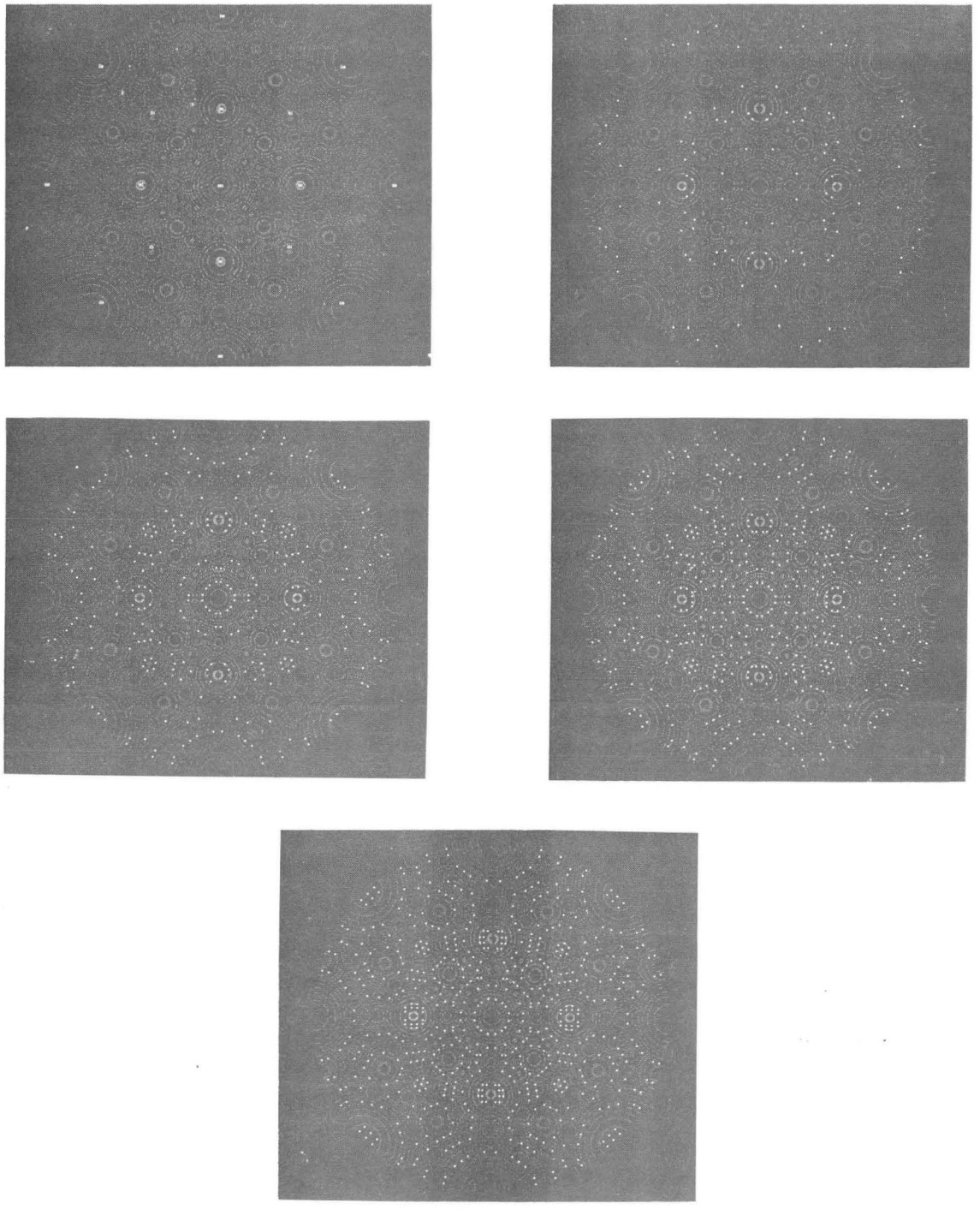

XBB 6911-7129

Figure 25

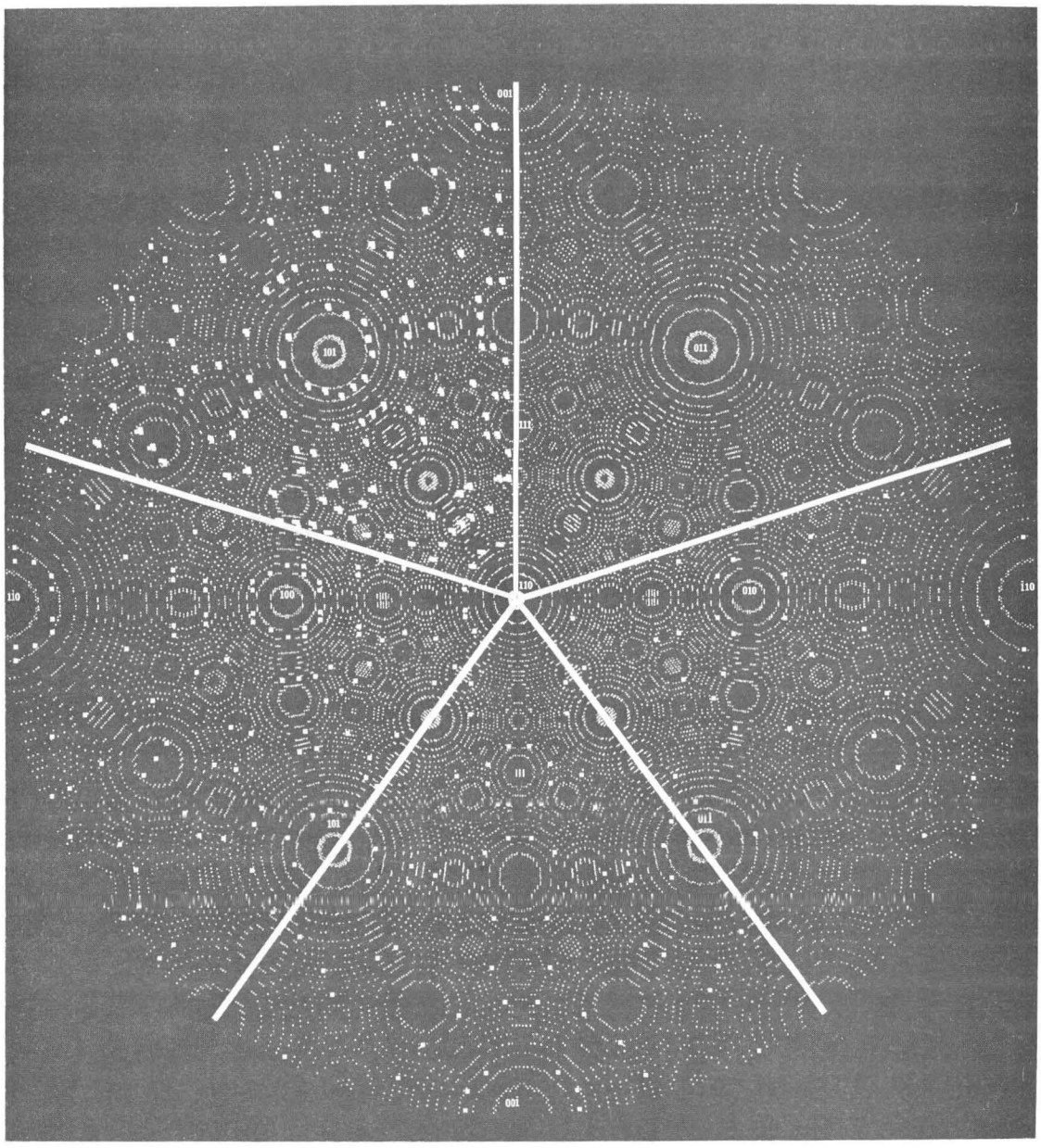

XBB 6911-6792

Figure 26

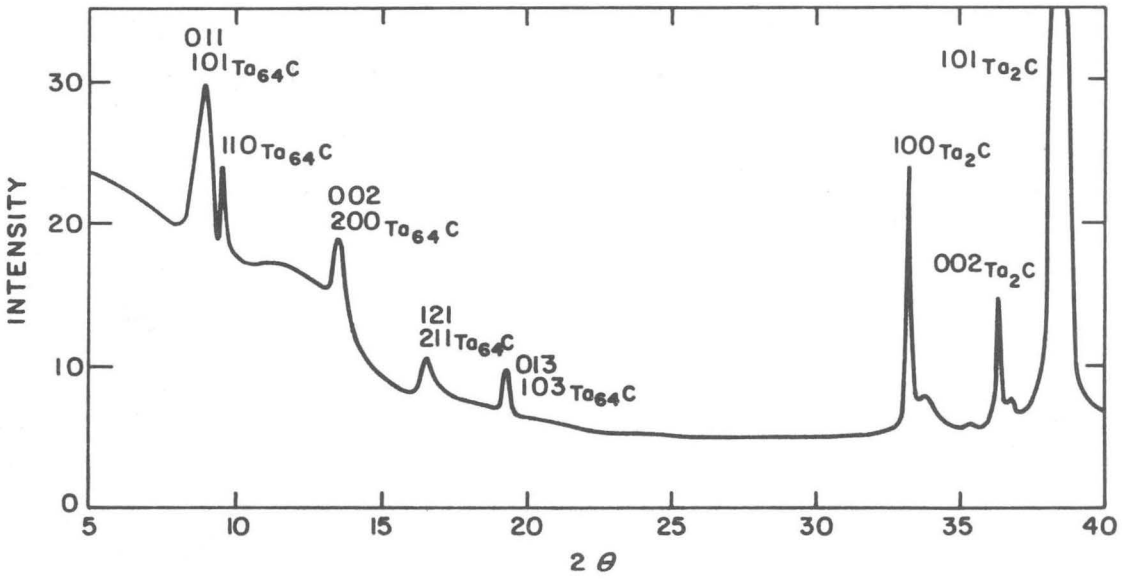

XBL 6910-5971

Figure 27

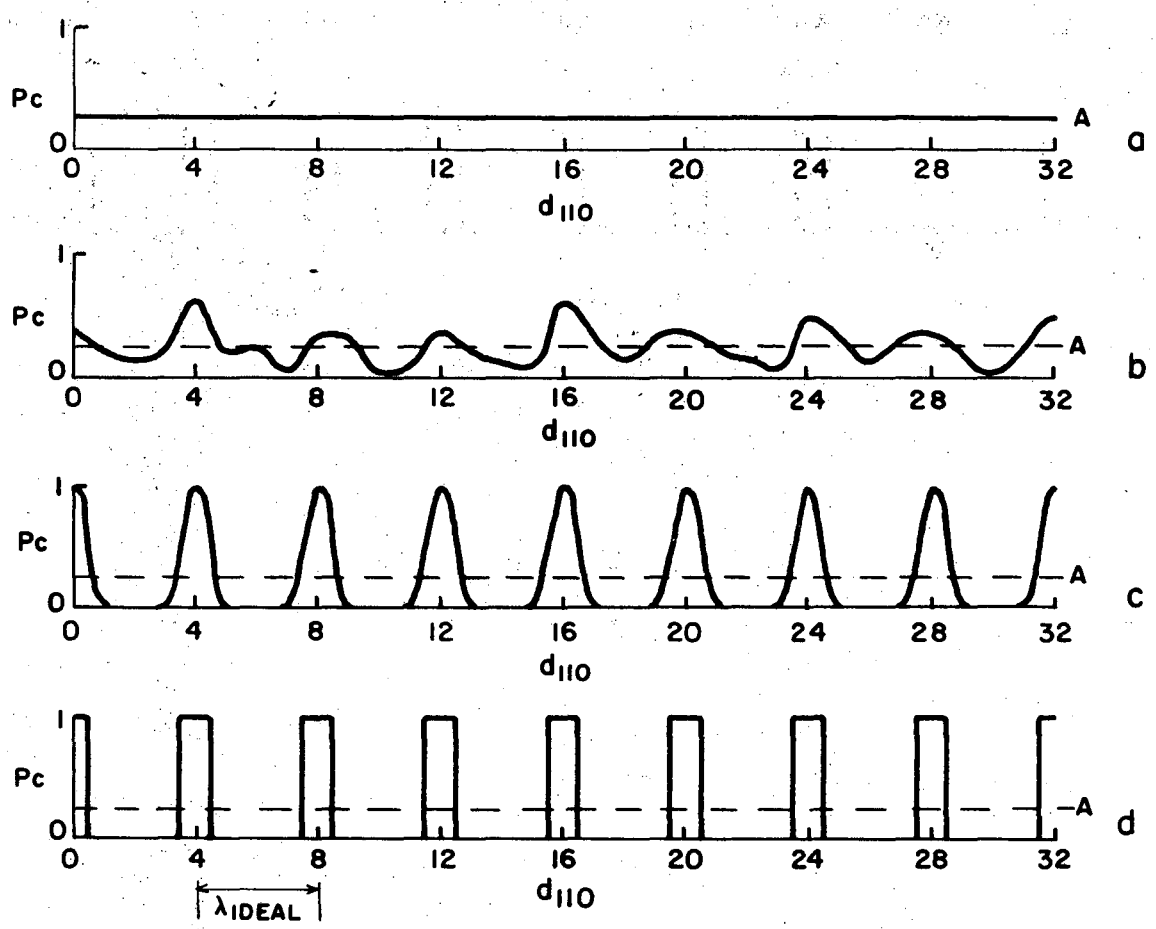

Pc = PROBABILITY OF FINDING A C ATOM ON (110) PLANE

A = AVERAGE C COMPOSITION

$\lambda_{IDEAL} = 4\,d_{(110)_{Ta}}$

XBL 6911-5994

Figure 28

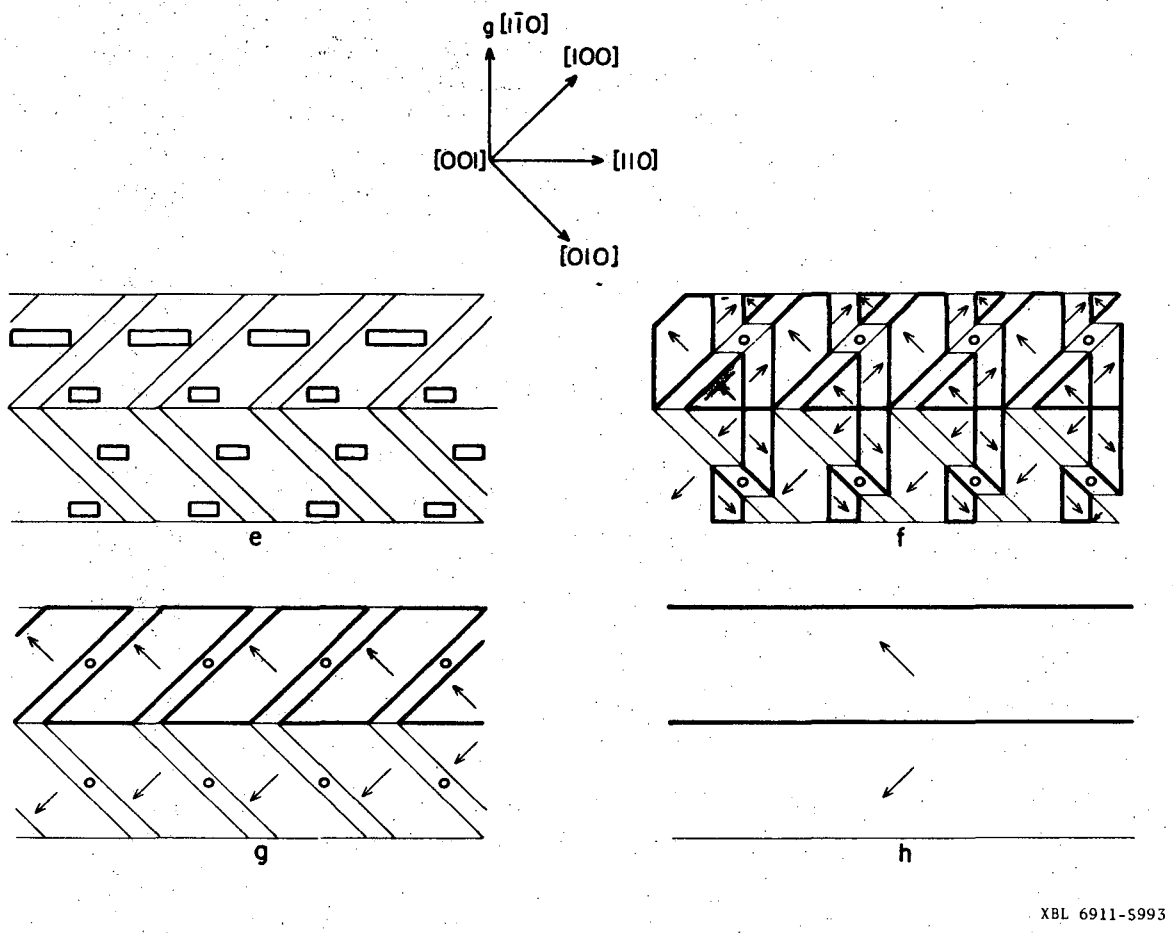

Figure 28e-h

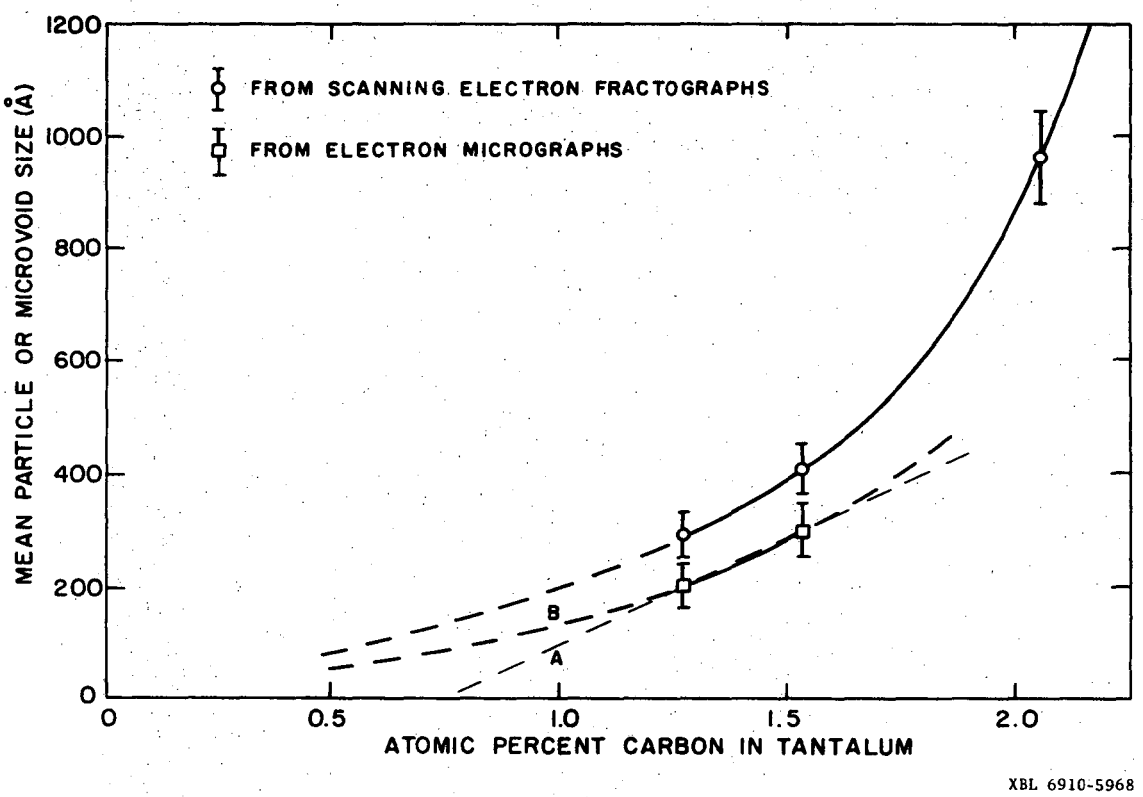
FROM SCANNING ELECTRON FRACTOGRAPHS
FROM ELECTRON MICROGRAPHS
MEAN PARTICLE OR MICROVOID SIZE (Å)
1200
1000
800
600
400
200
0
B
A
0
0.5
1.0
1.5
2.0
ATOMIC PERCENT CARBON IN TANTALUM
XBL 6910-5968

Figure 29

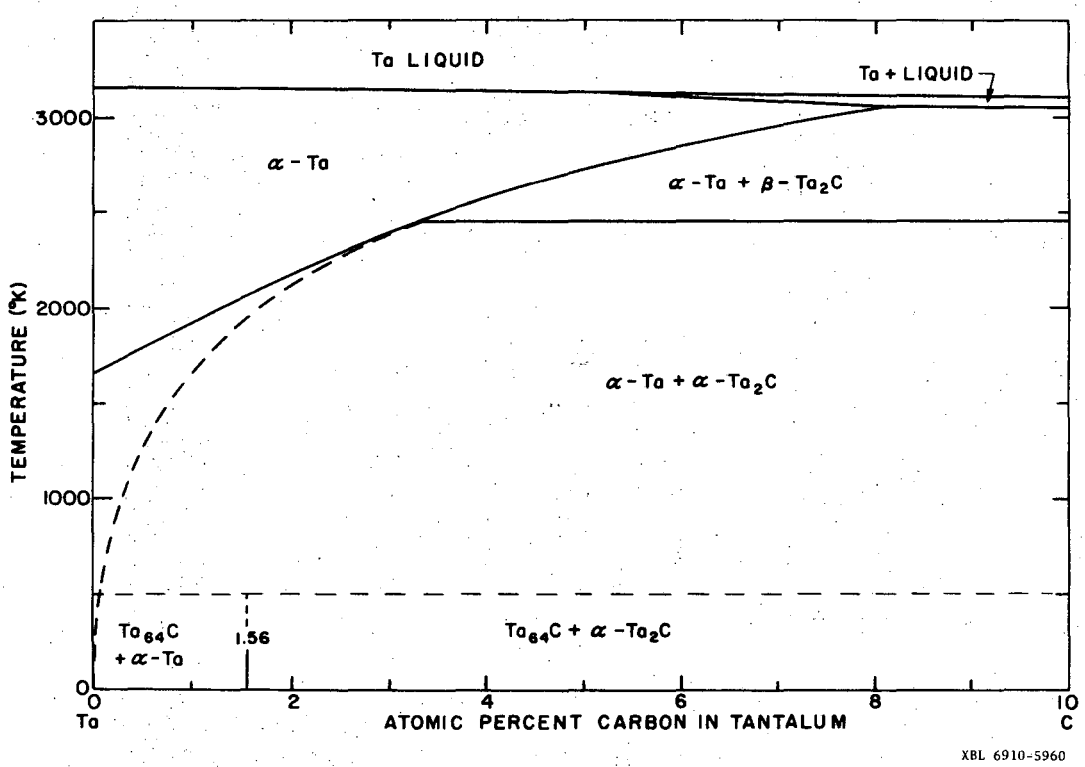
Ta LIQUID
Ta + LIQUID
α - Ta
α - Ta + β - Ta2C
α - Ta + α - Ta2C
Ta64C + α - Ta
1.56
Ta64C + α - Ta2C
TEMPERATURE (°K)
3000
2000
1000
0
0
2
4
6
8
10
Ta
C
ATOMIC PERCENT CARBON IN TANTALUM
XBL 6910-5960

Figure 30

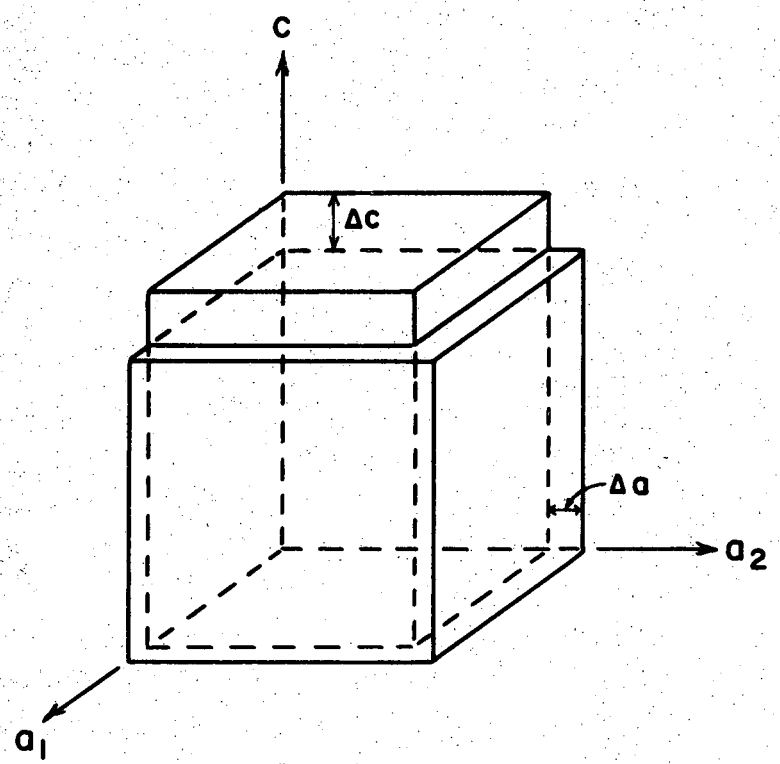

XBL 6911-5995

Figure 31

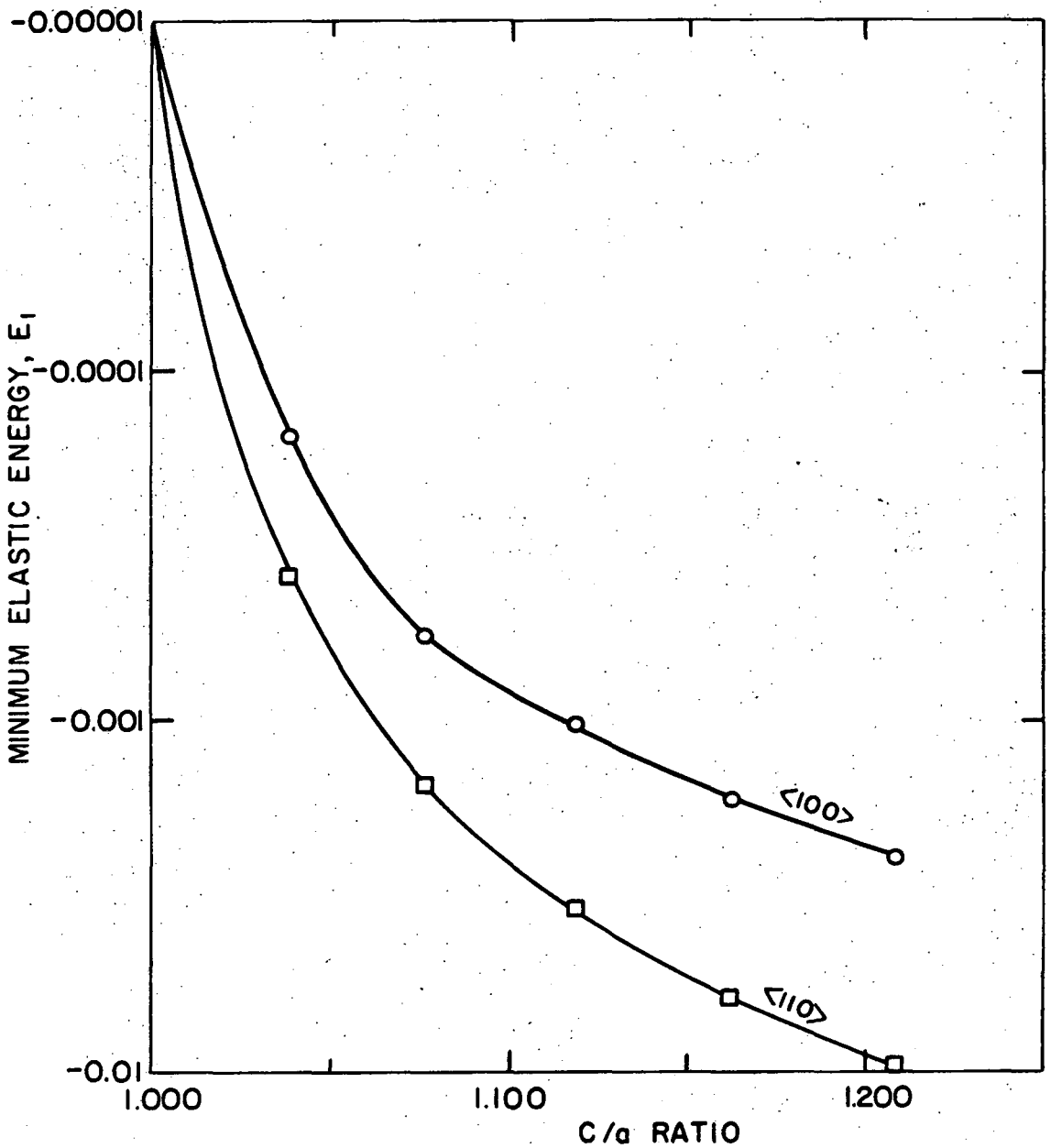

XBL 6911-5991

Figure 32

LEGAL NOTICE

This report was prepared as an account of Government sponsored work. Neither the United States, nor the Commission, nor any person acting on behalf of the Commission:

A. Makes any warranty or representation, expressed or implied, with respect to the accuracy, completeness, or usefulness of the information contained in this report, or that the use of any information, apparatus, method, or process disclosed in this report may not infringe privately owned rights; or

B. Assumes any liabilities with respect to the use of, or for damages resulting from the use of any information, apparatus, method, or process disclosed in this report.

As used in the above, "person acting on behalf of the Commission" includes any employee or contractor of the Commission, or employee of such contractor, to the extent that such employee or contractor of the Commission, or employee of such contractor prepares, disseminates, or provides access to, any information pursuant to his employment or contract with the Commission, or his employment with such contractor.

TECHNICAL INFORMATION DIVISION
LAWRENCE RADIATION LABORATORY
UNIVERSITY OF CALIFORNIA
BERKELEY, CALIFORNIA 94720